The Physics of High Energy Reactions

Alfredo Ferrari and Paola R. Sala

Istituto Nazionale di Fisica Nucleare, Sezione di Milano
Via Celoria 16, 20133 Milano, Italy

Lecture given at the

Workshop on Nuclear Reaction Data and Nuclear Reactors
Physics, Design and Safety

International Centre for Theoretical Physics
Miramare–Trieste, Italy, 15 April – 17 May 1996

Proceedings in press

The Physics of High Energy Reactions

Alfredo Ferrari, and Paola R. Sala
INFN, Sezione di Milano, Via Celoria 16, 20133 Milano, Italy

Abstract

The basic aspects of particle nuclear interactions in the energy range from a few tens of MeV up to several hundreds GeV, are presented, with particular emphasis on the intermediate energy range (from 20 MeV to $\approx$ 1-2 GeV). All topics concerning with hadron-nucleon interactions are discussed mainly on a phenomenological basis, while nuclear effects are presented in a more quantitative way. For both, the lecture is focussing on the general aspects, rather than going into details. A particular effort is made to illustrate the general features of the processes through the discussion of models of common use in practical calculations.

1 Introduction

The importance of shower simulations in many fields of present day particle physics has grown considerably during the last years, in parallel with the rapid increase in available CPU power. However there has been no corresponding development concerning the physical models used for such simulations, despite the strong impact that simulation studies have on the analysis of running experiments and on the design of future detectors.

A great importance has been attached instead to the development of sophisticated informatics packages to describe and visualize complex detectors and to provide the generic user with powerful interactive tools for detector modelling and data analysis. Perhaps the best example of such philosophy is the GEANT code [1], developed at CERN and widely used in the high energy physics community.

Besides physics experiment, there is an increasing interest for applications of accelerator beams. A new generation of intermediate energy proton and electron accelerators is under construction or planned in the near future, spanning a variety of applications, ranging from energy production, waste transmutation, synchrotron radiation to radiotherapy. Such applications call for more and more refined simulations tools, to be able to design and properly operate these facilities.

A good knowledge of radiation transport is critical also for other activities which apparently have very little in common with the new medical and industrial accelerators. Radiation background in the large experiments which are currently planned to be installed at the future LHC proton-proton collider will

be dominated by particle fluxes which can only be estimated by simulation of the whole hadronic cascade from several TeV down to thermal energies. Most of the particle production will take place at energies below 1 GeV. A similar situation arises in the assessment of the radiation dose affecting the crew of commercial airplanes or of space stations. The interplanetary radiation environment is indeed one of the major challenges of a possible manned mission to Mars, and the optimization of the spacecraft in order to maximize shielding while minimizing the weight is top priority. In general all aspects connected with the dosimetry of medium and high energy particles are still waiting for a fresh and more systematic treatment.

Detailed physical models are also required when designing and operating experiments based on calorimetry. A detailed comprehension of active device responses to subGeV hadrons will be a key issue for many of the future experiments, both at accelerator beams, or in underground laboratories. The recent question about the Kamiokande result on the deficit of atmospheric μ-neutrinos is a typical example. According to some calculations[2], the "signal" could be explained as due to π^0s produced by energetic neutrons generated in the surrounding rock by high energy muons. A precise knowledge of the full chain of muon photonuclear interactions, hadron showers, and finally pion production in the intermediate energy range is required to settle the question.

Despite they heavily rely on MonteCarlo modelling when designing and understanding their devices, and when analyzing experimental data for backgrounds and kinematical cuts, high energy physicists tend to consider all the complex phenomena of hadronic and electromagnetic showers occurring in their experimental apparatus as well understood physics, without recognizing the still large uncertainties connected with the physical description of nuclear interactions. While QCD inspired models are very powerful in predicting and describing the rare interesting phenomena searched for by high energy experiments, efforts in describing the bulk of high energy interactions, which cannot be understood in terms of perturbative QCD, are relatively rare.

Nuclear physicists are often working on a small subset of "interesting" phenomena related to nuclear interactions, and usually do not like to spend time on more general models which can be used for whichever application, particularly for technological ones. Very interesting physics researches are going on in the description of nucleon induced interactions below the pion threshold (see the reviews[3,4]), however little or no work is done in the understanding of interactions at higher energies, with possibly the exception of some interesting developments in the pion sector[5,6,7] and of Quantum Molecular Dynamics (QMD) models[8,9] when extended to the few GeV range. Anyway, new or updated models are seldom formulated in such a way as to allow a general

application. As a consequence, most applications must rely on models, like the glorious Bertini IntraNuclear Cascade code, which are 20 to 30 years old, and which are no longer up-to-date with the present knowledge.

As soon as the energy of a primary hadron beam exceeds few tens of MeV, inelastic interactions start to play a major role and secondaries have enough energies to trigger further interactions, giving rise to a hadronic shower. Whenever the beam energy is such that significant pion production can occur (the pion production threshold for nucleons interacting with stationary nucleons is around 290 MeV), an increasing fraction of the energy is transferred from the hadronic (HAD) to the electromagnetic (EM) sector due to production of mesons (mainly π^0 and η) which quickly decay into EM particles (e^+, e^-, and γ). Hadron and electromagnetic showers are very complex phenomena, whose description in terms of basic physical interactions requires a lot of knowledge. There are two basic differences between hadronic and EM showers. The first is that, while energetic hadronic showers are always giving rise to significant EM ones (and such EM component is more and more important with increasing primary energy), EM showers develop independently without further hadronic particle production, forgetting for a while the (small) probability of electro and photonuclear interactions. The second difference is that, while EM interactions are in principle well understood (see however [10]) and described by QED, the same does not apply to hadronic nuclear interactions, where such a complete theory does not exist and one has to resort to suitable models to have some insight into the physics of the processes.

The development of hadron initiated showers is determined both by atomic processes (dE/dx, multiple Coulomb Scattering etc), which take place very frequently, and by the relatively rare nuclear interactions (both elastic and nonelastic). EM showers are determined by the same atomic processes (dE/dx, multiple Coulomb Scattering etc), plus other atomic processes (Bremsstrahlung, pair production, Compton scattering etc), which are specific of $e^{\pm}$ and photons, while nuclear interactions play a minor role, and whenever the interest is not in the small amount of hadrons produced by EM particles, they can be safely neglected.

Therefore this lecture[a] will restrict mainly to hadron induced nuclear interactions with little or no discussion of those induced by real or virtual photons. The description of hadron-nucleus interactions is presented in sections 5,6. In particular section 5 describes hadronic inelastic interactions in the framework of the (Generalized) IntraNuclear Cascade approach, whose basis are presented in section 3. A discussion of practical implementations of (G)INC models, and

[a] This lecture is partially based on a similar one given at the *1995 Frederic Joliot Summer School in Reactor Physics* [19].

examples of performances are given in section 7.

Before going on with the proposed scheme, it is important to make the reader aware of a few important warnings and comments. The present lecture is based on the experience and feelings of the authors, who work since several years in the field of shower modelling, mainly for applications connected with high energy accelerators and experiments. Their opinions are not necessarily those of the majority of people working in the field.

Whenever presented, plots of cross sections etc are to be intended as indicative. Usually the data used for such plots are taken from the tabulations used by the author code (FLUKA). Whenever experimental data are plotted, the source is always indicated. Most of the examples have been computed again with FLUKA , just for convenience: indications whether they can be considered or not as typical examples are given every time.

No discussion is given about hadron interactions below, say, 20 MeV, both because they are outside the aim of this lecture (and they are perfectly covered by other authors at this school [11,12]), and because for most practical applications they are essentially restricted to neutron interactions, for which a huge and accurate body of experimental informations, sometimes supplemented by sophisticated modelling does exist in official compilations like ENDF-B, JEF, JENDL etc. It is always assumed that (nucleon) interactions below a few tens of MeV can be accurately described either with the models developed for this energy range [11,12,13,14,15], or making use of such (experimental) informations. The extension of these models [16,17,18], to higher energies close to the pion threshold, is of little or no interest for many applications since correlations among reaction products are forcibly lost due to the inclusive nature of the computed distributions. Such correlations are of fundamental importance whenever exclusive events are required, as for example in experiment analysis and design. The most popular solution for preserving the internal correlations of individual events are MonteCarlo based models. To the knowledge of the authors, no exclusive (MonteCarlo) model based on the refined physical basis of those models has been yet developed.

Furthermore, only single hadrons will be considered as possible projectiles. The extension to very light nuclei (deuterons and alphas), is relatively straightforward, at least for projectile energies much in excess of the binding of these nuclei, but will not be explicitly described. Models for complex nucleus-nucleus interactions will not be considered at all. Such interactions have indeed little or no interest for technological applications (with the possible exception of cancer therapy with ion beams), and for high energy experiment analysis (unless a primary ion beam is used).

The description of hadron-nucleon interactions above few GeV will be

forcibly limited to few remarks, because of space reasons and of the relative scarce interest of this energy range for accelerator technological applications. Nuclear effects will be presented in a more quantitative way, without however going into too many details. Anyway a comprehensive bibliography has been included in order to allow the reader to access more informations if required.

Finally, the title itself is rather misleading. "High energies" for people working in the nuclear field usually mean several tens of MeV, or few hundreds of MeV at most. They will probably feel rather exotic all parts dealing with interactions at several tens of GeV. On the contrary high energy physicists will be disappointed by the low energy trifles which fill a good fraction of this text.

2 Generalities

Before discussing specific aspects of hadronic interactions, there are a few comments which help in focussing the problem. Assuming one is dealing with some technological application of an accelerator beam (energy production, waste transmutation, cancer therapy etc), which kind of informations does he need? Without claiming that these are all the possible informations required, a reasonable list could be the following:

- Elastic and nonelastic cross sections as a function of projectile, energy and target
- Elastic scattering angular distributions
- Secondary particle yields as a function of energy and angle, following nonelastic interactions
- Residual nuclei produced by nonelastic interactions
- Internal correlations among produced particles in the same event

Ideally, our tool, from now identified with some MonteCarlo program, should be able to give us accurate predictions about all the above points, for any desired spatial mesh. Usually the degree of accuracy required for the different kind of informations is not the same. For example, residual nuclei are seldom required to an accuracy better than one order of magnitude, while neutron fluence can well be requested to be within a factor 10% or better.

In order to better focus our needs in the description of nuclear interactions, some general features of high energy showers are reported in the following (see [19] for details).

a) Energetic particles (often called *shower* particles) are concentrated mainly around the primary beam axis, regardless of their identity. Their dE/dx and the EM cascades associated with π^0 constitute the "core" of the energy profiles.

b) Neutral particles ($\rightarrow$ neutrons, since these are the only neutral hadrons with long enough lifetime) dominate at energies such that charged particle ranges become shorter than the interaction length. The energy deposition associated with "low" energy neutron interactions, both recoils and photons, constitute the long tails in the energy deposition profiles.

c) Most of the interactions are due to particles (mainly neutrons) of moderate energy, $\rightarrow$ a good description of this energy range is mandatory.

d) On the contrary the longitudinal shower development is ruled by *shower* particles, which carry a good fraction of the energy and have a longer interaction length. Taking into account that any approximation or inaccuracy in the first interactions cannot be recovered with a better physics in the following ones, this means that a good description of energetic particle interactions is also mandatory.

e) Pions can be only produced by *shower* particle interactions, so they are the real "tracer" of the high energy cascade. Neutrons and to less extent protons are copiously produced also in the final (evaporation) stages of nuclear interactions down to projectile energies comparable with their nuclear binding energy (see paragraph 5.8).

The term *shower* particles comes from the early experiments of high energy physics, where nuclear emulsions were often used as recording media. Charged particle tracks are therefore customarily classified in weakly ionizing, or *shower* tracks, medium ionizing, or *grey* tracks, and heavily ionizing, or *black* tracks, just according to their ionization rate. In practice, *shower* tracks correspond to (charged) particles with $\beta = \frac{v}{c} \geq 0.7$, *grey* tracks to $0.25 \leq \beta < 0.7$, and *black* tracks to $\beta < 0.25$. Forgetting the original meaning, but just retaining their velocity interval interpretation, such definitions are sometimes used also for neutral particles. $\beta = 0.7, 0.25$ corresponds to $\approx$ 400 MeV and 30 MeV for nucleons, and to $\approx$ 50 and 5 MeV for pions. Therefore black tracks are a good indicator of evaporation products, while grey tracks are often associated with nucleons emitted during intranuclear cascading. The bulk of shower tracks is due to secondaries produced during projectile primary interactions.

3 (Generalized)IntraNuclear Cascade

Hadron-nucleus non-elastic interactions will be described mostly in the framework of the IntraNuclear Cascade (INC) model. This model was developed at the very beginning (the original ideas go back at the end of the 40's) of the history of energetic nuclear interaction modelling, but it is still very valid and in some energy range it is the only available choice. The model is intrinsically a MonteCarlo model, well suited for numerical applications, while no closed analytical expression can be derived without severe approximations. Therefore INC models became more and more refined and widespread with the evolution of computer codes; currently available models can reach 100,000 lines of program.

In the energy range going from the pion production threshold ($\approx$ 290 MeV for a free nucleon, down to 200 MeV for nucleons in nuclei because of the Fermi motion) to high energies, INC models are practically the only available tools to model hadron-nucleus interactions. At lower energies, a variety of preequilibrium models can do a very good job, with physics foundations which become surely more robust than those of INC ones as the energy is going down.

However one of the fundamental requirements for a model describing nuclear interactions to be applied in practical calculations, is **speed**. Indeed there are two possible approaches to the speed problem: the former is to develop sophisticated models, not necessarily MonteCarlo ones, possibly very accurate and maybe slow, and to produce comprehensive tabulations of energy-angle spectra of all emitted particles for a fine mesh of energies of possible projectiles. Such an approach, very similar to that adopted for neutron calculations below 20 MeV, becomes soon very impractical. Indeed, assuming 20 points per energy decade for the energy mesh (still $\approx$ 10% inaccuracy), 3 energy decades (1-1000 MeV for example), 10 deg steps for angular distributions ($\rightarrow$ 18 points), tabulated data for at least p, n, π^+, π^-, π^0, and γ, it can be easily computed that $\approx$ 5-10 Mbytes of dynamic memory will be required for each (target) isotope present in the problem setup. Even assuming possible compression schemes, such a (still rough) mesh cannot be actually used without exploding memory requirements. Furthermore this kind of tabulations, while possibly suitable for many calculations, cannot be used for problems where internal correlations among different particles emerging from the same collision are important. Indeed problems like detector efficiencies, resolutions, coincidences background studies for rare events, etc, do often require the simulation of proper correlations among many particles inside each event, and therefore cannot be studied with approaches based on precomputed data, where such correlations are forcibly lost.

The second approach (used by the vast majority of practical applications in the energy domain of interest), is to use the MonteCarlo method, simulating at run time every interaction. One of reasons of the long dating success of INC models is just their ability to model in reasonable time, almost whichever target nucleus with whichever projectile, with no or small need for external input informations or preliminary calculations. The other great advantage is that all correlation among the different quantities and particles are fully reproduced. Of course, the speed of such a model is a key feature, since a large number of interactions must be simulated within reasonable time. Actually, most INC codes do their job fast enough that they do not represent any significant limitation to the CPU required, which is instead dominated by the transport time. Until this situation will continue, the push for complex and huge pre-tabulated libraries has no serious foundation, unless the physics is much better. Furthermore, while a code can be easily updated and/or corrected, every change in the underlying physical models will require a complete recalculation of the whole library, for all isotopes, particles and energies, making "de facto" such an hypothetical library a quickly obsoleting tool.

3.1 Basic assumptions of IntraNuclear Cascade (INC) models

Classical INC codes [20,21,22,23] are based on a more or less accurate treatment of hadron multiple collision processes in nuclei, the target being assumed to be a cold Fermi gas of nucleons in their potential well [24,25]. The hadron-nucleon cross sections used in the calculations are free hadron–nucleon cross sections. Usually, the only quantum mechanical concept incorporated is the Pauli principle. Possible hadrons are often limited to pions and nucleons, pions being also produce or absorbed via isobar (mainly Δ_{33}) formation, decay, and capture. The Fermi motion is taken into account when considering elementary collisions, both for the purpose of computing the interaction cross section, and to produce the final state particles. The basic assumptions of INC models can be summarized as follow:

1. Hadrons propagate like free particles in the nuclear medium, with interaction probability per unit length given by free space cross sections, properly averaged over the Fermi motion of the target nucleons, times the local nuclear density.

2. The particle motion is formulated in a classical way. It can be subject to an average nuclear mean potential, which must be added to the free particle kinetic energy when tracking through the nucleus. The radial and energy dependence of such field are model and particle dependent.

3. The effect of the nuclear mean field on the particle motion can either be null or can produce curved trajectories in a semiclassical approach, according to energy and momentum conservation, depending on the model. The curvature effects induced by the nuclear mean field are usually referred to as refraction and reflection effects.

4. Interactions occur like in free space in the Center of Mass System of the two colliding hadrons. Of course, because of the Fermi motion, the lab frame will not coincide with the frame where the target nucleon is at rest, but suitable Lorentz boosts (see Appendix A) have to be applied to transform back the secondary particles in the lab frame.

5. Interactions occur in a completely incoherent and uncorrelated way. No coherence or diffractive effect is included. No multibody or cluster process is included, with the possible exception of pion absorption (see next sections).

6. Quantum effects are mainly limited to Pauli blocking (see section 5): only few codes contain further quantum effects (see again section 5 for a discussion).

7. Secondaries are treated exactly like primary particles, with the only difference that they start their trajectory already inside the nucleus.

An obvious requirement arising from the previous points is that the wavelength associated to hadron motion must be much shorter than the hadron mean free path inside the target nucleus, and also much shorter than the average distance among two neighboring nucleons. That is:

$$\lambda_h = \frac{2\pi\hbar}{p} \ll \frac{1}{\sigma_{hN}\rho} \tag{1}$$

$$\lambda_h = \frac{2\pi\hbar}{p} \ll \left(\frac{3}{4\pi\rho}\right)^{1/3} \tag{2}$$

The nucleon density at the center of nuclei is typically $\rho \approx 0.17$ fm^{-3}, therefore the latter condition would require a particle momentum in excess of 1 GeV/c. For a projectile nucleon, again at central density, the former condition is fulfilled only starting from 200 MeV (see fig. 1 for evaluating σ_{hN}). From these back of the envelope estimates it would appear that INC models cannot work at all, unless the projectile energy is above a few hundreds MeV. Furthermore, the transport and reinteraction inside the nucleus of secondary particles, which are at lower energies, cannot easily comply with the above requirements. Fortunately the situation is not so bad as it could appear. Pauli blocking and other

effects contribute to increase particle mean free paths. In particular Pauli blocking is more effective for low energy particles, in such a way partially compensating the increase in nucleon-nucleon cross sections at low energies. Furthermore, hadronic interactions are mostly surface effects (as can be easily checked both from mean free paths and realizing that hadron-nucleus cross sections scale with the target atomic mass approximately like $A^{2/3}$). Hence the nuclear reactions mostly occur at densities significantly lower than the central one, therefore partially mitigating the requirements on particle energies. However it is clear that the physical foundations of INC are not very sound for primary or secondary particle momenta below a few hundreds of MeV/c. According to these considerations, the quality of results which can be obtained by INC codes is somewhat surprising.

3.2 The Steps of an INC simulation

A typical INC code usually follows the following logic:

- Target nucleus description, typically realized through a few concentric spheres of different density and Fermi energy
- Geometrical cross section, corresponding to the nuclear radius or to the maximum possible impact parameter
- Impact parameter selection with a constant probability over the geometrical cross section area. More than one selection can be required if the particle crosses the nucleus without interacting
- Interaction point selection and projectile tracking through the nucleus, according to Fermi motion averaged hadron-nucleon cross sections and possibly to the nuclear mean field, including the Coulomb field
- Target nucleon selection according to σ_{hp}, σ_{hn} and local Fermi energy
- Interaction simulation according to free hN interactions, local Fermi energy and Pauli blocking
- Secondary tracking into the nucleus, until interaction, escape, or energy cut-off
- (Possible) preequilibrium stage, whenever all excited nucleons are below a given energy threshold (typically a few tens of MeV). This stage is included only in the most recent developments

- Evaporation stage whenever the preequilibrium stage is finished, or all particles are below a given threshold (usually of the order of the binding energy), and the system can be assumed to be equilibrated
- Final deexcitation stage when the excitation energy is below the threshold for particle emission and it is spent through photon emission

A description of the physics involved in all stages can be found in the next sections. It is important to remark that in principle INC codes are able to compute reaction cross sections by themselves. Indeed, the reaction cross section is given by the geometrical one times the probability of interaction. The latter information can be easily derived from the ratio of the impact parameter selections which gave rise to interactions and the total number of selected impact parameters.

3.3 Advantages and Limitations of INC models

A few of the strong points of INC codes have been already touched in the introduction to this section, however they are repeated here for completeness:

- No other model available for energies above the pion threshold (with the exception of QMD models, which however include a substantially similar approach for including hadron-nucleon nonelastic interactions)
- No other model for projectiles other than nucleons
- Easily available for on-line integration into transport codes
- Every target-projectile combination, without any extra information
- Particle-to-particle correlations preserved
- Equally valid on very light as well as on very heavy nuclei (with some question mark on evaporation)
- Capability of computing reaction cross section where unknown

Before going into details about weak points of INC codes, it must be remarked that many of the historical weaknesses have been mitigated or even completely solved in some of the most recent developments [26,27,28]. In the following list, points flagged with an asterisk refer to glorious but old models, typically the Bertini model [21,29,30], but are partially or completely solved in state-of-the-art codes.

- *Low projectile energies ($E \leq 100 - 200$ MeV) are badly described

- *Binding energy: the commonly used assumption of a constant binding energy makes the end points, shapes, and absolute intensities of emitted particle spectra increasingly meaningless for energies below 100 MeV, particularly for reactions like (p, xn) or (n, xp)

- *Backward angle emission poorly described (see [31,32,33,34,35])

- *Coulomb barrier effect: neglected when refraction/reflection are not modelled or no Coulomb potential is included

- *Cross section calculations: crazy when no potential effect is included for E <100 MeV, and anyway at low energies. This point is particularly critical for codes, like HETC [44], which make use of INC computed cross sections for particle transport

- *Secondary transport threshold: down to energies much lower than any safe limit for the theory

- Quasielastic peaks above 100 MeV are usually too sharp when compared with experimental data [36]

- Coherent effects as well as direct transitions to discrete states are not included

- Nuclear medium effects which can alter interaction properties are not taken into account (see [37,38,39] for example)

- Multibody processes, like interaction on nucleon clusters, are not included in INC approaches (with the possible exception of pion absorption)

- Composite particle emission (d, t, ^{3}He, α) cannot be easily accomodate into INC codes, but for the evaporation stage.

It must be stressed that a relevant part of the improvements achieved by recent developments is due to the inclusion of a preequilibrium stage, which prevents the INC part from working in an unsafe energy range, and strongly improves the modelling of reactions at the lowest energies. Since most of the interactions for a real shower occur in this energy range, it is highly questionable the use of codes which are still based on sloppy physics in this region.

4 Hadron-Nucleon interactions

The basic assumption in calculations of intranuclear cascades is that nuclear reactions involving incident particles of high energy can be described in terms of hadron-nucleon collisions within the nucleus. Models for such elementary interactions are supposed to be available from phenomenology complemented by theoretical analysis. Therefore a description, mainly phenomenological, of hadron-nucleon interactions is essential in understanding the following more complex treatment of nuclear interactions and is given in this section.

4.1 Preliminary

We remind here a few concepts and formulae of general utility.

We will deal with elastic and inelastic scatterings, thus the quantities to be calculated , and sampled, will be mainly total or differential cross sections. Plenty of books exist on this subject. We re-write here well known formulae: the differential cross section as a function of scattering angle and centre of mass energy can be written in terms of a *scattering amplitude* $f(\theta, s)$:

$$\frac{d\sigma}{d\Omega}(\theta) = |f(\theta)|^2 \tag{3}$$

The scattering amplitude is a complex quantity, and it is determined by the interaction matrix. A very useful theorem is the *optical theorem*, that links scattering amplitude and total (elastic scattering + reaction) cross section:

$$\sigma_T = \frac{4\pi}{k}\mathrm{Imf}(0) \tag{4}$$

The scattering amplitude can be separated in partial amplitudes corresponding to the different values of the angular momentum l; in the case of spinless particles one has:

$$f(\theta) = \frac{1}{k}\sum_l (2l+1) f_l P_l(\cos\theta) \tag{5}$$

where the P_l are the Legendre Polynomials. More details about partial wave expansions and the corresponding *impact parameter* representation of scattering amplitudes can be found in Appendix B.

The experimental observation of charge invariance of nuclear forces suggested the introduction of the isotopic spin vector T. For instance, the proton and the neutron can be described as the two states of a single entity, the nucleon, having total isospin $T = \frac{1}{2}$, and possible projections $T_z = \pm\frac{1}{2}$. In the

case of the nucleon, the charge is given by $q = \frac{1}{2} + T_z$. From charge independence, it follows that nuclear interactions depend only on the total isospin value, and not on its projection. Cross sections and other matrix element can be separated in isospin channels; Coulomb forces must then be treated as a correction. The isospin formalism is analogous to the spin formalism, and the Pauli principle is taken into account by (anti)-symmetrization of the wave function also with respect to isospin.

4.2 Nucleon-Nucleon elastic interactions

Below the pion production threshold, the only possible interaction between two nucleons is just elastic scattering. The cross sections for p–p (or n–n) and n–p total and elastic scattering are plotted in fig. 1. There are two basic features of these cross sections (which are the total ones up to roughly 300 MeV). The former is the rapid increase of both cross sections with decreasing energy, while the latter is the factor three at the lowest energies between the n–p and the p–p cross sections, as expected on the basis of symmetry and isospin considerations. The total cross section for the two isospin components are shown in fig. 2, according to $\sigma_T^1 = \sigma_{pp}$ and $\sigma_T^0 = 2\sigma_T^{np} - \sigma_T^{pp}$. The same decomposition can be shown to apply for the elastic and the reaction cross sections too.

The angular distributions of the p–p reaction is fairly isotropic up to $\approx$ 300 MeV, while the n–p one starts to exhibit a significant anisotropy at much lower energies [47].

As soon as the energy exceeds a few hundred MeV, both reactions start to develop strong forward peaks, while the backward "charge exchange" peak of n–p becomes progressively smaller than the forward one, on the contrary of what can be observed at lower energies. Such a behaviour is partially reflected also in nuclear collisions, where nucleon-nucleon elastic interactions are the dominant process for nucleon induced reactions below 1 GeV. Above few GeV the behaviour of the bulk of the angular distribution is well described by a standard diffraction-like expression (see Appendix C):

$$\frac{\mathrm{d}\sigma}{\mathrm{dt}} = B\sigma_0 \mathrm{e}^{\mathrm{Bt}} \tag{6}$$

where t is the four-momentum transfer (see Appendix A).

4.3 Pion-Nucleon Elastic and Charge Exchange Interactions at Intermediate Energies

Inelastic processes in Pion-Nucleon collisions remain negligible up to a pion laboratory energy of about 250 MeV, although the kinematic threshold for

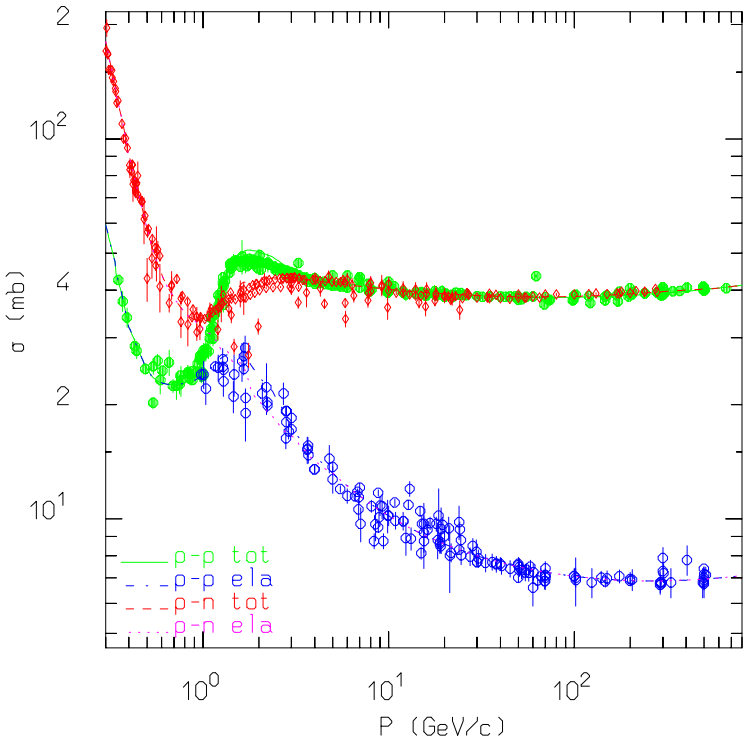

Figure 1: Total and elastic cross section for p–p and p–n scattering, together with experimental data

pion production is at 170 MeV. Up to these energies the most important processes are elastic and charge exchange scattering. Elastic, charge exchange and inelastic π^+ cross sections extracted from tabulations in [48] are shown in fig. 3. All show sharp peaks, distinctive of resonances. These peaks are most conveniently examined in the Isotopic Spin formalism. The total isotopic spin for the pion is $T = 1$, and the three charge states correspond to the three values of T_z. Thus, in the pion-nucleon system two values of T are allowed : $T = \frac{1}{2}$ and $T = \frac{3}{2}$, and two independent scattering amplitudes, $A_{\frac{1}{2}}$ and $A_{\frac{3}{2}}$, enter in the cross sections. From Clebsch-Gordan coefficients one obtains the scattering amplitudes A in the different charge states:

$$A\left(\pi^+ p \to \pi^+ p\right) \quad = \quad A_{\frac{3}{2}} \tag{7}$$

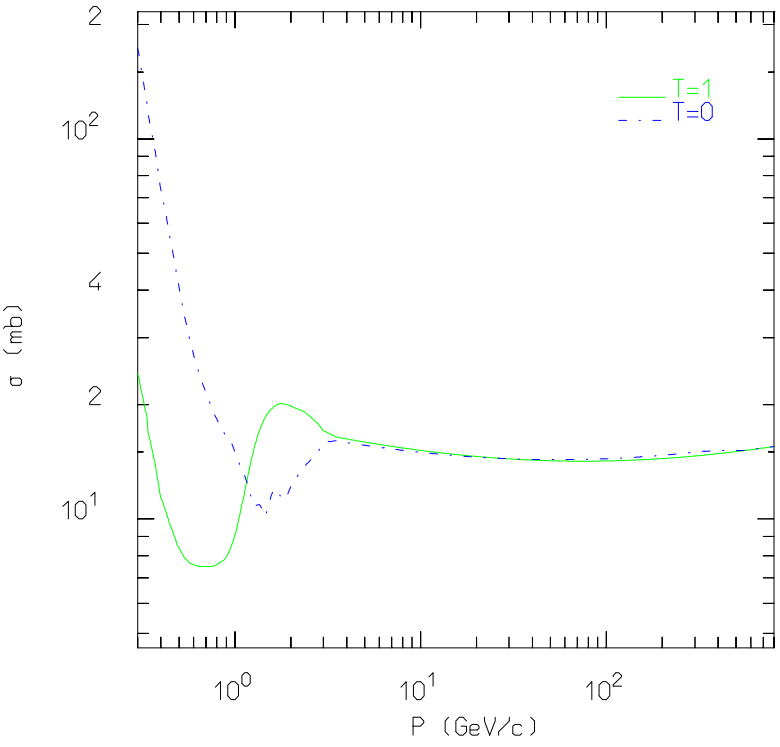

Figure 2: Total cross section for $T = 1$ and $T = 0$ isospin channels for nucleon-nucleon scattering

$$
\begin{aligned}
A\left(\pi^- p \to \pi^- p\right) &= \frac{1}{3}\left(2A_{\frac{1}{2}} + A_{\frac{3}{2}}\right) \\
A\left(\pi^- p \to \pi^0 n\right) &= \frac{1}{3}\left(\sqrt{2}A_{\frac{3}{2}} - \sqrt{2}A_{\frac{1}{2}}\right) \\
A\left(\pi^0 p \to \pi^0 p\right) &= \frac{1}{3}\left(2A_{\frac{3}{2}} + A_{\frac{1}{2}}\right) \\
A\left(\pi^0 p \to \pi^+ n\right) &= A\left(\pi^- p \to \pi^0 n\right) \\
A\left(\pi^- n \to \pi^- n\right) &= A\left(\pi^+ p \to \pi^+ p\right) \\
A\left(\pi^+ n \to \pi^+ n\right) &= A\left(\pi^- p \to \pi^- p\right) \\
A\left(\pi^+ n \to \pi^0 p\right) &= A\left(\pi^- p \to \pi^0 n\right)
\end{aligned}
$$

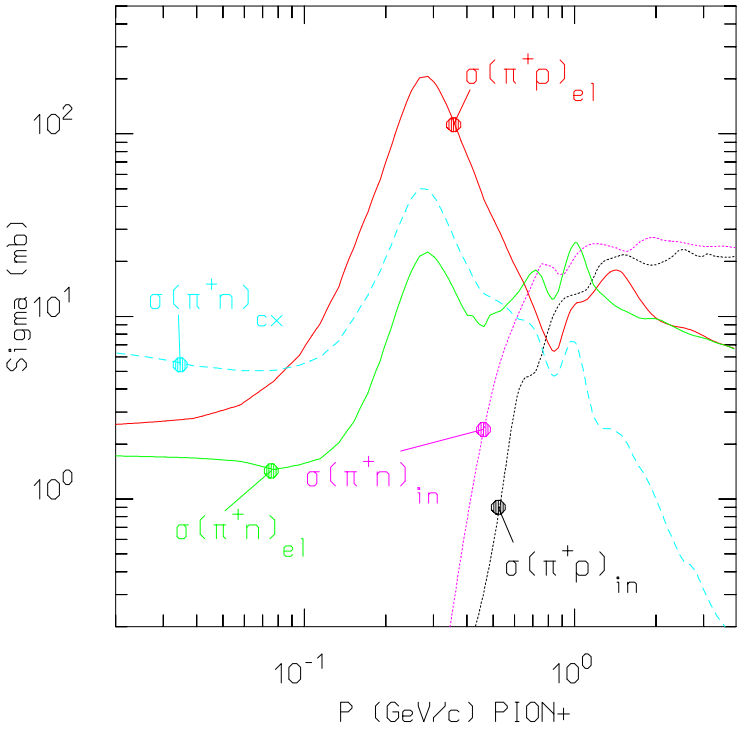

Figure 3: Cross sections for π^+ p and π^+ n reactions

$$\begin{aligned} A\left(\pi^0 n \to \pi^0 n\right) &= A\left(\pi^0 p \to \pi^0 p\right) \\ A\left(\pi^0 n \to \pi^- p\right) &= A\left(\pi^0 p \to \pi^+ n\right) \end{aligned}$$

Using these relations all differential cross sections can be derived from the three measured ones: $\sigma\left(\pi^+ p \to \pi^+ p\right)$, $\sigma\left(\pi^- p \to \pi^- p\right)$, $\sigma\left(\pi^- p \to \pi^0 n\right)$. Care must be taken to include the effect of the mass differences between charged and neutral pions, and between neutron and proton [49]. At low energies also Coulomb effects should be taken into account.

From 7 and from the optical theorem 4 the total cross sections for the $T = \frac{1}{2}$ and $T = \frac{3}{2}$ states can be isolated:

$$\sigma_T^{\frac{3}{2}} = \sigma_T\left(\pi^+ p\right)$$

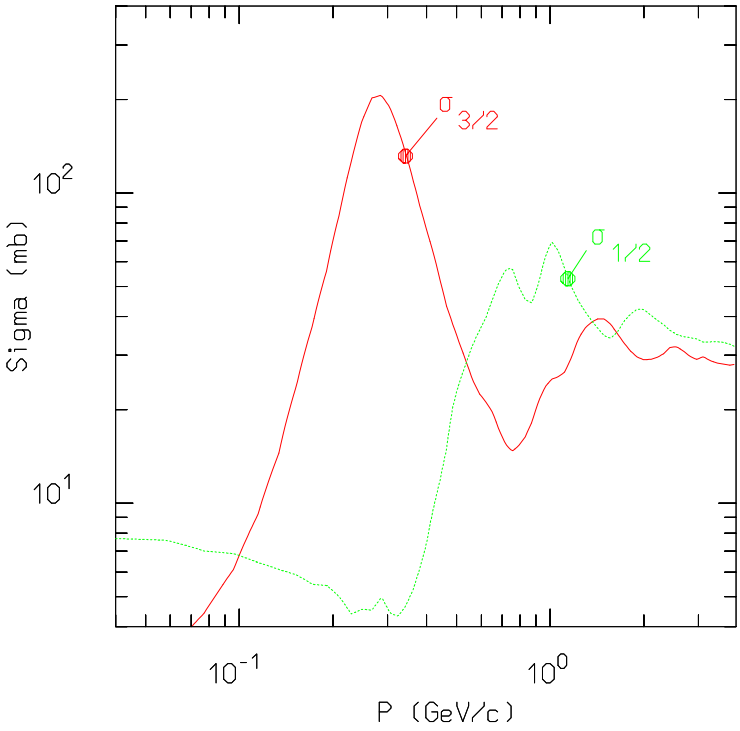

Figure 4: Total cross section for the $T = \frac{3}{2}$ and $T = \frac{1}{2}$ channels for pion-nucleon reactions

$$\sigma_T^{\frac{1}{2}} = \frac{3}{2}\sigma_T\left(\pi^- p\right) - \frac{1}{2}\sigma_T\left(\pi^+ p\right) \tag{8}$$

These are plotted in fig. 4 and show the dominant role of the $\Delta(1232)$ (also called Δ_{33} or simply Δ) resonance in the $T = \frac{3}{2}$ channel at $\approx$ 180 MeV lab. energy, and the presence of several N^* resonances in the $T = \frac{1}{2}$ channel at higher energies.

The same relations for the two possible isospin channels shown in eq. 8 for the total cross sections, can be demonstrated to hold also for the elastic + charge exchange and non-elastic (reaction) cross sections.

$$\sigma_r^{\frac{3}{2}} = \sigma_r\left(\pi^+ p\right)$$

$$\sigma_r^{\frac{1}{2}} = \frac{3}{2}\sigma_r\left(\pi^- p\right) - \frac{1}{2}\sigma_r\left(\pi^+ p\right) \tag{9}$$

$$\begin{aligned} \sigma_{el+cx}^{\frac{3}{2}} &= \sigma_{el}\left(\pi^+ p\right) \\ \sigma_{el+cx}^{\frac{1}{2}} &= \frac{3}{2}\left[\sigma_{el}\left(\pi^- p\right) + \sigma_{cx}\left(\pi^- p\right)\right] - \frac{1}{2}\sigma_{el}\left(\pi^+ p\right) \end{aligned} \tag{10}$$

Detailed phase shift analysis have been performed for $\pi^+ p$ and $\pi^- p$ scatterings up to centre of mass energies of 2.5 GeV[48]. For kinetic energies below 300 MeV the interaction is strongly dominated by s- and p-waves. The Δ resonance occurs in the $l = 1$, $J^P = \frac{3}{2}^+$, $T = \frac{3}{2}$ channel (where J is the total angular momentum, P the parity and T the isospin), at a centre-of-mass energy of $\approx$1232 MeV and with a width of $\approx$120 MeV. The branching for decay into π N is $\approx$100%. The cross sections for π^+ on p and n for the elastic, charge exchange, and inelastic (pion production) channels are shown in fig. 3.

In the Δ region the angular distribution of pions after elastic or charge exchange scattering closely follows the theoretical expectation:

$$P(\cos\theta)\mathrm{d}\Omega \quad \propto \quad (1 + 3\cos^2\theta)\mathrm{d}\Omega$$

For energies larger than 1 GeV, the elastic scattering angular distribution becomes progressively more peaked, approaching the usual exponential behaviour in the 4-momentum transfer t described in Appendix C, as for the nucleon-nucleon case.

4.4 Pion production at Intermediate Energies

Pion production is the first non-elastic channel (particle production) to be open both in pion-nucleon and nucleon-nucleon interactions, obviously because of the small pion mass. The reaction $N_1 + N_2 \to N_1' + N_2' + \pi$ has its threshold around 290 MeV, and it starts to be important around 700, while the reaction $\pi + N \to \pi' + \pi'' + N'$ opens at 170 MeV. The dominance of the Δ resonance and of the N^* resonances at higher energies, in the π N channel, suggest to treat both reactions in the framework of the isobar model, that is to assume that they all proceed through an intermediate state containing at least one resonance. For instance, in the case of nucleon induced single pion production, the following channels can be considered:

$$\begin{aligned} N_1 + N_2 &\to N_1' + \Delta(1232) \to N_1' + N_2' + \pi \\ N_1 + N_2 &\to N_1' + N^*(1440) \to N_1' + N_2' + \pi \end{aligned}$$

where the $N^*(1440)$ is a $\mathrm{T}(\mathrm{J}^P)=\frac{1}{2}\left(\frac{1}{2}^+\right)$ baryon resonance with sizeable decay channels into one or two pions plus one nucleon.

The situation for pion induced reactions is a bit different due to the possible direct production of s-channel resonances (that is $\pi\ N$ going into one resonance, like the Δ), which are not possible in the $N\ N$ system since no dibaryon resonance has ever been discovered. Pion induced single pion production can therefore be described by (among all possible channels):

$$\begin{aligned}
\pi + N &\rightarrow N^*(1440) \rightarrow \rho(770) + N' \rightarrow \pi' + \pi'' + N' \\
\pi + N &\rightarrow \Delta(1600) \rightarrow \pi' + \Delta(1232) \rightarrow \pi' + \pi'' + N' \\
\pi + N &\rightarrow \rho(770) + N' \rightarrow \pi' + \pi'' + N' \\
\pi + N &\rightarrow \pi' + \Delta(1232) \rightarrow \pi' + \pi'' + N'
\end{aligned}$$

where the first two reactions are examples of s-channel direct resonance production. $\rho(770)$ is a $\mathrm{T}(\mathrm{J}^P)=1\,(1^+)$ meson resonance with 100% decay branching into $\pi\pi$.

The isobar model easily accommodates multiple pion production, for example allowing the presence of more than one resonance in the intermediate state[50]. Double pion production opens already at 600 MeV in nucleon-nucleon reactions, and at about 350 MeV in pion-nucleon ones. In case of nucleon-nucleon reactions, two pion production can be obtained considering for example (many more channels are possible):

$$\begin{aligned}
N_1 + N_2 &\rightarrow \Delta_1(1232) + \Delta_2(1232) \rightarrow N_1' + \pi_1 + N_2' + \pi_2 \\
N_1 + N_2 &\rightarrow N_1' + N^*(1440) \rightarrow N_1' + \pi_1 + \Delta(1232) \rightarrow N_1' + \pi_1 + N_2' + \pi_2 \\
N_1 + N_2 &\rightarrow N_1' + \Delta(1600) \rightarrow N_1' + \pi_1 + N^*(1440) \rightarrow N_1' + \pi_1 + N_2' + \pi_2
\end{aligned}$$

and for pion-nucleon:

$$\begin{aligned}
\pi + N &\rightarrow \Delta(1600) \rightarrow \pi' + N^*(1440) \rightarrow \pi' + \pi'' + \Delta(1232) \\
&\rightarrow \pi' + \pi'' + \pi''' + N' \\
\pi + N &\rightarrow \omega(782) + N' \rightarrow \pi' + \pi'' + \pi''' + N' \\
\pi + N &\rightarrow \rho(770) + \Delta(1232) \rightarrow \pi' + \pi''' + \pi'' + N'
\end{aligned}$$

Summarizing, all reactions can be thought to proceed through channels like:

$$h + N \rightarrow X \rightarrow x_1 + ... + x_n \tag{11}$$

$$h + N \rightarrow X + Y \rightarrow x_1 + ... + x_n + y_1 + ... + y_m \tag{12}$$

where X and Y can be real resonances, or stable particles (n, p, π) directly.

Resonances which appear in the intermediate states can be treated as real particles, that is, in a MonteCarlo code they can be transported and then transformed into secondaries according to their lifetimes and decay branching ratios.

These definitions can be obviously extended to elastic and charge exchange scattering too, for example:

$$\begin{aligned} \pi^+ + n &\rightarrow \Delta^+ \rightarrow \pi^+ + n \\ \pi^+ + n &\rightarrow \Delta^+ \rightarrow \pi^0 + p \\ p + n &\rightarrow p + n \end{aligned}$$

Reactions described by eq. 11 are examples of s-channel direct resonance production, and therefore they show up in the corresponding isospin cross section as bumps around the centre-of-mass energy corresponding to the resonance nominal mass (see fig. 4). The reactions proceeding like in 12, due to the presence of two particles in the intermediate state with the associated extra degree of freedom of their relative motion, do not exhibit a resonant behaviour, but rather a relatively fast increase starting from a centre-of-mass energy, $\sqrt{s} \approx M_X + M_Y$, followed by a smooth behaviour. N N reactions are all of this latter type and therefore no resonant structure can be find in N N cross sections (see fig. 2).

For a practical use, all hadron-nucleon cross sections must be decomposed into channels like those of eqs. 11 and 12, and the relative angular distribution of the two resonances of the latter case must be known, together with the decay branching ratios and possible anisotropic decay matrix elements for all considered resonances. Unfortunately the experimental information about exclusive channels is far from being complete. However, resorting again to isospin decomposition both for deriving quantities for charge states different from the experimentally known ones, and for correctly isolating the contributions of the different resonances, together with the constraints given by the measured inclusive cross sections for one-, two- and many pion production, a reasonable description can be achieved. Example of analysis and parametrizations of nucleon induced pion production in terms of isospin can be found in [51,52]. An example of a model aiming to describe all exclusive channels up to few GeV is given in [50].

However, as soon as the incident hadron energy exceeds 3-4 GeV, the description of nonelastic interactions via quasi two-body reactions with formation and decay of resonances starts to become difficult. The number of possible channels (and consequently of resonances) to be considered grows very rapidly,

the relevant resonances are often not well established and sometimes their decay channels are unknown. More fundamentally, an inspection of experimental data clearly shows how the produced particles are no longer associated with the projectile/target fragmentation region in the centre-of-mass frame, but they start to preferentially populate the "central" region (see Appendix A), in contrast with the naive picture of two excited objects with some transverse momentum in the CMS, decaying into particles in the forward and backward emisphere.

Fortunately as soon as the energy is beyond the resonance region (above a few GeV), different models can be used. These models are also more appealing since their theoretical basis are stronger, and their dependence on experimental phenomenology weaker than for the isobar model.

4.5 Hadron-Nucleon High Energy Inelastic and Diffractive Interactions

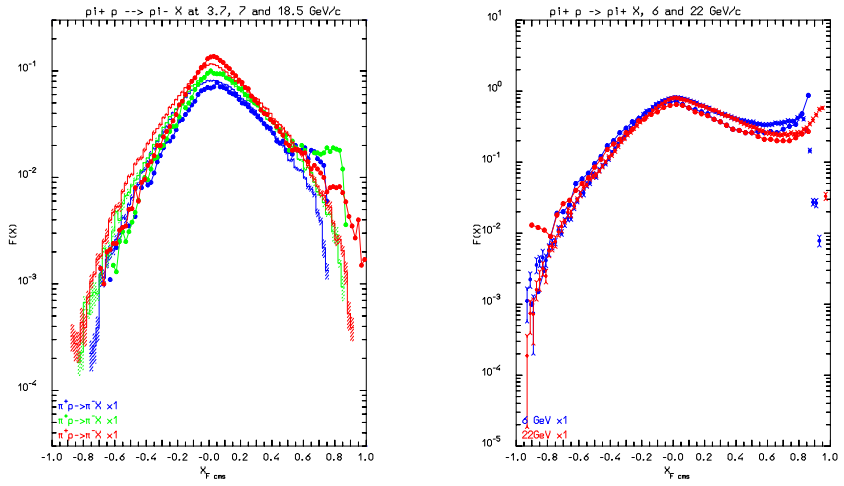

Figure 5: Invariant cross section spectra, as a function of Feynman x_F^* of negative (left), and positive (right) pions emitted for π^+ on protons at various momenta. Symbols are exp. data, dashed histograms are the FLUKA result

Hadron nucleon interactions at high energy can be described by QCD based models only at relatively large transverse momenta. Up to fairly high energies (several tens of TeV in the lab, where minijet production can no longer be neglected), the bulk of hadron-nucleon inelastic collisions is due to processes with small transverse momentum. In this regime, QCD calculations become impractical because of the large coupling constant, which prevents the use of

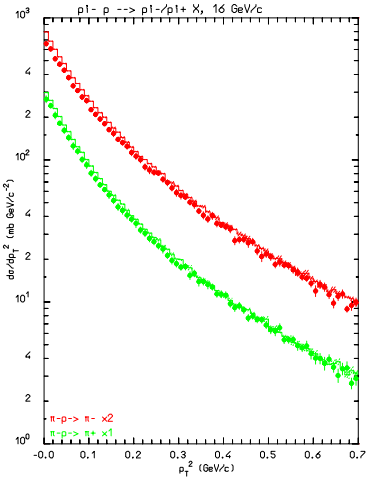

Figure 6: p_T spectra of π^+ and π^- produced by 16 GeV/c π^- incident on an hydrogen target. Symbols are exp. data, the dashed histogram is the FLUKA result

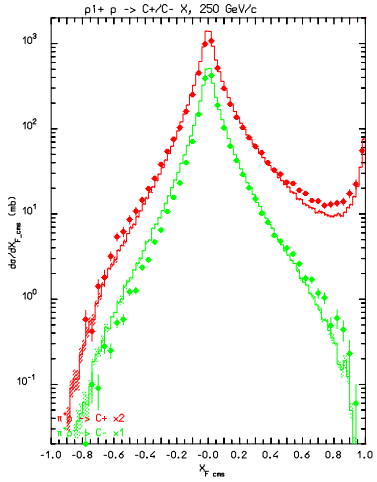

Figure 7: Feynman x_F^* spectra of positive particles and π^- produced by 250 GeV/c π^+ incident on an hydrogen target. Symbols are exp. data, the dashed histogram is the FLUKA result

perturbation methods, and because transverse momenta well in excess of 1 GeV are required to prevent scattered quarks to undergo multiple interactions with the spectator quarks.

The produced particle distributions essentially reflect the motion of the internal constituents, valence and sea quarks. Therefore the longitudinal distribution of produced particles is intimately linked with the longitudinal motion of the projectile and target parton constituents, while the p_T distribution has a roughly gaussian shape, typical of multiple collisions. The scale of the p_T distribution is directly linked to the uncertainty principle, taking into account that hadrons are composite objects with a rms radius ≈ 0.8 fm, $p_T \approx \frac{\hbar}{0.8} \approx 200 - 300$ MeV/c. The shape of the p_T distribution is fairly independent from the projectile energy up to at least several TeV in the lab, and can be well described in terms of invariant cross section (see Appendix A) by:

$$\sigma_{inv} = E\frac{d^3\sigma}{d^3\vec{p}} \propto \mathrm{e}^{-\mathrm{BM_T}} \tag{13}$$

The longitudinal momentum distributions of produced particles approximately scale with the incident energy. Such a scaling is often quoted as the hypothesis of *limiting fragmentation*[53] (see Appendix A for details). A consequence of this

approximate scaling is that the produced particle multiplicity does not increase linearly with the system invariant mass, $\sqrt{s}$, ($\sqrt{s} \propto \sqrt{E_{beam}}$, for $E_{beam} \gg M$), but increases roughly logarithmically with s.

An example of the invariant cross section distribution, $F(x) = \frac{1}{\sigma}\frac{2E_{CM}}{\pi\sqrt{s}}\frac{\mathrm{d}\sigma}{\mathrm{dx_F}}$, of negative pions produced in the $\pi^+ + p \to \pi^- + X$ reactions at 3.7, 7, and 18.5 GeV is presented in fig. 5. A similar plot for $\pi^+ + p \to \pi^+ + X$ is also shown in the same figure. All the experimental data have been taken from the compilation[54]. Both figures show the characteristic concentration of particles in the central region. The scaling violation occurring in that region (the scaling hypothesis originally proposed by Feynman for high energy particle production would predict that the invariant cross section when plotted as a function of the Feynman x variable does not depend on the projectile energy in the central region too) is also evident in the π^- plot. Diffractive production for π^+ at large x_F is apparent from that figure.

In order to describe these features, more or less phenomenological models have to be used, even though motivated by physical ideas. Such models usually work at the constituent level, that is with the constituent quarks (often called *valence* quarks), and possibly also with the so called *sea* quarks which are also present inside real hadrons. The momentum or energy distribution of the constituents must be given (it is the equivalent for soft collisions of the structure functions used for hard collisions), and proper hadronization models must be provided.

The Dual Parton Model

One of the most successful models in this field is the so called Dual Parton Model (DPM), originally developed in Orsay in 1979[55]. It provides the theoretical framework for the model developed for FLUKA in order to describe hadron-nucleon interaction from several GeV onwards. Only few words will be given here, since the main purpose of this lecture is to introduce the reader to the aspects specific of nuclear interactions. Of course hadron-nucleon interactions are an essential basis for nuclear interactions, however they are not our main goal. The interested reader can find all relevant details in a recent review[56].

In principle one would like to derive all features of "soft" interactions (low-p_T interactions) from the QCD Lagrangian, as it is done for hard processes. Unfortunately the large value taken by the running coupling constant prevents the use of perturbation theory.

Indeed, in QCD, the color field acting among quarks is carried by the vector bosons of the strong interaction, called gluons, which are "colored" themselves.

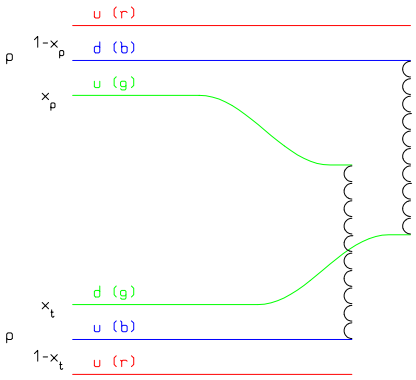

Figure 8: Leading two-chain diagram in DPM for $p - p$ scattering. The color (red, blue, and green) and quark combination shown in the figure is just one of the allowed possibilities

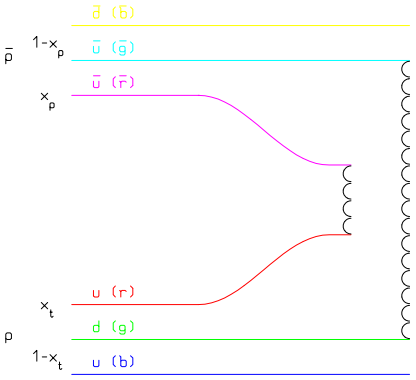

Figure 9: Leading two-chain diagram in DPM for $\bar{p} - p$ scattering. The color (red, blue, and green) and quark combination shown in the figure is just one of the allowed possibilities

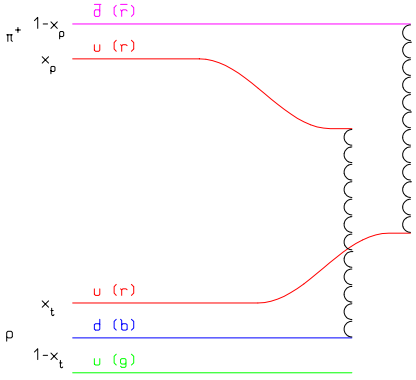

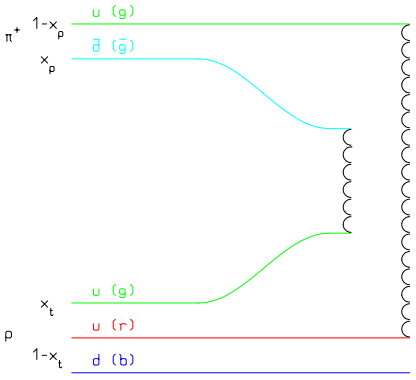

Figure 10: Leading two-chain diagrams in DPM for $\pi^+ - p$ scattering. The color (red, blue, and green) and quark combination shown in each figure is just one of the allowed possibilities

Therefore the characteristic feature of gluons (and QCD) is their strong self-interaction, on the contrary of what occurs for example in QED, where the force carriers, the photons, are chargeless and therefore do not interact among

themselves. If we imagine that quarks are held together by color lines of force, the gluon-gluon interaction will pull them together into the form of a tube or a string. Since quarks are confined, the energy required to "stretch" such a string is increasingly large until it suffices to materialize a quark-antiquark couple from the vacuum and the string breaks into two shorter ones, with still quarks at both ends.

Therefore it is not unnatural that because of quark confinement, theories based on interacting strings emerged as a powerful tool in understanding QCD at the soft hadronic scale, that is in the non-perturbative regime. An interacting string theory naturally leads to a topological expansion. At high energies, such an expansion was developed already before the establishment of QCD, that is the Reggeon-Pomeron calculus in the framework of perturbative Reggeon Field Theory (for a review of Regge theory applied to high energy scattering see[57]). Regge theory makes use explicitly of the constraints of analyticity and duality, and the Dual Parton Model is built introducing partonic ideas into a topological expansion which explicitly incorporates the constraints of duality and unitarity.

In DPM a hadron is a low-lying excitation of an open string with quarks, antiquarks or diquarks sitting at its ends. In particular mesons (all naturally occuring mesons are explained as colorless combination of a quark and an antiquark $q\bar{q}$) are described as strings with their valence quark and antiquark at the ends. (Anti)baryons (all baryons are colorless combinations of three quarks, qqq) are treated like open strings with a (anti)quark and a (anti)diquark at the ends, made up with their valence quarks.

At sufficiently high energies, when all Reggeon (IR) exchange amplitudes become negligible (see Appendix C), the leading term in high energy scattering corresponds to a Pomeron (IP) exchange (a closed string exchange), which has a cylinder topology. When an unitarity cut (think about the optical theorem) is applied to the cylindrical Pomeron two hadronic chains are left as the sources of particle production. While the partons (quarks or diquarks) out of which chains are stretched carry a net color, the chains themselves are built in such a way to carry no net color, or to be more exact to constitute color singlets like all naturally occuring hadrons. In practice, as a consequence of color exchange in the interaction, each colliding hadron splits into two colored system, one carrying color charge c and the other $\bar{c}$. These two systems carry together the whole momentum of the hadron. The system with color charge c ($\bar{c}$) of one hadron combines with the system of complementary color of the other hadron, in such a way to form two color neutral chains. These chains appear as two back-to-back jets in their own centre-of-mass systems.

The exact way of building up these chains depends on the nature of

the projectile-target combination (baryon-baryon, meson-baryon, antibaryon-baryon, meson-meson): examples are shown in figs. 8,9 and 10, and explained in the following.

In the case of baryon-baryon scattering, indicating with q_p^v the valence quarks of the projectile, and with q_t^v those of the target, and assuming that the quarks sitting at one end of the baryon strings carry momentum fraction x_p^v and x_t^v respectively, the resulting chains are $q_t^v - q_p^v q_p^v$ and $q_p^v - q_t^v q_t^v$, as shown in fig. 8.

For meson-baryon scattering, indicating with q_p^v the valence quarks of the projectile, and with q_t^v those of the target, and indicating with x_p^v and x_t^v respectively the energy/momentum fractions carried by the two quarks sitting at the chain ends, the resulting chains are $q_t^v - \bar{q}_p^v$ and $q_p^v - q_t^v q_t^v$, as shown in fig. 10.

For antibaryon-baryon scattering, adopting the same notation, the chains are $q_t^v - \bar{q}_p^v$ and $\bar{q}_p^v \bar{q}_p^v - q_t^v q_t^v$, as shown in fig. 9.

For all cases, the energy, and momentum in the centre-of-mass system of the collision, as well as the invariant mass squared of the two chains, can be obtained from:

$$\begin{aligned} E^*_{ch1} &\approx \frac{\sqrt{s}}{2}(1 - x_p^v + x_t^v) \\ E^*_{ch2} &\approx \frac{\sqrt{s}}{2}(1 - x_t^v + x_p^v) \\ p^*_{ch1} &\approx \frac{\sqrt{s}}{2}(1 - x_p^v - x_t^v) = -p^*_{ch2} \\ s_{ch1} &\approx s(1 - x_p^v)x_t^v \\ s_{ch2} &\approx s(1 - x_t^v)x_p^v \end{aligned} \tag{14}$$

The single Pomeron exchange diagram is the dominant contribution, however higher order contributions with multi-Pomeron exchanges become important at energies in excess of 1 TeV in the laboratory. They correspond to more complicated topologies, and DPM provides a way for evaluating the weight of each, keeping into account the unitarity constraint. When cut, every extra Pomeron exchanged gives rise to two extra chains which are built using two $q\bar{q}$ couples excited from the projectile and target hadron sea respectively. The inclusion of these higher order diagrams is usually referred to as *multiple soft collisions*.

Two more ingredients are required to completely settle the problem. The former is the momentum distribution for the x variables of valence and sea quarks. Despite the exact form of the momentum distribution function,

$P(x_1,..,x_n)$, is not known, general considerations based on Regge arguments allow to predict the asymptotic behaviour of this distribution whenever each of its arguments goes to zero. The behaviour turns out to be singular in all cases, but for the diquarks. A reasonable assumption, always made in practice, is therefore to approximate the true unknown distribution function with the product of all these asymptotic behaviours, treating all the rest as a normalization constant.

Under this approximation, indicating with $x_{q\,i}^{sea}$, and $x_{\bar{q}\,i}^{sea}$, the energy/momentum fractions carried by the sea quarks and with X_i^{sea} the sum of $x_{q\,i}^{sea}$ and $x_{\bar{q}\,i}^{sea}$, the total momentum distribution function for a(n) (anti)baryon in the case of n_{IP}-cut Pomerons can be written as:

$$\begin{aligned} P(\bar{x})\mathrm{d\bar{x}} &\approx C_b\; x_q^{-\frac{1}{2}} x_{\bar{q}q}^{\frac{3}{2}} \prod_i^{n_{IP}-1} (X_i^{sea})^{-1} (x_{q\,i}^{sea})^{-\frac{1}{2}} (x_{\bar{q}\,i}^{sea})^{-\frac{1}{2}} \\ &\cdot \quad \delta(1-x_q-x_{qq}-\sum_i^{n_{IP}-1} X_i^{sea})\;\mathrm{d\bar{x}} \qquad (15) \\ \bar{x} &\equiv x_q \cdot x_{qq} \prod_i^{n_{IP}-1} \left(x_{\bar{q}\,i}^{sea} \cdot x_{q\,i}^{sea}\right) \end{aligned}$$

where C_b is a normalization factor. The momentum distribution function for a meson reads:

$$\begin{aligned} P(\bar{x})\mathrm{d\bar{x}} &\approx C_m\; x_q^{-\frac{1}{2}} x_{\bar{q}}^{-\frac{1}{2}} \prod_i^{n_{IP}-1} (X_i^{sea})^{-1} (x_{q\,i}^{sea})^{-\frac{1}{2}} (x_{\bar{q}\,i}^{sea})^{-\frac{1}{2}} \\ &\cdot \quad \delta(1-x_q-x_{\bar{q}}-\sum_i^{n_{IP}-1} X_i^{sea})\;\mathrm{d\bar{x}} \qquad (16) \\ \bar{x} &\equiv x_q \cdot x_{\bar{q}} \prod_i^{n_{IP}-1} \left(x_{\bar{q}\,i}^{sea} \cdot x_{q\,i}^{sea}\right) \end{aligned}$$

The latter ingredient is of course a hadronization model, which must take care of transforming each chain into a sequence of physical hadrons, stable ones or resonances. The basic assumption is that of *chain universality*, which assumes that once the chain ends and the invariant mass of the chain are given, the hadronization properties are the same regardless of the physical process which originated the chain. Therefore the knowledge coming from hard processes and e^+e^- collisions about hadronization can be used to fulfill this task.

There are many more or less phenomenological models which have been developed to describe hadronization (examples can be found in [58,59]). In principle hadronization properties too can be derived from Regge formalism[60,61].

Summarizing, DPM provides recipes for performing the following tasks:

- determining the number of cut Pomerons, and therefore the number of chains contributing to the reaction
- forming the chains using the valence and possibly sea quarks of the two colliding hadrons
- determining the energy and momentum carried by each chain, according to the momentum distribution functions of the two colliding hadrons
- hadronizing each chain producing the final hadrons, stable ones or resonances

The last step is not exactly a part of DPM, but rather DPM is factorized in such a way that it can be accomplished using whichever hadronization scheme. Indeed DPM is intrinsically factorized, and this strongly constrains the model. In principle there is little or no freedom in each individual step, therefore strenghtening the predictive power of the model. Actually, in the energy range of interest for experiments, that is with showers in the apparatus with energies from few GeV up to several hundreds GeV, threshold effects are still very important. While DPM is assumed to be valid in the asymptotic regime, and treats massless partons at energies large enough to neglect hadron masses (the limit in which eq. 14 is derived), most practical implementations deal with chains with invariant masses so small that only very few particles can be produced out of the chain itself. In this regime the treatment of finite mass effects both when building chains, with the possibility of cutting-off secondary chains because of insufficient energy, and during hadronization, is very important. As an example, the centre-of-mass energy for 450 GeV protons on protons (the maximum laboratory energy obtainable with the CERN accelerator complex on fixed targets) is $\sqrt{s} \approx 30\ GeV$. For $x_q^v \approx 0.2$ which is a typical value, the two chains have invariant masses of $\sqrt{s_{1/2}} \approx 12$ GeV each. Therefore, already 6 GeV in the global centre-of-mass frame are "wasted" into chain motion, and each chain consists of two back-to-back jets with ≈ 6 GeV each, which cannot produce much more than 2-3 particles/resonances, taking into account that typical resonance masses are of the order of 1 GeV and still some motion between resonances created out of the same jet must be provided. Moreover, a centre-of-mass energy of 30 GeV is not obviously negligible with respect to the two proton masses, of ≈ 1 GeV each. Of course such finite mass and threshold

effects are even more important at lower energies, where however we still would like to use DPM due to the lack of valid alternatives. Indeed with a proper treatment of these effects, models based on DPM can be successfully used at lower energies, as shown in the examples reported in this section.

It is possible to extend DPM to hadron-nucleus collisions too [55,56], making use of the Glauber-Gribov approach (see the next section). Furthermore DPM provides a theoretical framework for describing hadron diffractive scattering both in hadron-hadron and hadron-nucleus collisions. The approach to diffractive scattering will not be touched here, however general informations on diffraction can be found in [62] and details as well as practical implementations in the DPM framework in [56,63,64].

At very high energies, those of interest for cosmic ray studies (10–10^5 TeV in the lab), or for collisions at present and future colliders ($\sqrt{s}$=0.2–20 TeV), hard processes cannot be longer ignored. They can be included in DPM through proper unitarization schemes which consistently treat soft and hard processes together. Again we are not going to give any detail on this subject, but the interested reader can find more informations as well as practical implementations and results in [56,65,66,67].

It must be stressed that DPM is not the only model which has been developed an successfully compared with experimental data for high energy interactions. Other models are available, but most of them share an approach based on string formation and decay. For example, the *Quark Gluon String Model* [68] has been developed more or less in parallel with DPM. This model shares most of the basic features of DPM, while differing for some details in the way chains are created and in the momentum distribution functions.

No effort will be made to illustrate the many successes of DPM in predicting experimental observables. The quoted references include a vast amount of material showing the capabilities of the model when compared with experimental data. Only examples computed with the DPM based model implemented in the FLUKA code have been included.

One of the few models available for high energy interactions [69], which is used in many flavors in HETC88 [45], LAHET [46], HERMES [43], and GEANT, has been developed in the DPM framework, originally for the FLUKA code. FLUKA does now include a much more advanced version, which however is still based on the same physical basis. It includes the leading order contribution (one pomeron exchange) as well as diffraction, and for the hadronization it makes use of an advanced version of the model described in [59], with particular emphasis on a correct description down to the lowest energies (a few GeV in the lab).

As an example of p_T distributions, the experimental data (and the MC simulation) of the p_T spectra of pions produced by 16 GeV/c π^- on Hydrogen

are shown in fig. 6 (experimental data from[54]). The longitudinal distribution of positive particles and negative pions produced by 250 GeV/c π^+ on Hydrogen are shown in fig. 7 (experimental data from[70]). Again the diffractive peak in the positive particle distribution is clearly visible in fig. 7.

5 Nonelastic Nuclear Interactions

Hadronic nuclear interactions are by far the most complex topic of this lecture. A thorough discussion of their characteristics and of the relevant physics is outside the aims of this lecture (and perhaps of the knowledge of the lecturer). The approach followed is just to describe the basic ideas underlying the most successful models used in practice to describe such interactions. In particular the intranuclear cascade model will be described, mainly because it is still the only one able to cover the full energy range of interest for hadron interactions. However plain INC models like those developed in the seventies become unreliable both at the lower (< 100-200 MeV) and higher (> 2-3 GeV) ends of the energy scale, and show limitations (see 3.3 and the examples reported in 7) also when used in the proper energy range.

Once suitable models for describing hadron-nucleon interactions are available, the high energy regime can be properly handled provided the spacetime characteristics of high energy interactions and multiple primary collisions according to the Glauber approach (see after) are taken into account. Models which includes these features are often referred to as *Formation Zone IntraNuclear Cascade* or *Glauber Cascade* approaches (see for example[71,72]).

However important changes to the original INC approach must be done also at the lowest energies, and are mainly related with quantum nuclear effects and multibody interactions, besides the introduction of a preequilibrium stage.

IntraNuclear Cascade approaches which make use both of the high energy and low energy extensions can be called *(Generalized) IntraNuclear Cascade* models, and will be referred as such in the next sections.

Most of the description of the next paragraphs will follow the layout of the (G)INC model implemented in the FLUKA code, whose low-medium energy part (up to few GeV) is called PEANUT (for PreEquilibrium Approach to NUclear Thermalization). A few words about the latter model are given in the following paragraph in order both, to allow the reader to understand how the model is built, and to present a practical example of INC model.

After this brief introduction, a description of the main physical ingredients will be presented; the physical grounds will be discussed in general, giving some details about the actual implementation in PEANUT .

5.1 PEANUT *: Generalities*

Presently, PEANUT handles interactions of nucleons, pions, kaons, γ rays, and stopping negative muons with nuclei from about 2.5 GeV down to reaction threshold (or 20 MeV for neutrons). As concerns photonuclear reactions which will not be discussed in the next paragraphs, details can be found in [73].

The reaction mechanism is modelled in PEANUT by explicit intranuclear cascade smoothly joined to statistical (exciton) preequilibrium emission [4,74]. The full INC treatment stops, and the statistical treatment starts, when all the secondary nucleons have energies smaller than 50 MeV (as calculated in the continuum). To ensure continuity, however, secondary nucleons with 10<E<50 MeV are transported by the INC algorithm till they either escape or reinteract in the nucleus. In the latter case no explicit interaction is performed: only an average Pauli rejection factor [75] is applied and the exciton number is increased, leaving to the preequilibrium stage the further development of the configuration.

In both stages, INC and exciton, the nucleus is modelled as a sphere with density given by a symmetrized Woods-Saxon [76] shape for A>16,

$$\begin{aligned} \rho(r) &= \rho_0 \frac{\sinh(\mathrm{R_0/a})}{\cosh(\mathrm{r/a}) + \cosh(\mathrm{R_0/a})} \\ &\approx \frac{\bar{\rho}_0}{1 + \exp\frac{r - R_0}{a}} \end{aligned} \tag{17}$$

and by a harmonic oscillator shell model for light isotopes (see [77]). It is radially divided in 16 zones of constant density, and its boundary is set at the radius (R_{nuc}) where the density is one hundredth of the central one. Six radial zones are added to allow a suitable description of the nuclear potential ouside the nucleus, and finally 10 extra radial bins are there for charged particles to describe the long range effect of the Coulomb potential. Primary and secondary particles are transported inside these radial zones according to their nuclear mean field and to the Coulomb potential.

Proton and neutron densities are generally different, according again to shell model ones for A<16, and to the droplet model [78,79] for heavier nuclei.

Binding Energies (B_{en}) are obtained from mass tables, depending on particle type and on the actual composite nucleus, which may differ from the initial one in the case of multiple particle emission. Relativistic kinematics is applied, with accurate conservation of energy and momentum, and with inclusion of the recoil energy and momentum of the residual nucleus.

5.2 Nucleon Fermi Motion

Some properties of nuclear matter can be explained in a very simple way by the Fermi gas model (for descriptions of this and other nuclear models see for instance [80,81,82]). Nucleons are described as non-interacting fermions constrained in a cubic box of linear dimension a. The confinement is somehow equivalent to the introduction of an attractive interaction among nucleons that keeps them inside the nucleus. The nucleon wave functions are those of a free-particle with the condition $\Psi(x, y, z) = 0$ at the nuclear boundary, thus with constraints on the three components of the momentum:

$$K_x a = n_x \pi \quad K_y a = n_y \pi \quad K_z a = n_z \pi \tag{18}$$

where the n's are positive integers. Each set of integers defines a solution of the Schrödinger equation with energy given by:

$$E(n_x, n_y, n_z) = \frac{\hbar^2}{2M} |K|^2 \tag{19}$$

$$|K|^2 = (K_x^2 + K_y^2 + K_z^2) \tag{20}$$

Nucleons must obey the Pauli principle, thus for each set of n's, that is for a given momentum state, there can be at most four nucleons, namely two protons and two neutrons, each pair with opposite spin. The ground state of the nucleus will be that with all the lowest-lying states occupied. The number of possible states can be easily calculated in momentum space: from the above quantization it follows that each solution occupies a box in momentum space given by $\left(\frac{\pi}{a}\right)^3$; thus the number of states with momentum comprised between K and $K + dK$ is given by the volume of the spherical shell of radius K and thickness dK divided by the volume occupied by each single solution, and divided again by eight since we consider only positive values of n_x, n_y, n_z:

$$\mathrm{dN} = \frac{|\mathrm{K}|^2}{2\pi^2} \Omega \mathrm{dK}, \quad \Omega = \mathrm{a}^3 \tag{21}$$

re-expressed as a function of energy :

$$\mathrm{dN} = \frac{\Omega \mathrm{m}}{2\pi^2 \hbar^3} \sqrt{2\mathrm{mE}} \mathrm{dE} \tag{22}$$

Integrating eq. 21 up to a given momentum $|K_F|$, one obtains the total number of states with momentum smaller than $|K_F|$:

$$n(K_F) = \frac{4\pi}{3} \frac{K_F^3}{8(\pi/a)^3} \tag{23}$$

These n levels must be occupied by N neutrons and Z protons. If we take N=Z=A/2, and place 4 nucleons on each level, we get:

$$A = \frac{2\Omega}{3\pi^2} K_F^3 \tag{24}$$

it follows that the momentum of the highest occupied state depends only on the nuclear density $\rho = A/\Omega$:

$$\rho = \frac{2}{3\pi^2} K_F^3 \tag{25}$$

From the observed density of nuclei, $\rho = 1.7 \times 10^{38}$ nucleons/cm^3, one obtains

$$K_F = 1.36 \text{ fm}^{-1} \quad \text{E}_\text{F} = 38 \text{ MeV} \tag{26}$$

These are called the *Fermi momentum* and *Fermi Energy*. In nuclei with $N \neq Z$, two different values of the Fermi energy can be defined:

$$\begin{aligned} \rho_n = \frac{N}{A}\rho &= \frac{(K_F^n)^3}{3\pi^2} \\ \rho_p = \frac{Z}{A}\rho &= \frac{(K_F^p)^3}{3\pi^2} \end{aligned} \tag{27}$$

The so defined Fermi energies are obviously kinetic energies, that is energies counted from the bottom of a potential well that in this model must be input from outside. The total depth of the potential should be such to place the so-called Fermi level, i.e. the last occupied level, at a total energy corresponding to the separation energy for the nucleus considered. This gives an average potential depth of about 38+8=46 MeV. The Fermi kinetic energy distribution can be used with success in many applications. The model is also able to predict the order of magnitude of some empirical nuclear parameters, such as surface energy and asymmetry energy.

The model can be extended to account for realistic nuclear density distributions, which are not uniform, but present a zone of gradual decrease called nuclear skin. The Fermi energy of eq. 25 can be made radius-dependent in a straightforward way, through the so called *local density approximation*:

$$\rho(r) = \frac{2}{3\pi^2} K_F^3(r) \tag{28}$$

Since the density distribution is experimentally well determined, this last formulation of the Fermi energy could provide the radial behaviour and value of the nuclear potential. This is of widespread use in intranuclear cascade codes.

Moreover, the same assumption, i.e. nuclear matter as a gas of noninteracting nucleons, linked with thermodynamics, leads to the definition of nuclear temperature and to a general expression for the density of nuclear excited states as a function of excitation energy. An other important quantity that can be calculated in this model is the so-called correlation function, that must be taken into account in intranuclear cascade codes, expecially when dealing with multibody processes. Due to the antisymmetrization of the fermion's wave function, given a nucleon in a position $\vec{r}$ in a nucleus with density ρ_0, the probability of finding another like nucleon in a position $\vec{r}\,'$ is decreased for small values of the distance $r = |\vec{r} - \vec{r}\,'|$ by a factor

$$g(x) = 1 - \frac{1}{2}\left[\frac{3}{x^2}\left(\frac{\sin x}{x} - \cos x\right)\right]^2 \tag{29}$$

where $x = K_F \cdot r$, and the factor $\frac{1}{2}$ in front of the parenthesis accounts for the two possible spin orientations.

5.3 Nuclear Potential

The approximation of independent motion of nucleons inside a common single-particle potential is possible due to the fact that the average inter-nucleon distance is large with respect to the range of the nucleon-nucleon interaction. This is partly ensured by the Pauli principle, and partly by the presence of a repulsive core in the nucleon-nucleon interaction. The single particle potential can be thought as the mean field resulting from all the two-body interactions among nucleons. Many possible shapes of this potential have been proposed, either on the basis of self-consistency (Hartree-Fock like) or of computational usefulness linked with agreement with experimental quantities (harmonic oscillator, Nilsson anharmonic oscillator, Woods-Saxon, all with spin-orbit coupling). These potential are able to reproduce the observed level spacings and ordering, and other nuclear quantities. They are, however, less useful in scattering or reaction processes. In these application, the so called *Optical Potential* is introduced. It is a complex potential that enters in the Schrödinger equation for the projectile. The real part describes the scattering, the complex part describes the absorption: to illustrate this, let us suppose that the optical potential $V(\vec{r}) = -[U(\vec{r}) + \mathrm{iW}(\vec{\mathrm{r}})]$ has the shape of a square well. The wave functions can then be described by plane waves, and the solution of the Schrödinger equation

$$\left\{-\frac{\hbar^2}{2M}\nabla^2 + V - E\right\}\Psi_K = 0 \tag{30}$$

inside the range of the potential will be

$$\begin{aligned} \Psi_{\vec{K}} &= A\mathrm{e}^{\mathrm{i}\vec{\mathrm{K}}\cdot\vec{\mathrm{r}}-\frac{\mathrm{i}}{\hbar}\mathrm{Et}} \\ E &= \frac{\hbar^2 K^2}{2M} - U - \mathrm{iW} \end{aligned} \tag{31}$$

since E is real and equal to the energy before the collision, $\vec{K}$ must be a complex vector, thus if one looks at the dependence of the particle probability density $|\Psi|^2$ as a function of $\vec{r}$, and assuming for simplicity $K \parallel z$, one obtains

$$|\Psi|^2 \propto \mathrm{e}^{-2\mathrm{ImK}\cdot\mathrm{z}} \tag{32}$$

That means that the particle can be absorbed in the nucleus with a mean free path

$$\lambda = \frac{1}{2\mathrm{ImK}}$$

From eq. 31 one has $\mathrm{ImK} = \frac{2\mathrm{M}}{\hbar^2}\frac{\mathrm{W}}{2\mathrm{ReK}}$, and, assuming that the absorptive potential W is small with respect to $E+U$, $\mathrm{ReK} \approx \left[\frac{2\mathrm{M}}{\hbar^2}(\mathrm{E}+\mathrm{U})\right]^{\frac{1}{2}}$, from which

$$\lambda^{-1} \approx 2\frac{W}{\hbar}\left[\frac{M}{2(E+U)}\right]^{\frac{1}{2}} \tag{33}$$

this becomes

$$\lambda^{-1} \approx 2\frac{W}{v\hbar} \tag{34}$$

where v is the particle velocity. The nucleon mean free path in a nucleus should be given, at least in first approximation, by the cross section on a single nucleon multiplied by the nuclear density: $\lambda^{-1} = \rho \cdot \sigma_{NN}$, thus a link between the absorptive nuclear potential and the nucleon nucleon cross section is immediately derived:

$$W = \frac{\hbar}{2} v \rho \sigma_{NN} \tag{35}$$

We shall see in sec. 5.6 that many effects invalidate this simple relation, which however remains a first order estimate.

The optical potential can be derived from the convolution of the interactions between the projectile and all the nucleons in the nucleus, or can be fitted to the scattering data with preliminary assumptions about its radial dependence. The real part of the optical potential is also sometimes used to describe bound states. As life is always complicated, both the optical potential and the self consistent nuclear potential turn out to be energy dependent, but we stop here.

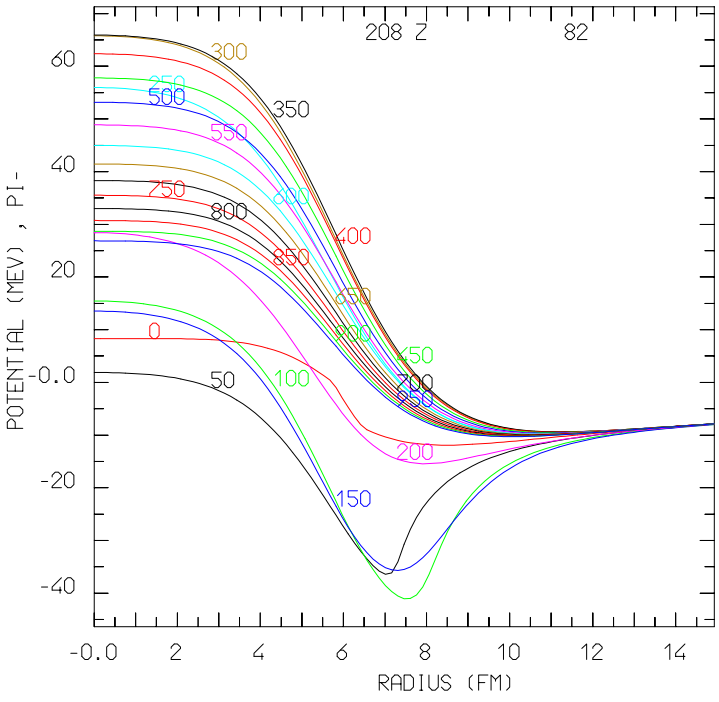

Figure 11: Nuclear potential for π^- in a Pb nucleus as a function of radius. Different curves refer to different pion kinetic energies (MeV). Coulomb potential is included

For pions, a standard nuclear potential exists [83]. It must be written in relativistic form, because the pion mass is small (about 139 MeV) and can be comparable with its kinetic energy. In coordinate space, and in the frame in which the nucleus is at rest, this is written as (the upper and lower signs refer to π^+ and π^-, respectively, while π°s are not sensitive to N-Z asymmetry):

$$2\omega U_{opt}(\omega,r) = -\beta(\omega,r) + \frac{\omega}{2M}\nabla^2\alpha(\omega,r) - \nabla\cdot\frac{\alpha}{1+g\alpha(\omega,r)}\nabla \quad (36)$$

$$\beta = 4\pi\left[\left(1+\frac{\omega}{M}\right)\left(b_0(\omega)\mp b_1(\omega)\frac{N-Z}{A}\right)\rho(r)+\right.$$

$$\left(1+\frac{\omega}{2M}\right)B_0(\omega)\rho^2(r)\Big] \tag{37}$$

$$\alpha = 4\pi\left[\frac{1}{1+\frac{\omega}{M}}\left(c_0(\omega)\mp c_1(\omega)\frac{N-Z}{A}\right)\rho(r)+\right.$$
$$\left.+\frac{1}{1+\frac{\omega}{2M}}C_0(\omega)\rho^2(r)\right] \tag{38}$$

where ω is the first component of the pion 4-momentum, M is the nucleon mass, U_{opt} is the optical potential, $b_0, b_1, c_0, c_1, B_0, C_0$ are complex parameters, g is the Lorentz-Lorenz correction parameter[83] (here and in the following the natural system of units, $\hbar c = 1$, is used). The functional form of this potential derives from that of the pion-nucleon scattering amplitude: b 's are related to s-wave pion-nucleon interaction, while c 's are related to p-wave interaction. The terms in ρ^2 account for two-nucleon mechanisms. This potential contains a divergence operator, thus it is non-local, that means that it depends on the pion velocity besides on position, or, equivalently, the potential in a given position depends on the value of the wave function at different positions. A semiclassical approximation of the particle trajectory is in principle not possible for a non-local potential. However, many localization procedures have been already devised for it[84,86]. We do not go into details, but just give the result to understand its properties :

$$2\omega U_{opt}(\omega, K) = -\beta - K^2\frac{\alpha}{1+g\alpha} + \frac{\omega}{2M}\nabla^2\alpha \tag{39}$$

where K is the pion wave number inside the nucleus and the nuclear density that enters in α and β is the local one. It can be seen that the dependence on momentum is strong. In the literature, the Klein-Gordon equation for the pion in the nuclear optical potential is always written as:

$$\left[(\omega - V_c)^2 - 2\omega U_{opt} - K^2\right]\Psi = m_\pi^2\Psi \tag{40}$$

From eq. 40 applying energy conservation and calling k_0 the linear momentum of the pion outside the potential range, one obtains an equation for K^2:

$$K^2 = k_0^2 + V_c^2 - 2\omega V_c^2 - 2\omega U_{opt}(\omega, K) \tag{41}$$

substituting eq. 39

$$K^2 = \frac{k_0^2 + V_c^2 - 2\omega V_c^2 + \beta - \frac{\omega}{2M}\nabla^2\alpha}{1-\bar{\alpha}} \tag{42}$$
$$\bar{\alpha} = \frac{\alpha}{1+g\alpha}$$

The real part of K^2 gives then the real part of the potential from eq. 41. As pointed out by Johnson and Bethe [87], the denominator of eq. 42 approaches zero for normal nuclear densities. In ref. [87,88] they suggested a correction which takes into account the effects of correlated scattering centers, and reduces the values of the potential as the density increases. The values of the optical potential parameters at low energies (below 50 MeV) are known [83,89] from pionic atoms and scattering data. At higher energies, however, only an extrapolation based on pion-nucleon phase shifts is available [89]. For the dependence of the p-wave parameters on energy a resonant shape can also be assumed, following the theoretical behaviour of the pion-nucleon scattering amplitude, which is dominated by the Δ resonance channel.

The resulting potential has again a resonant shape, with strong dependences on nuclear density. Its depth reaches several tens of MeV, therefore its introduction, although complex, is essential to correctly describe the pion transport and interaction in nuclear matter. An example is shown in fig. 11 for pions in Lead, as a function of pion energy and nuclear radius. In making this plot, a nuclear density of the form of eq. 17 has been used.

5.5 Multibody Absorption of Pions

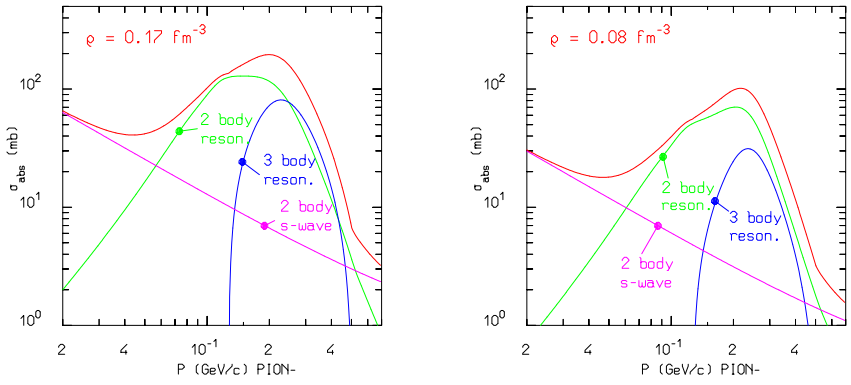

Figure 12: Charged pion absorption cross section for infinite symmetric nuclear matter at two different density values ($\lambda_{abs}^{-1} = \sigma_{abs} \cdot \frac{1}{2}\rho = \sigma_{abs} \cdot \rho_{pro} = \sigma_{abs} \cdot \rho_{neu}$)

Negative pions at rest can be captured on atomic orbits, forming pi-mesic atoms, jump on more internal orbitals with the emission of X-rays and finally be captured by the nucleus. This process is a long-studied one [84], and led to

the construction of very detailed models of low-energy pion-nucleus interactions. But this is not the only possible absorption: the in-flight one exists, and its cross section can amount to about one third of the total pion-nucleus cross section, and about one half of the reaction one. For free pions and nucleons the non-radiative absorption process does not occur since energy and momentum cannot be conserved, and the radiative absorbtion is a very weak process. Conversely, pion absorption in complex nuclei can proceed via multinucleon processes: the basic process is absorption on two nucleons, thus the simplest case to be examined is the absorption on the deuteron. Both total cross sections and angular distribution of emitted nucleons have been extensively measured in the $\pi d \to pp$ reaction, and show again the dominance of the $\Delta(1232)$ resonance[83,85]. At very low energies, the s-wave non-delta interaction is important and the cross section rises as the inverse of the relative velocity. Turning to absorption on an arbitrary pair of nucleons, this dominance of non-resonant s-wave and resonant p-wave absorption is the guide to describe the process. Again, the isospin decomposition turns out to be a very useful tool. The outgoing nucleon pair can have $T = 0$ or 1, thus these are the two isospin channels allowed. The initial state is composed by a pion, and again an isospin $I = 0$ or 1 nucleon pair. If we label the amplitudes as f_{IT}, some passages of momentum combination algebra help to demonstrate that, given a pion with isospin projection λ, and a nucleon pair with isospin projection i,

$$\sigma(\lambda, t) \propto \sum_{IT} |(Ii1\lambda|Tt)|^2 \cdot |f_{IT}|^2 \ , \quad t = i + \lambda \tag{43}$$

If, now, we consider the intermediate state, in order to extract the Δ contribution, we can use the Racah coefficients to recouple the isospin and explicitate the pion-nucleon intermediate state, always in a definite total T state . In this case the amplitudes will be denoted by $g_{\frac{3}{2},T}$ and $g_{\frac{1}{2},T}$, and the link between the f and the g is given by

$$\begin{aligned} f_{01} &= \frac{1}{\sqrt{3}} \left(\sqrt{2} g_{\frac{3}{2},1} + g_{\frac{1}{2},1} \right) \\ f_{11} &= \frac{1}{\sqrt{3}} \left(-g_{\frac{3}{2},1} + \sqrt{2} g_{\frac{1}{2},1} \right) \\ f_{10} &= g_{\frac{1}{2},0} \end{aligned} \tag{44}$$

If we assume Δ dominance, and put $g_{\frac{1}{2},T}$=0, from eqs. 44 and 43 we obtain that for charged pions the absorption cross section on a (p,n) pair is five times that on a (p,p) (or (n,n)) pair. Moreover, the isospin 0 channel has no contribution from the Δ resonance.

The formal treatment of this process inside a real nucleus is quite complex, because the pion can interact with other nucleons before being absorbed, it acquires a potential energy due to its average interaction with nucleons and to the Coulomb field, and the Δ properties, in particular the partial widths, are modified by nuclear matter. Inside nuclear matter, the Δ can either decay, resulting in elastic scattering or charge exchange, or interact with other nucleons, resulting in pion absorption: its width is broadened with respect to the free one [5,6,7,90]. Modern calculations [6] take these effects into account by calculating energy and nuclear density dependent partial widths for the Δ decay:

$$\frac{1}{2}\Gamma_T = \frac{1}{2}\Gamma_F - \mathrm{Im}\Sigma_\Delta \tag{45}$$

$\Sigma_\Delta = \Sigma_Q + \Sigma_2 + \Sigma_3$, where Σ_Q, Σ_2 and Σ_3 are the partial widths for quasielastic scattering, two body and three body absorption. The nuclear density dependence of two and three body absorption turns out to be of the type ρ^β and ρ^γ, respectively with $\beta < 2$ and $\gamma < 3$, thus different from the simple ρ^2 (ρ^3) dependence one expects for a two-body (three-body) process. In this way pion scattering, charge exchange, two-body and even three-body absorption can be treated in a consistent way as two-step processes, the first one being the excitation of a Δ from a pion-nucleon interaction, the second being the propagation and rescattering or decay of the resonance in the nucleus. The inclusion of this process in an INC code allows to keep into account processes that are called FSI (final state interaction) and ISI (initial state interaction), that are absorption preceeded (or followed) by scattering of the projectile or of the secondaries, and the effect of the Coulomb field. These processes represent a significant complication when theoretical calculations of absorption are compared to experimental data in medium-heavy nuclei.

In addition, a two-body s-wave absorption cross section can be derived from the optical model [83] as

$$\sigma_s^A(\omega) = \frac{4\pi}{p}(1 + \frac{\omega}{2m})\mathrm{ImB_0}(\omega)\rho \tag{46}$$

where ω is the pion energy in the lab frame and B_0 is a parameter of the pion optical potential.

As a result, the absorption cross section on nuclei still resembles in shape that on the deuteron, with a resonance-like behaviour, but the resonance is smoothed, and an enhancement of the π^- cross section with respect to the π^+ one arises, both due to the Coulomb field and to the neutron excess in heavy nuclei. The absorption cross section, both 2 and 3 body resonant, and 2 body non resonant, is shown in fig. 12, for two different values of the nuclear density.

The figure is based on the approach outlined in[27]. The values must be taken as indicative, mainly because no difference between neutron and proton densities has been included.

5.6 Hadron Mean Free Paths in the Nucleus and Pauli Blocking

As already mentioned, the plain use of hadron nucleon-nucleon cross sections leads to values of the mean free path of hadrons which are by far too short with respect to reality. There are many effects that influence the in-medium cross sections. The first, and better known, effect, is *Pauli blocking*. Any secondary nucleon created in an intranuclear interaction must obey the Pauli exclusion principle, thus it must have enough energy to jump from the Fermi sea where it lies before the interaction to an unoccupied state, above the Fermi level. As a result, interactions with small momentum transfer are partially inhibited. Here two points must be mentioned: the former is that the kinetic energy of the projectile inside the nucleus is different with respect to the free one because of the presence of the nuclear potential. The latter is that the target nucleons possess themselves a kinetic energy, distributed accordingly to the Fermi distribution 22. The interaction kinematics must be applied in the correct frame, that of the projectile-target nucleon center of mass, to get the correct cross section and outgoing particle distribution.

Analytical calculations for the combined effect of Fermi motion and Pauli blocking on the in-nucleus nucleon-nucleon cross section can be performed under a few approximations, such as isotropy of the angular distribution and either independence on or inverse proportionality to energy of the cross section[75]. The reduction of the cross section with respect to the free one depends on the projectile energy and on the Fermi energy. For instance taking $E_F = 40$ MeV, the reduction factor is ≈ 0.3 at 20 MeV incident Energy (measured outside the nucleus) and ≈ 0.6 at 100 MeV. Even with these corrections, the mean free path of a 60 MeV nucleon results as small as 2 fm.

In a MonteCarlo cascade code, the aforementioned approximations can be avoided, by explicitly checking after each interaction that the momenta of all secondary nucleons are above the Fermi level. Pauli blocking is of course effective also in pion-nucleus interactions, both scattering and absorption.

Mechanisms other than Pauli blocking are effective in increasing the particle mean free path in nuclear medium. These mechanisms are important to prevent the well known problems[91] met by INC codes which includes refraction and reflection because of strong secondary absorption in the nucleus core, and to match at low energies the mean free paths obtained from optical model analysis.

- The formation zone [92] concept after pion or nucleon inelastic (pion production) interactions
- Nucleon antisymmetrization effects [82], which decrease the probability for secondary particles to reinteract on a nucleon of the same type very close to the production point (see eq. 29)
- Nucleon-nucleon hard-core correlations (see for example [93]) which also prevent secondary particles to collide again too close to the production point. Typical hard-core radii used are in the range 0.5-1 fm
- "Coherence" length after elastic or charge exchange hadron-nucleon scatterings. In analogy with the formation zone concept, such interactions cannot be localized better than the position uncertainty connected with the four-momentum transfer of the collision. Reinteractions occurring at distances shorter than the coherence length would undergo interference and cannot be treated anyway as independent interactions on other nucleons. It must be stressed that this mechanism is rather selective on the outgoing direction. Forward scattered particles are preferably emitted as well as backward scattered ones if the colliding particles are identical, pp or nn for example.

5.7 Preequilibrium Emission

The intranuclear cascade model is the most straightforward approach when writing a MonteCarlo code, and has been successfully used for decades in the intermediate energy region. However, its physical foundation becomes approximate at low energies as seen in the previous sections, resulting in a decrease of its accuracy. Moreover, it can be very time consuming, since many particles must be followed down to very low energies.

On the other hand, a description based simply on direct reaction plus compound nucleus evaporation is surely not sufficient. Already in 1966 Griffin [74] described the spectra following nucleon-induced reactions in terms of a *preequilibrium* model, that is, a transition between the first step of the reaction and the final thermalization.

Since then, many models have been developed (see [4] for an exhaustive review). The two leading approaches (with many different implementations) are the quantum-mechanical multistep model [94], which has a very good theoretical background, but is complex and poses some difficulties to the description of multiple nucleon emission, and the exciton model [4,74,95], which relies on statistical assumptions. This makes it very simple and fast, but of course leads to some limitations, especially for medium-high energy projectiles.

The approach described here is that adopted in PEANUT and used for the examples reported at the end of this lecture. Before describing the actual preequilibrium model, it is important to discuss how the transition from the INC part to the preequilibrium stage occurs.

The INC step goes on until all nucleons are below 50 MeV (with the further specifications discussed before) *and* all particles but nucleons (typically pions) have been emitted or absorbed. At the end of the INC stage a few particles may have been emitted and the nuclear configuration is characterized by the total number of protons, Z^0_{pre}, and neutrons, N^0_{pre}, by the number of particle-like excitons (nucleons excited above the Fermi level), n_p ($n_p = n_{pro} + n_{neu}$), and of hole-like excitons (holes created in the Fermi sea by the INC interactions), n_h, by the "compound" nucleus excitation energy (actually the nucleus is not yet at all in a equilibrated state and the term "compound" is somewhat incorrect), E ($E = \sqrt{s} - M_{N^0,Z^0}$, where $\sqrt{s}$ is the center of mass energy of the system), and by the "compound" nucleus momentum components, $p_{i\ comp}$. All the above quantities can be derived by proper counting what occurred during the INC stage and they represent the input configuration for the preequilibrium stage.

It must be stressed that in our approach the typical problems of INC codes with binding energies and reaction Qs are completely solved, thanks to the use of the "running" binding energy, which evolves with the reaction evolution and accounts at every emission stage for the proper Q.

The exciton formalism employed in PEANUT follows that of M. Blann and coworkers[96,97,98,99], called Geometry Dependent Hybrid Model (GDH). Indeed there are a few modifications, regarding mainly the way the nuclear geometry is accounted for, inverse cross sections, and exciton reinteraction rates.

The preequilibrium process in the exciton model is described as a chain of steps, each step corresponding to a certain number of "excitons", where an exciton can be either a particle above the Fermi surface or a hole below the Fermi surface. The statistical assumption underlying the exciton model states that any partition of the excitation energy E among n, $n = n_h + n_p$, excitons has the same probability to occur. The nucleus proceeds in the chain through nucleon-nucleon collisions which increase the exciton number by two units, thus assuming that the probability of having an interaction that decreases the exciton number or lets it unchanged can be neglected (the so called "never come back" approximation). The chain stops, and equilibrium is reached, when either the exciton number n is sufficiently high ($n = \sqrt{2gE}$), where g is the single particle level density, or the excitation energy is below any emission threshold.

The initial number of excitons depends on the reaction type and on the cascade history.

At each step there is a definite probability $P_{x,n}(\epsilon)$ of emitting a nucleon of type x and energy ϵ in the continuum. This probability can be factorized in two parts, one giving the fraction of n-exciton states in which one exciton is unbound and has energy ϵ in the continuum, the other giving the probability for the exciton to escape from the nucleus during its mean lifetime[96]:

$$P_{x,n}(\epsilon)\mathrm{d}\epsilon = \frac{\rho_{\mathrm{n}}(\mathrm{U},\epsilon)\mathrm{g}\mathrm{d}\epsilon}{\rho_{\mathrm{n}}(\mathrm{E})}\frac{\mathrm{r_c}(\epsilon)}{\mathrm{r_c}(\epsilon)+\mathrm{r_+}(\epsilon)} \tag{47}$$

where n_{p_x} is the number of particle-like excitons which are of type x, g is the single-particle state density, U is the residual nucleus excitation energy ($U = E - \epsilon - B_{en}$), $\rho_n(E)$ is the density (MeV^{-1}) of exciton states, and is given by:

$$\rho_n(E) = \frac{g(gE)^{n-1}}{n!(n-1)!} \tag{48}$$

$r_c(\epsilon)$ is the rate of emission in the continuum, and is related to the cross section of the inverse process (σ_{inv}) by the detailed balance principle (see par.5.8),

$$r_c = \sigma_{inv}\frac{\epsilon}{g_x}\frac{(2s+1)\,8\pi m}{h^3} \tag{49}$$

and $r_+(\epsilon)$ is the exciton reinteraction rate. The $r_+(\epsilon)$ can be calculated from the nucleon mean free path in nuclear matter[75] ($V = E_F + B_{en}$, f_{Pauli} is the Pauli blocking suppression factor, see[75] for explicit expressions),

$$r_+^{NN} = f_{Pauli}(\epsilon, E_F)\left[\rho_{pro}\sigma_{xp} + \rho_{neu}\sigma_{xn}\right]\left[\frac{2(\epsilon+V)}{m}\right]^{1/2} \tag{50}$$

or from the optical model (W is the imaginary part of the optical potential).

$$r_+^W = \frac{2W}{\hbar} \tag{51}$$

The value of the single particle density is often taken as g=Z/14 (N/14) MeV^{-1} for protons(neutrons), although it could be a complex function of energy[100].

This formulation has been refined in the GDH[97] to account for the experimentally established importance of peripheral collisions. This has been accomplished through two mechanisms, both applied to the first step of the exciton chain. As first, all position dependent parameters (density, Fermi energy, imaginary part of the optical potential etc) entering the quantities in

eq. 47, 49,50(51) are no longer constant, but depend on the impact parameter and are chosen according to an average carried out along a straight line crossing the nucleus at constant impact parameter. The relative importance of different impact parameters is then established through the use of transmission coefficients obtained from optical models.

Secondly, the exciton state density is modified from eq. 48 by the assumption that any hole-like exciton cannot carry an excitation energy larger than the (local→ impact parameter averaged) Fermi energy. Explicit formulae for the constrained exciton state densities can be found in [99]. Both mechanisms contribute to the enhancement of the hardest part of the emitted particle spectra.

Our approach is similar but with a few differences. First of all geometry dependent quantities are no longer averaged as a function of the impact parameter, but real point like values are used, since the position of the first interaction is known from INC part where anyway the projectile is tracked into the nucleus until the first interaction occurs (remember that the interaction can or can be not modelled through the INC stage depending on the projectile energy, but tracking is always performed). Therefore when entering the preequilibrium stage PEANUT knows the actual values of the nuclear density and of the (local) Fermi energy corresponding to the hole(s) generated in the INC step at positions $\vec{x}_i$. At the first step only one hole has been created and therefore the local nuclear density and Fermi energy are those corresponding to the interaction position. However, since the preequilibrium stage follows the intranuclear cascade step, at sufficiently high energy it can be reached when already two or more holes have been created. In this a proper average must be taken. In general for n_h holes already present when reaching the preequilibrium stage:

$$\rho^{loc}_{n_h} = \frac{\sum_{i=1}^{n_h} \rho(\vec{x}_i)}{n_h} \tag{52}$$

$$E^{loc}_{F\,n_h} = \frac{\sum_{i=1}^{n_h} E_F(\vec{x}_i)}{n_h} \tag{53}$$

The local Fermi energy defined in eq. 53 is then used when computing the exciton state densities for constrained exciton states, since these are truly local quantities. Constrained exciton state densities are in fact used in PEANUT for the configurations 1p-1h, 2p-1h, 1p-2h, 2p-2h, 3p-1h and 3p-2h, which cover most of the emission spectra.

However the Fermi energy and the nuclear density enter also the definition of r_+ if the nucleon-nucleon cross section approach is used (and it is used in PEANUT). For such purpose the use of point values would not be correct, since

a possible subsequent reinteraction will take place at some distance. Therefore the following quantities are introduced and used when computing reinteraction rates as representative of the nuclear matter in the neighborhood of the point where the nucleon originated,

$$\rho^{nei}_{n_h} = \frac{n_h \rho^{loc}_{n_h} + \rho^{ave}}{n_h + 1} \tag{54}$$

$$E^{nei}_{F\ n_h} = \frac{n_h E^{loc}_{F\ n_h} + E^{ave}_F}{n_h + 1} \tag{55}$$

where ρ^{ave} and E^{ave}_F are the nuclear density and the Fermi energy respectively averaged over the whole nucleus. At each step of the preequilibrium stage the exciton number is increased and $n_h \rightarrow n_h + 1$, and of course the position of the last interaction is not known. Our prescription is to use for the new local values

$$\rho^{loc}_{n_h+1} = \rho^{nei}_{n_h} \tag{56}$$

$$E^{loc}_{F\ n_h+1} = E^{nei}_{F\ n_h} \tag{57}$$

which implicitly assumes that the density and the Fermi energy of the last generated hole are given by ρ^{ave} and E^{ave}_F respectively. It is clear that as soon as the number of steps becomes large all quantities naturally converge to the nucleus averaged values. Summarizing our treatment of geometry dependent effects is much more "local" for the first interaction(s), where not only impact parameters but complete positions are explicitly selected and taken into account, and becomes less and less local, in contrast with the original GDH approach as soon as the number of interactions increases, according to a description where larger and larger volumes of the nucleus are involved in the reaction.

For the exciton reinteraction rate nucleon-nucleon cross sections corrected[75] for Fermi motion and Pauli principle, have been used. Further corrections connected to nucleon correlations and to coherence considerations after scattering events have been introduced when computing the reinteraction rate, for consistency with what is done in the INC part. These corrections proved to be very useful and prevented the need for arbitrary reduction factors of the nucleon-nucleon cross sections, which were often required in similar models to match the experimental data.

In our approach an energy dependent form for g is usually assumed, which follows the main features described in [100] for simple cases.

In the exciton model the angular dependence has to be somehow added, since it is not intrinsic in the formulation. Many different approaches have been

recently developed, most of which rely on the fast particle approximation. A non-isotropic angular distribution has been implemented in PEANUT , following the fast particle approximation[101], as implemented by Akkermans *et al.*[102]. In this model the angular orientation of the nucleus at each step is defined by the direction of the fast particle, which changes gradually in a series of two-body collisions. The transition rate between different exciton states is supposed to be factorizable in an energy-dependent and an angle-dependent factor. The same factorization holds then for the resulting emission probability :

$$\frac{\mathrm{dP_{x,n,\theta}}(\epsilon)\mathrm{d}\epsilon}{\mathrm{d}\Omega} = P_{x,n}(\epsilon)\mathrm{d}\epsilon \cdot \sum_{\mathrm{l}} \mathrm{a_l^m P_l}(\cos(\theta)) \tag{58}$$

where $P_{x,n}(\epsilon)d\epsilon$ is the angle-integrated emission probability from an n-exciton state as given by GDH, the a_l^m are coefficients that depend on the number of steps m in the exciton chain and θ in the original formulation is the polar angle with respect to the direction of the projectile. Besides the fast particle one, other approximations are introduced in the calculations leading to eq. 58: in the binary collisions the Fermi motion of target nucleons and the Pauli exclusion principle are neglected, as are reflection/refractions at the nuclear boundary.

Since in PEANUT the exciton stage may be reached after one or more cascade steps, possibly with particle emission, care must be taken in defining the initial step number and the reference direction. The adopted choice has been to define the reference axis as that of the residual momentum of the system at the step under consideration (it coincides with that of the projectile if no particles have been yet emitted). If this total momentum is comparable with the average Fermi momentum, the angular distribution is assumed to be isotropic. As for the step number m, it is taken equal to the number of holes below the Fermi level.

For projectile energies below 30 MeV, where only tracking up to the first interaction is performed in the INC stage, the preequilibrium model must provides also the angular distribution for nucleons scattered only once. The adopted approach is to consider an angular distribution kernel obtained assuming isotropic nucleon-nucleon scattering and folding with the Fermi motion of the target nucleon and with (average) refraction and reflection effects in the entrance and exit channels. Such a kernel is properly correlated with the selected nucelon emission energy.

At the end of the preequilibrium stage, a true compound nucleus is left with Z_{res} and N_{res}, moving with $\vec{p}_{res}$, and with excitation energy U. The Evaporation/fission/fragmentation stage is then performed starting from this configuration.

5.8 Evaporation/Fragmentation

At the end of the exciton chain, or of the INC part whenever no preequilibrium stage is included in the calculation, the residual nucleus is supposed to be left in an equilibrium state, in which the excitation energy U is shared by a large number of nucleons. Such equilibrated compound nucleus is supposed to be characterized by its mass, charge and excitation energy with no further memory of the steps which led to its formation. The excitation energy can be higher than the separation energy, thus nucleons and light fragments (α, d, ^{3}H, ^{3}He) can still be emitted: they constitute the low-energy (and most abundant) part of the emitted particles in the rest system of the residual nucleus, having an average energy of few MeV. The emission process can be well described as an evaporation from a hot system. The treatment starts from the formula of Weisskopf [103], that is an application of the detailed balance principle, linking the probabilities $P_{i\to f}$ to go from a condition i to a condition f and viceversa through the density ρ of states in the two systems:

$$P_{i\to f}\rho(i) = P_{f\to i}\rho(f) \tag{59}$$

$P_{f\to i}$ is the probability per unit time of capturing a particle and form a composite nucleus, and is given by the product of the compound nucleus cross section σ_{inv} times the particle flux. Restricting to a volume Ω, the particle flux is $\frac{v}{\Omega}$, and

$$P_{f\to i} = \sigma_{inv}\frac{v}{\Omega}$$

Thus the evaporation probability for a particle of type j , mass m_j, spin $S_j \cdot \hbar$ and kinetic energy E is given by

$$P_j(E)\mathrm{dE} = \frac{(2\mathrm{S_j}+1)\mathrm{m_j}}{\pi^2\hbar^3}\sigma_{\mathrm{inv}}\frac{\rho_{\mathrm{f}}(\mathrm{U_f})}{\rho_{\mathrm{i}}(\mathrm{U_i})}\mathrm{EdE} \tag{60}$$

where ρ's are the nuclear level densities ($\rho_f(U_f)$ for the final nucleus, $\rho_i(U_i)$ for the initial one), $U_i \equiv U$ is the excitation energy of the evaporating nucleus, $U_f = U - E - Q_j$ that of the final one, Q_j is the reaction Q for emitting a particle of type j from the original compound nucleus, and σ_{inv} is the cross section for the inverse process. The non-relativistic phase space density for a free particle of spin S in a volume Ω has been used (eq. 22 with a spin term) and entered in the final state density.

Eq. (60) must be implemented with a suitable form for the nuclear level density and the inverse cross sections. Many recipes have been suggested for both. In the original work of Dostrovsky [106], where the evaporation process has been translated into a MonteCarlo code for the first time,

$\rho(U) \approx C \exp(2\sqrt{aU})$, with $a = A/8$ MeV^{-1} has been used for the level density dependence on the excitation energy U, an expression inspired to the Fermi gas one. This has led to a simple form for the evaporation probability:

$$P_j(E)\mathrm{dE} = \frac{(2\mathrm{S_j}+1)\mathrm{m_j}}{\pi^2\hbar^3}\sigma_{\mathrm{inv}}\frac{\mathrm{e}^{2\sqrt{\mathrm{a(U-E-Q_j)}}}}{\mathrm{e}^{2\sqrt{\mathrm{aU}}}}\mathrm{EdE}. \tag{61}$$

In the same work, the inverse cross sections have been parametrized in a very simple way, so that expression (61) can be analytically integrated and used for MC sampling. The same formulation is used in the examples reported in this work, with, however, a different choice of a, taking into account that the Fermi expression for the nuclear density must be refined, essentially allowing the value of a to depend both on nuclear species and on excitation energy (see below). As a first step the so-called backshifted level density should be used, where $\rho(U) = C\mathrm{e}^{2\sqrt{\mathrm{aU}}}$ is substituted by $\rho(U) = C\mathrm{e}^{2\sqrt{\mathrm{a(U-\Delta)}}}$, Δ being the pairing gap in the nucleus considered.

To get a first idea of the spectrum of emitted nucleons, one can isolate the dominant dependence on the outgoing particle energy, in the case of neutrons, where one can assume an almost constant σ_{inv}:

$$\begin{aligned} P_j(E)\mathrm{dE} &\propto E\frac{\mathrm{e}^{2\sqrt{\mathrm{a(U-E-Q_j)}}}}{\mathrm{e}^{2\sqrt{\mathrm{aU}}}}\mathrm{dE} \\ &\approx E\frac{\mathrm{e}^{2\sqrt{\mathrm{aU}}\left(1-\frac{1}{2}\frac{\mathrm{E+Q_j}}{\mathrm{U}}\right)}}{\mathrm{e}^{2\sqrt{\mathrm{aU}}}}\mathrm{dE} \\ &\approx E\mathrm{e}^{-\frac{\mathrm{E}}{\mathrm{T}}}\mathrm{dE} \end{aligned} \tag{62}$$

from which the evaporative Maxwellian shape of the spectrum is evident, once the nuclear temperature $T \approx \sqrt{\frac{U}{a}}$ is introduced (this definition of nuclear temperature follows from the thermodynamical definition $T = [\mathrm{d}(\ln\rho(\mathrm{U}))/\mathrm{dU}]^{-1}$). Taking for instance U=20 MeV in an A=80 nucleus ($a = 10$), the emitted neutron spectrum is peaked at about 2.8 MeV, that is quite a low energy. The emission of protons is reduced and the spectrum is shifted toward higher energies due to the Coulomb barrier.

The total width for neutron emission can be found by integrating Eq. (60) between zero and the maximum possible ejectile energy $(U - Q_j)$

$$\Gamma_j = \frac{(2S_j+1)m_j}{\pi^2\hbar^2}\int_0^{(U-Q_j)}\sigma_{\mathrm{inv}}(E)\frac{\rho_f}{\rho_i}E\mathrm{dE} \tag{63}$$

The same applies to charged particles, where the integration actually goes from some effective Coulomb barrier where $\sigma_{\rm inv}$ drops to zero, up to the maximum energy.

The evaporative process is in competition with another equilibrium process, that is fission [110]. A fraction of the excitation energy may be spent to induce a collective deformation. As the nucleus shape departs from sphericity the surface energy increases but the Coulomb energy decreases. The potential energy reaches a maximum at a deformation stage that is called "saddle point". The height of the potential energy over the ground state is the fission barrier B_f. Once a nucleus reaches the saddle point, the fission occurs, and the nucleus separates, most of the times into two heavy fragments. The height of the fission barrier can be in first order calculated with the liquid drop model, although shell effects have to be incorporated. For the fission probability, a statistical method can be used [103,111]: it will be equal to the probability of reaching the saddle point, because this is a no-way-back point. Given the excitation energy U, this will be divided between a relative kinetic energy of the two fragments E and a residual excitation. All the procedure is like the one for evaporation, where now the spectrum is that of the kinetic energy at the saddle point, the $P_{f\to i}$ is simply one times the flux of "ingoing" fragments, but the system is confined to one dimension because of the path to saddle point. The total fission width can be expressed as:

$$\Gamma_F = \frac{1}{2\pi}\frac{1}{\rho_i(U)}\int_0^{(U-B_F)} \rho_F(U-B_F-E)\mathrm{dE} \qquad (64)$$

where B_F is the fission barrier, and $\rho_F(U_F) \approx C\exp(2\sqrt{a_F U_F})$, the level density of the fissioning nucleus at the saddle point, where the excitation energy U_F is given by the initial one minus the fission barrier. Fission barriers vary roughly with the fissility parameter $\frac{Z^2}{A}$: measured values range from about 25-30 MeV at $\frac{Z^2}{A}\approx 30$ to 6 MeV for $\frac{Z^2}{A} > 34$. Fission for nuclei with $Z < 70$ can be neglected in most practical calculations. In other nuclei, the fission width has to be compared with the evaporation widths to determine the relative importance of the two processes. The level density at the saddle point ρ_F is different from that of the nucleus in its ground state. From comparison to experimental data, it turns out that a_F is greater than the a used for evaporation of about 10% at low excitation energies, and the two a's become equal at large excitation energies. Moreover, $\tilde{a} = a/A$, and $\tilde{a}_F = a_F/A$, are found to be all but constant parameters: they possess a dependence on A and Z, due to shell and deformation effects, and a dependence on excitation energy. Both effects have been experimentally observed, and have been subject of many phenomenological and theoretical investigations (see [100,104,105,107,108,109]).

After scission, the fragments acquire kinetic energy from the Coulomb repulsion between them. Their mass distribution depends on Z and on the excitation energy of the fissioning nucleus: for low Z fissioning system the mass distribution is centered around the half mass, while for high Z nuclei, the mass distribution has a symmetric component and an asymmetric one in which one of the fragment has always a mass around 140. The relative importance of the symmetric component grows with growing excitation energy.

In the examples presented in the following paragraphs and obtained with the FLUKA code, the prescriptions of Atchison [112] have been used to calculate the quantities entering in Eq. (64), except, again, for the level density parameter a_F, and for the omission of the "ad hoc" reduction factor for the fission width.

In both $\rho_F(U)$ and $\rho(U)$ the so-called backshifted level density have been used, using $U - \Delta$ rather than U, where Δ is the pairing energy. For a, a_F, the N and Z dependence of ref. [109] has been used, and complemented with the energy dependence prescription of Ignatyuk [107,108].

$$\begin{aligned} a &= A \cdot [\bar{a} \cdot f(U) + \tilde{a} \cdot (1 - f(U))] \\ \bar{a} &= a_0 + 9.17 \times 10^{-3} \cdot [S_{\mathrm{Z}}(Z) + S_{\mathrm{N}}(N)] \\ \tilde{a} &= 0.154 - 6.3 \times 10^{-5} \cdot A \\ f(U) &= \frac{1 - \mathrm{e}^{-0.054 \cdot (\mathrm{U} - \Delta)}}{0.054 \cdot (U - \Delta)} \end{aligned} \tag{65}$$

where according to [109], a_0 is given by 0.142 and 0.12 MeV^{-1} for undeformed and deformed nuclei respectively, and $S_{\mathrm{Z}}(Z)$ and $S_{\mathrm{N}}(N)$ are the shell correction terms for protons and neutrons. The unit of energy used throughout eq. 65 are MeV.

We use $a_F \approx 1.08a$, with a smooth A dependence. After fission occurs, the two fragments are treated like independent residual nuclei with their own excitation and can possibly emit further particles.

For light nuclei, the statistical assumptions and the sequential emission scheme underlying the classical evaporation models become less and less sound, because:

- Already moderate excitation energies can represent a substantial fraction of the (total) binding energy of such nuclei.
- The level structure of such nuclei is usually highly specific and anyway level spacings can be comparable with the excitation energy.
- The "evaporation" of light fragments other than p or n becomes meaningless, since the mass of the "evaporated" fragment can be comparable

or even larger than the mass of the residual nucleus.

Therefore other deexcitation mechanisms are more suitable for these light (typically A$\leq$16) residual nuclei. A possible choice (adopted for all presented examples) for this calculations is the so called Fermi Break-up model [113,114], where the excited nucleus is supposed to disassemble just in one step into two or more fragments, with branching given by plain phase space considerations. In particular, the probability for disassembling a nucleus of N neutrons, Z protons, and U excitation energy (total mass $M^* = U + M_{A,Z}$) into n fragments ($n \geq 2$) of the same total charge and baryon number, is given by:

$$W = \frac{g}{G}\left[\frac{V_{\rm br}}{(2\pi\hbar)^3}\right]^{n-1}\left(\frac{1}{M^*}\prod_{i=1}^{n} m_i\right)^{3/2}\frac{(2\pi)^{3(n-1)/2}}{\Gamma(\frac{3}{2}(n-1))}E_{\rm kin}^{3n/2-5/2} \tag{66}$$

where the spin factor g, and the permutation factor G are given by (n_j is the number of identical particles of jth kind)

$$g = \prod_{i=1}^{n}(2S_i+1), \qquad G = \prod_{j=1}^{k} n_j! \tag{67}$$

and $E_{\rm kin}$ is the total kinetic energy of all fragments at the moment of break-up. $V_{\rm br}$ is a volume of the order of the initial residual nucleus volume. Therefore, the final state can be conveniently selected by means of a MC procedure, by evaluating such an expression for all possible combinations of fragments energetically allowed and making a random selection.

In the examples reported in this paper, all combinations formed by ≤ 6 fragments have been considered, unless the residual "nucleus" is composed by A like particles (p or n), in which case it is disintegrated into A fragments according to phase space. All particle stable states with $A \leq 16$ have been included, plus the particle unstable levels with sizeable γ decay branching ratios. Also a few known particle unstable isotopes, like ^{8}Be, have been included and, if produced, are let to decay according to the experimental branching. Once the final state configuration has been selected, the kinematical quantities of each fragment are chosen according to n-body phase space distribution. Such a selection must be performed having care to subtract from the available energy the Coulomb repulsion of all charged particles: the Coulomb energy is then added back to the charged particles alone, to simulate properly the effect of the Coulomb repulsion. In practice $E_{\rm kin}$ at disassembling will be given by:

$$E_{\rm kin} = U - \left(\sum_{i=1}^{n} m_i c^2 - M_{A,Z}c^2\right) - B_{\rm Coul} \tag{68}$$

where it must be recalled that the emitted fragments can be in an excited state. The total Coulomb barrier $B_{\rm Coul}$ of the selected configuration is distributed to charged particles after disassembling, in their own c.m. system.

According to the picture of the compound nucleus like an equilibrated system determined only by its mass, charge and excitation energy, with no memory of previous steps of the interaction, Fermi Break-up is activated in the model every time the current compound nucleus has mass number $A \leq 17$, including possible light fission fragments.

A similar process occurs also in medium-heavy nuclei, although it becomes important only at multi-GeV proton induced reactions or in heavy ion induced reactions. This is called *nuclear fragmentation* and is characterized by the emission of low energy complex fragments with $A \geq 5$ from a thermalized nucleus. Reviews of this topic can be found in [117,120,118]. Fragmentation is expected to occur when the excitation energy per nucleon exceeds about 3 MeV [115], that in A=100 mass nucleus correspond to 300 MeV of excitation energy *after* all direct and preequilibrium emissions. As an example, the cross sections for emitting Sodium or Magnesium isotopes in proton induced reaction on gold are or the order of 0.03 mb at 0.5 GeV, 0.5 mb at 1 GeV and saturate at values between 3 and 10 mb for incident energies larger than 10 GeV. This is not a process that will influence the development of a shower or the average energy deposition, but it is the only one that can produce residual nuclei very far both from the target mass and from the fission product distribution, thus it must be taken into account for a detailed analysis of residual nuclei.

Theoretical descriptions of fragmentation model it as a two-stage process, the first being the production of a sufficiently hot compound nucleus, the second being the fragmentation itself. For the first stage, both intranuclear cascade [119,115], and Fluidodynamical [116] models have been employed. The second stage can be described in terms of statistical methods or in terms of the fluctuations of the nuclear mean field. The statistical approach of [115] and that of [121] are among the few examples of implementation in a MonteCarlo code.

5.9 Residual Nucleus Deexcitation

The evaporation process continues till it is energetically possible, and leaves generally the residual nucleus in an excited state. The residual excitation energy is then dissipated by emission of γ rays. Actually γ emission occurs even during evaporation, as a competing process, but with a small branching ratio.

The evaporation stage ends when the nuclear excitation energy becomes

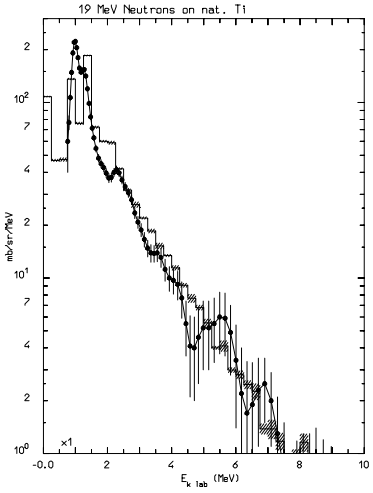

Figure 13: Photon spectrum following the reaction Ti(n,x) at 19 MeV. The dashed histogram represents MonteCarlo results with errors. Dots are experimental data from [128]

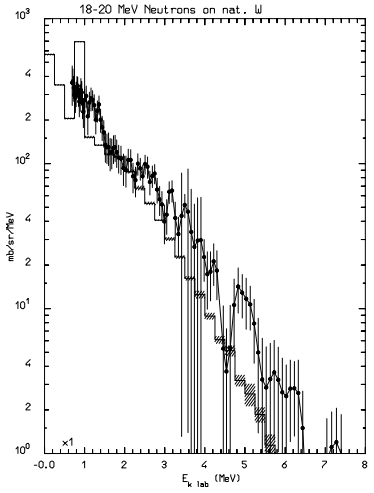

Figure 14: as in fig.13 for Tungsten. Experimental points are from [129]

lower than all separation energies for nucleons and fragments. This residual excitation energy is then dissipated through emission of photons. In reality, gamma emission occurs even during the preequilibrium and evaporation stages, in competition with particle emission, but its relative probability is low, and it can safely neglected in most practical applications.

Gamma deexcitation proceeds through a cascade of consecutive photon emissions, until the ground state is reached. The cascade is assumed to be statistical as long as the excitation energy is high enough to allow the definition of a continuous nuclear level density. Below a (somewhat arbitrary) threshold, set at the pairing gap value in the presented examples, the cascade goes through transitions between discrete levels.

The statistical model formulation for the gamma ray emission probability is again similar to those for evaporation and fission [122,123]:

$$P(E_\gamma)\mathrm{dE}_\gamma = \frac{\rho_\mathrm{f}(\mathrm{U_f})}{\rho_\mathrm{i}(\mathrm{U_i})} \sum_\mathrm{L} \mathrm{f(E_\gamma, L)dE}\gamma \tag{69}$$

where L is the multipolarity of the γ transition. The strength functions $f(E, L)$ can be either derived from photoabsorption cross sections or calculated from single-particle estimates of transition strengths. The former approach is more

sophisticated but requires the knowledge of the resonance parameters for all isotopes; the latter approach is easier and sufficent for a first order estimate of the γ spectral distribution. In the following the procedure used to compute the examples and implemented in the PEANUT code is briefly described. We assume

$$f(E_\gamma, L) = c_L \cdot F_L(A) \cdot E_\gamma^{(2L+1)} \tag{70}$$

where $E_\gamma^{(2L+1)}$ is the energy dependence for multipolarity L. For the c_L coefficients the Weisskopf single particle estimates[124]can be used. The $F_L(A)$ factors have been included to partially account for the many effects that bring to deviations from the single particle estimates; they are rough A dependent averages of the hindrance and enhancement factors given in [125]. Only E1, M1 and E2 transitions have been considered. The assumed level density is the same as in the evaporation part, but the ratio of exponentials coming from the level densities has been approximated as first order expansion around $E_\gamma = 0$. This is equivalent to the assumption of a constant nuclear temperature at low excitation energies, that is often used in the analysis of gamma emission following neutron capture[122,126]

As a result, one obtains the expressions for the emission probabilities for the considered multipoles. Since competition between photon and particle emission is neglected at the present status of the model, only the relative values are of interest:

$$\begin{aligned} P(L, E_\gamma)\mathrm{dE}_\gamma &= \tilde{C}_L E_\gamma^{(2L+1)} \mathrm{e}^{\frac{\mathrm{E}_\gamma}{\mathrm{T}}} \mathrm{dE}_\gamma \\ \frac{\tilde{C}_{M1}}{\tilde{C}_{E1}} &= 0.31 A^{\frac{-2}{3}} \frac{F_{M1}(A)}{F_{E1}(A)} \\ \frac{\tilde{C}_{E2}}{\tilde{C}_{E1}} &= 7.2 \cdot 10^{-7} A^{\frac{2}{3}} \frac{F_{E2}(A)}{F_{E1}(A)} \quad \mathrm{MeV}^{-2} \end{aligned} \tag{71}$$

T is the nuclear temperature at the initial excitation energy U, taken as $U - \Delta = aT^2$, a being the usual level density constant and Δ the pairing energy.

A first sampling is performed on the integrated gamma emission probabilities to choose the character (electric or magnetic) and the multipole order of the emitted photon, and a second sampling is performed to determine the emission energy according to the selected multipolarity. For both steps the full energy range $0 \leq E_\gamma \leq U$ is used, even though the intrinsic limit of validity would be $0 \leq E_\gamma \leq (U - \Delta)$. After emission, all parameters are updated on the basis of the new excitation energy, and another statistical emission is performed, until the excitation energy falls below the preset "discrete level threshold". This threshold has been set to the pairing energy for even-even

or odd mass nuclei; for odd-odd nuclei the threshold corresponds to the first excited level.

For many isotopes the experimentally determined values of the first and second excited levels have been tabulated in the code, for the others a rotational like structure is assumed, with level energy given by :

$$U_I = \frac{\hbar^2}{2\mathcal{I}} I(I+1) \tag{72}$$

where I is the level spin (integer for even-mass, half integer for odd mass nuclei, 0 or 1/2 for the ground state), and $\mathcal{I}$ is the nuclear moment of inertia, taken as 0.4 times that of a rigid body . The last steps of the γ cascade consist of δI=2 transitions among these rotational levels, down to the ground state. When known levels are tabulated, the cascade is forced to pass through them. All photons are emitted isotropically, since from the evaporation stage no information on the residual nucleus spin and polarization is available; it would be possible to implement angular distributions based on angular momentum estimates and on average experimental values of substate distributions [127].

This γ deexcitation model has been developed and tested within the PEANUT [27] model. Anyway the process is supposed to depend only on the residual nucleus mass, Z and excitation energy after evaporation, and not on the details of the preceeding interaction history. Two examples of its performances are shown in figs. 13 and 14. Both the total gamma multiplicity and the shape of the spectra are well reproduced.

5.10 High Energy Interactions: Generalities

Once suitable models are available for the description of hadron-nucleon (hN from now) interactions (see paragraph 4.5), there are still two basic ingredients to be added for a sensible description of hadron-nucleus (hA from now) interactions at high energies. Both stem from experiments which show some distinct features of these interactions when compared with hN interactions at the same energy, or with hA interactions at lower energies, and are supported by convincing theoretical modelling. The former is the increasing number of shower particles produced with increasing mass number of the target. The latter is the apparently reduced cascading into the nucleus when compared with naive expectations based on hN cross sections and hN multiplicities.

5.11 Glauber Model for High Energy Hadron-Nucleus Interactions

To better appreciate the increase of shower particle multiplicity as a function of the target mass number, fig. 15 shows the experimental rapidity distributions of

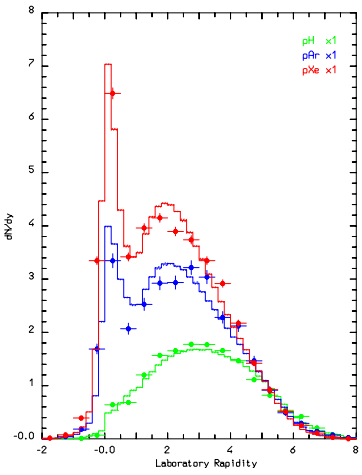

Figure 15: Rapidity distribution of charged particles produced in 200 GeV proton collisions on Hydrogen, Argon, and Xenon targets, symbols exp. results [133], histo FLUKA results

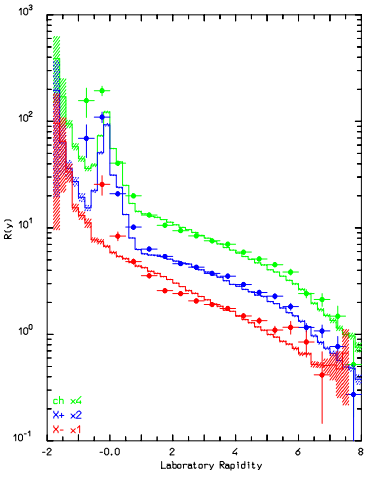

Figure 16: Ratio of rapidity distribution of charged, positive, and negative particles produced in 200 GeV proton collisions on Xenon and Hydrogen, symbols exp. results [133], histo FLUKA results

charged particles produced in interactions of 200 GeV protons with Hydrogen, Argon, and Xenon. The ratios of the rapidity distribution of charged, positive, and negative particles produced on Xenon and Hydrogen are shown in fig. 16. Both experimental data, taken from [133] (which are actually pseudorapidity spectra above about 1 GeV) and FLUKA results are presented. The peak at low rapidity in the Argon and Xenon data is due to grey particles emitted following cascading of secondaries produced in primary interactions, which are mainly slow protons produced by cascading into the target nucleus.

These results cannot be interpreted as due to increased cascading in heavier nuclei of secondaries produced in the projectile-nucleon primary interaction. There are two main difficulties connected with this naive interpretation.

- the rapidity distributions on medium-heavy nuclei are indeed somewhat shifted toward lower values with respect to hN ones, but the amount of this shift and the overall shape of the distributions are not in agreement with those expected for the simple reinteraction hypothesis. Indeed, looking at the p–p distribution in fig. 15, it is clear how most of the secondaries in p–p collisions are produced in the central region, around mid-rapidity. For p–p collisions at 200 GeV, mid-rapidity (the rapidity of the centre-of-mass system) is around 3, while the projectile rapidity

is twice that value, around 6. Particles created in the first interaction, when undergoing further collisions, will produce particles with rapidity distributions similar in shape to that for p–p at 200 GeV, but extending from ≈0 to the rapidity of the reinteracting particle → typically around 3. Clearly the distributions of particles created in the first generation of reinteractions will be centered around 1.5, that of the second around 0.75 and so on. The net result would be a distribution steadily increasing towards low rapidities, with no plateau, and showing when compared to the p–p one a depletion in all the forward emisphere (from mid-rapidity upward), with an overall spectrum much softer than the p–p one. Actually the experimental evidence is very different, showing an increase with respect to the p–p case already at rapidity 4-5, with only a slight decrease in the extreme projectile fragmentation region, with a well defined plateau just slightly below mid-rapidity. Furthermore there is no evidence of the large number of slow particles which are foreseen by the reinteraction hypothesis

- the reinteraction of fast particles produced by primary collisions is strongly inhibited by Lorentz contraction and uncertainty considerations. These arguments will be developed in more details in paragraph 5.12.

Therefore, the standard interpretation of these results is that the projectile itself undergoes multiple primary interactions with one or more target nucleons, and that the number of such interactions is increasing with the target mass. Experimentalists have developed suitable methods to "count" these primary interactions [133,134], and their outcomes for the average number of "primary" collisions are in agreement with:

$$< \nu >= \frac{A \cdot \sigma_{hN}}{\sigma_{hA}} \tag{73}$$

where σs are to be intended as absorption (≈reaction) cross sections. A rigorous demonstration of eq. 73 in the framework of the Glauber model will be given in the following paragraphs, together with the exact definition of absorption cross section. Since high energy hA absorption cross sections scale well with the mass number:

$$\sigma_{hA} = \sigma_0 \cdot A^{\alpha} \tag{74}$$

with σ_0 usually some 20-30% higher than σ_{hN} and α very close to 2/3, it is easy to verify that the average number of primary collisions scales roughly like $< \nu > \propto A^{1/3}$, with the proportionality constant slightly smaller than unity. Therefore $< \nu >$ can be significantly larger than unity for heavy nuclei, giving

rise to a substantial increase of shower particle multiplicity with respect to the hN case. The theoretical explanation of this multiple collision approach is the so called Glauber-Gribov cascade [135,136,137,138,139,141,140,142]. Within such an approach multiple collisions of primary particles are naturally accounted for, and their distribution as a function of the impact parameter can be computed once σ_{hN} is known. It is important to stress again that the term "multiple collisions" must not be interpreted as several successive interactions of the primary particle, or maybe of the leading particle coming from the previous interaction but rather as an expansion of the interaction cross section into several diagrams, the first one representing the exchange of "something" in between the primary particle and one target nucleon, the second one with two nucleons etc.

The Glauber formalism provides also the most powerful approach for calcuting total and elastic hadron-nucleus cross sections, and elastic differential cross section from few hundreds of MeV up to the highest energies.

In the following a derivation of the original Glauber approach is sketched out, and the most relevant formulae for non-elastic interactions are demonstrated.

Basic Assumptions and Formulae

According to eq. 187 in Appendix B, the nuclear scattering amplitude can be written as:

$$f(\vec{q},s) = \frac{\mathrm{ik}}{2\pi}\int \mathrm{d}^2\vec{\mathrm{b}}\ \mathrm{e}^{\mathrm{i}\vec{\mathrm{q}}\cdot\vec{\mathrm{b}}}\Gamma_{\mathrm{hA}}(\vec{\mathrm{b}},\mathrm{s}) \tag{75}$$

where the nuclear profile function, Γ_{hA}, is defined as a function of the complex phase shift χ_{hA}, by (see again Appendix B):

$$\Gamma_{hA}(\vec{b},s) = 1 - S_{hA}(\vec{b},s) = 1 - \mathrm{e}^{\mathrm{i}\chi_{\mathrm{hA}}(\vec{\mathrm{b}},\mathrm{s})} \tag{76}$$

and the total, reaction and elastic cross sections can be expressed as:

$$\begin{aligned}
\sigma_{hA\ T}(s) &= 2\int \mathrm{d}^2\vec{\mathrm{b}}\ \mathrm{Re}\Gamma_{\mathrm{hA}}(\vec{\mathrm{b}},\mathrm{s}) \\
\sigma_{hA\ r}(s) &= \int \mathrm{d}^2\vec{\mathrm{b}}\ \left[1 - |\mathrm{S}_{\mathrm{hA}}(\vec{\mathrm{b}},\mathrm{s})|^2\right] \\
\sigma_{hA\ el}(s) &= \int \mathrm{d}^2\vec{\mathrm{b}}\ |\Gamma_{\mathrm{hA}}(\vec{\mathrm{b}},\mathrm{s})|^2
\end{aligned} \tag{77}$$

Under the following assumptions:

- the phase shifts $\chi_{hA}(\vec{b},s)$ are mainly imaginary $\rightarrow$ the scattering amplitude f mainly imaginary as well and mostly absorptive
- the elastic scattering is mostly forward peaked
- the momentum transfer to individual nucleons is negligible
- there is no correlation among nucleons (but for the obvious constraint on the centre of mass position)

it is reasonable to assume that the nuclear phase shift, χ_{hA}, is the sum of the phase shifts out of individual nucleons, that is changes in the amplitude are mutiplicative. For a purely absorptive amplitude this assumption simply tells that the overall attenuation factor due to the nuclear target is simply obtained as the convolution($\rightarrow$ multiplication) of the attenuation due to individual nucleons. Such a behaviour strictly resembles those of light rays in an absorbing/diffracting medium, where the net effect can be obtained as the multiplication of the effects of the layers constituting the medium. This *phase shift additivity* hypothesis despite its simplicity and naturality, has consequences which go far beyond. Indeed, under such hypothesis alone, the Glauber approach allows to derive all properties connected with hadron-nucleus scattering, making use only of hadron-nucleon interaction and nuclear ground state properties. Suppose we have a specific configuration of the nucleons, characterized by the position vectors $\vec{r}_j$ ($\vec{r}_{j\perp}$ when projected onto a plane perpendicular to the incident beam direction), then the phase shift additivity hypothesis translates into:

$$\tilde{\chi}_{hA}(\vec{b},s) = \sum_{j=1}^{A} \chi_{hN}(\vec{b}-\vec{r}_{j\perp},s) \tag{78}$$

$$\tilde{S}_{hA}(\vec{b},s) = \prod_{j=1}^{A} S_{hN}(\vec{b}-\vec{r}_{j\perp},s) \tag{79}$$

$$\tilde{\Gamma}_{hA}(\vec{b},s) = 1-\tilde{S}_{hA}(\vec{b},s) = 1-\prod_{j=1}^{A}\left[1-\Gamma_{hN}(\vec{b}-\vec{r}_{j\perp})\right] \tag{80}$$

$$\tilde{f}_{hA}(\vec{q},s) = \frac{\mathrm{ik}}{2\pi}\int \mathrm{d}^2\vec{\mathrm{b}}\ \mathrm{e}^{\mathrm{i}\vec{\mathrm{q}}\cdot\vec{\mathrm{b}}}\tilde{\Gamma}_{\mathrm{hA}}(\vec{\mathrm{b}},\mathrm{s}) \tag{81}$$

$$\tilde{\sigma}_{hA\ T}(s) = \frac{4\pi}{k}\mathrm{Im}\tilde{\mathrm{f}}_{\mathrm{hA}}(0,\mathrm{s}) = 2\int \mathrm{d}^2\vec{\mathrm{b}}\ \mathrm{Re}\tilde{\Gamma}_{\mathrm{hA}}(\vec{\mathrm{b}},\mathrm{s}) \tag{82}$$

where tilded values indicate that all quantities refer to that specific nuclear configuration and quantities labelled hN refer to elementary hadron–nucleon

scattering. In principle such quantities depend on the considered nucleon too (for example p or n) and therefore an index j should be also present. Such index is not explicitly indicated both in order to simplify the notation and because $h-n$ and $h-p$ scatterings are very similar at high energies. Whenever the (in)equality of $h-p$ and $h-n$ scattering will be explicitly used, it will be explicitly mentioned.

Now, in order to compute the observable total cross section, one needs to average the scattering amplitude over all posibble nucleon configurations of the specific initial and final nuclear states under consideration. For this purpose let us introduce:

$$\tilde{g}_{hA}(\vec{q},\vec{b},s) = \mathrm{e}^{\mathrm{i}\vec{\mathrm{q}}\cdot\vec{\mathrm{b}}}\tilde{\Gamma}_{\mathrm{hA}}(\vec{\mathrm{b}},\mathrm{s}) \tag{83}$$

$$g_{hA}(\vec{q},\vec{b},s) = \mathrm{e}^{\mathrm{i}\vec{\mathrm{q}}\cdot\vec{\mathrm{b}}}\Gamma_{\mathrm{hA}}(\vec{\mathrm{b}},\mathrm{s}) \tag{84}$$

and write the scattering amplitude as:

$$f_{hA}(\vec{q},s) = \frac{\mathrm{ik}}{2\pi}\int \mathrm{d}^2\vec{\mathrm{b}}\ \mathrm{e}^{\mathrm{i}\vec{\mathrm{q}}\cdot\vec{\mathrm{b}}}\Gamma_{\mathrm{hA}}(\vec{\mathrm{b}},\mathrm{s}) = \frac{\mathrm{ik}}{2\pi}\int \mathrm{d}^2\vec{\mathrm{b}}\ \mathrm{g}_{\mathrm{hA}}(\vec{\mathrm{q}},\vec{\mathrm{b}},\mathrm{s}) \tag{85}$$

then the (averaged) scattering amplitude corresponding to the transition from an initial nuclear state i to a final one f can be obtained in terms of the respective wave functions, Ψ_i and Ψ_f.

$$\begin{aligned} g_{hA\ fi}(\vec{q},\vec{b},s) &\equiv < f|\tilde{g}_{hA}|i >= \\ &= \int\prod_{j=1}^{A}\mathrm{d}^3\vec{\mathrm{r}}_\mathrm{j}\ \Psi^*_\mathrm{f}(\vec{\mathrm{r}}_1,...,\vec{\mathrm{r}}_\mathrm{A})\Psi_\mathrm{i}(\vec{\mathrm{r}}_1,...,\vec{\mathrm{r}}_\mathrm{A})\tilde{\mathrm{g}}_{\mathrm{hA}}(\vec{\mathrm{q}},\vec{\mathrm{b}},\mathrm{s}) \end{aligned} \tag{86}$$

$$\begin{aligned} S_{hA\ fi}(\vec{b},s) &\equiv < f|\tilde{S}_{hA}|i >= \\ &= \int\prod_{j=1}^{A}\mathrm{d}^3\vec{\mathrm{r}}_\mathrm{j}\ \Psi^*_\mathrm{f}(\vec{\mathrm{r}}_1,...,\vec{\mathrm{r}}_\mathrm{A})\Psi_\mathrm{i}(\vec{\mathrm{r}}_1,...,\vec{\mathrm{r}}_\mathrm{A})\tilde{\mathrm{S}}_{\mathrm{hA}}(\vec{\mathrm{b}},\mathrm{s}) \end{aligned} \tag{87}$$

$$\begin{aligned} \Gamma_{hA\ fi}(\vec{b},s) &\equiv < f|\tilde{\Gamma}_{hA}|i >= \\ &= \int\prod_{j=1}^{A}\mathrm{d}^3\vec{\mathrm{r}}_\mathrm{j}\ \Psi^*_\mathrm{f}(\vec{\mathrm{r}}_1,...,\vec{\mathrm{r}}_\mathrm{A})\Psi_\mathrm{i}(\vec{\mathrm{r}}_1,...,\vec{\mathrm{r}}_\mathrm{A})\tilde{\Gamma}_{\mathrm{hA}}(\vec{\mathrm{b}},\mathrm{s}) \end{aligned} \tag{88}$$

The $i \to f$ transitions include also transition to excited nuclear states besides the elastic channel ($f = i$). A cross section for the transition from the i (ground) state to the f final state can be defined according to:

$$\sigma_{hA\ fi}(s) = \int \mathrm{d}\Omega_{\mathrm{k}'}\ \frac{\mathrm{k}'}{\mathrm{k}}|\mathrm{f}_{\mathrm{fi}}(\mathrm{k},\mathrm{k}')|^2 \tag{89}$$

where k' is the momentum of the outgoing hadron. Since we are neglecting $k - k'$, and using formula 184 from Appendix B, it turns out:

$$\sigma_{hA\ fi}(s) = \frac{1}{k^2} \int \mathrm{d}^2\vec{\mathrm{q}}\ |\mathrm{f}_{\mathrm{hA\ fi}}(\vec{\mathrm{q}},\mathrm{s})|^2 \tag{90}$$

where using eq. 86:

$$f_{hA\ fi}(\vec{q},s) = \frac{\mathrm{ik}}{2\pi} \int \mathrm{d}^2\vec{\mathrm{b}}\ \Gamma_{\mathrm{hA\ fi}}(\vec{\mathrm{b}},\mathrm{s}) \mathrm{e}^{\mathrm{i}\vec{\mathrm{q}}\cdot\vec{\mathrm{b}}} = \frac{\mathrm{ik}}{2\pi} \int \mathrm{d}^2\vec{\mathrm{b}}\ < \mathrm{f}|\check{\mathrm{g}}_{\mathrm{hA\ fi}}(\vec{\mathrm{q}},\vec{\mathrm{b}},\mathrm{s})|\mathrm{i} > \tag{91}$$

In order to evaluate $\sigma_{hA\ fi}$ and to give a closed expression for $S_{hA\ fi}$ and $\Gamma_{hA\ fi}$ it is convenient to simplify the notation, introducing:

$$\vec{u} \equiv (\vec{r}_1, ..., \vec{r}_A) \tag{92}$$

$$\mathrm{d}^3\vec{\mathrm{u}} \equiv \prod_{i=1}^{A} \mathrm{d}^3\vec{\mathrm{r}}_{\mathrm{j}} \tag{93}$$

Making use of eqs. 79,80 together with 87 and 88:

$$S_{hA\ fi}(\vec{b},s) = \int \mathrm{d}^3\vec{\mathrm{u}}\ \Psi_{\mathrm{f}}^*(\vec{\mathrm{u}})\Psi_{\mathrm{i}}(\vec{\mathrm{u}}) \prod_{\mathrm{j}=1}^{\mathrm{A}} \mathrm{S}_{\mathrm{hN}}(\vec{\mathrm{b}} - \vec{\mathrm{r}}_{\mathrm{j}\perp}, \mathrm{s}) \tag{94}$$

$$\Gamma_{hA\ fi}(\vec{b},s) = \int \mathrm{d}^3\vec{\mathrm{u}}\ \Psi_{\mathrm{f}}^*(\vec{\mathrm{u}})\Psi_{\mathrm{i}}(\vec{\mathrm{u}}) \left\{ 1 - \prod_{\mathrm{j}=1}^{\mathrm{A}} \left[1 - \Gamma_{\mathrm{hN}}(\vec{\mathrm{b}} - \vec{\mathrm{r}}_{\mathrm{j}\perp}, \mathrm{s}) \right] \right\} \tag{95}$$

$$\begin{aligned} |\Gamma_{hA\ fi}(\vec{b},s)|^2 &= \int \mathrm{d}^3\vec{\mathrm{u}} \int \mathrm{d}^3\vec{\mathrm{u}}\,'\ \Psi_{\mathrm{f}}(\vec{\mathrm{u}})\Psi_{\mathrm{f}}^*(\vec{\mathrm{u}}\,')\Psi_{\mathrm{i}}^*(\vec{\mathrm{u}}\,')\Psi_{\mathrm{i}}(\vec{\mathrm{u}}) \\ &\cdot \left\{ 1 - \prod_{l=1}^{A} \left[1 - \Gamma_{hN}^*(\vec{b} - \vec{r}_{l\perp}', s) \right] \right\} \\ &\cdot \left\{ 1 - \prod_{j=1}^{A} \left[1 - \Gamma_{hN}(\vec{b} - \vec{r}_{j\perp}, s) \right] \right\} = \\ &= \int \mathrm{d}^3\vec{\mathrm{u}} \int \mathrm{d}^3\vec{\mathrm{u}}\,'\ \Psi_{\mathrm{f}}(\vec{\mathrm{u}})\Psi_{\mathrm{f}}^*(\vec{\mathrm{u}}\,')\Psi_{\mathrm{i}}^*(\vec{\mathrm{u}}\,')\Psi_{\mathrm{i}}(\vec{\mathrm{u}}) \\ &\cdot \left[1 - \prod_{l=1}^{A} S_{hN}^*(\vec{b} - \vec{r}_{l\perp}', s) \right] \left[1 - \prod_{j=1}^{A} S_{hN}(\vec{b} - \vec{r}_{j\perp}, s) \right] \end{aligned} \tag{96}$$

Total, Elastic, Quasi–Elastic, and Absorption Cross Section Definition

Making use of the closure relation [136] for the final states f:

$$\sum_f \Psi_f(\vec{u})\Psi_f^*(\vec{u}\,') = \delta^{3\mathrm{A}}(\vec{\mathrm{u}} - \vec{\mathrm{u}}\,') \tag{97}$$

one can write, introducing μ's as in Appendix B, and summing over all possible nuclear states:

$$\begin{aligned}
\sigma_{hA\ \Sigma f}(s) &\equiv \sum_f \sigma_{hA\ fi}(s) \equiv \sum_f \int \mathrm{d}^2\vec{\mathrm{b}}\ \mu_{\mathrm{hA\ fi}}(\vec{\mathrm{b}},\mathrm{s}) = \\
&= \int \mathrm{d}^2\vec{\mathrm{b}} \sum_{\mathrm{f}} |\Gamma_{\mathrm{hA\ fi}}(\vec{\mathrm{b}},\mathrm{s})|^2 = \\
&= \int \mathrm{d}^2\vec{\mathrm{b}} \int \mathrm{d}^3\vec{\mathrm{u}}\ |\Psi_{\mathrm{i}}(\vec{\mathrm{u}})|^2 |\tilde{\Gamma}_{\mathrm{hA}}(\vec{\mathrm{b}},\mathrm{s})|^2 = \\
&= \int \mathrm{d}^2\vec{\mathrm{b}} \int \mathrm{d}^3\vec{\mathrm{u}}\ |\Psi_{\mathrm{i}}(\vec{\mathrm{u}})|^2 \left| \left[1 - \prod_{\mathrm{j}=1}^{\mathrm{A}} \mathrm{S}_{\mathrm{hN}}(\vec{\mathrm{b}} - \vec{\mathrm{r}}_{\mathrm{j}\perp},\mathrm{s}) \right] \right|^2 \qquad (98) \\
\sigma_{hA\ el}(s) &\equiv \sigma_{hA\ ii}(s) \equiv \int \mathrm{d}^2\vec{\mathrm{b}}\ \mu_{\mathrm{hA\ el}}(\vec{\mathrm{b}},\mathrm{s}) = \\
&= \int \mathrm{d}^2\vec{\mathrm{b}} \left| \int \mathrm{d}^3\vec{\mathrm{u}}\ |\Psi_{\mathrm{i}}(\vec{\mathrm{u}})|^2 \left[1 - \prod_{\mathrm{j}=1}^{\mathrm{A}} \mathrm{S}_{\mathrm{hN}}(\vec{\mathrm{b}} - \vec{\mathrm{r}}_{\mathrm{j}\perp},\mathrm{s}) \right] \right|^2 \qquad (99)
\end{aligned}$$

where $\sigma_{hA\ \Sigma f}$ represents the cross section for both elastic scattering and inelastic scattering to excited states, and does not include contributions from individual hN non-elastic interactions. The total cross section can be expressed, using eqs. 77,94, as:

$$\begin{aligned}
\sigma_{hA\ T}(s) &\equiv \int \mathrm{d}^2\vec{\mathrm{b}}\ \mu_{\mathrm{hA\ T}}(\vec{\mathrm{b}},\mathrm{s}) = 2\int \mathrm{d}^2\vec{\mathrm{b}}\ \mathrm{Re}\Gamma_{\mathrm{hA\ ii}}(\vec{\mathrm{b}},\mathrm{s}) = \\
&= 2\int \mathrm{d}^2\vec{\mathrm{b}} \int \mathrm{d}^3\vec{\mathrm{u}}\ |\Psi_{\mathrm{i}}(\vec{\mathrm{u}})|^2 \mathrm{Re}\tilde{\Gamma}_{\mathrm{hA}}(\vec{\mathrm{b}},\mathrm{s}) = \qquad (100) \\
&= 2\int \mathrm{d}^2\vec{\mathrm{b}} \int \mathrm{d}^3\vec{\mathrm{u}}\ |\Psi_{\mathrm{i}}(\vec{\mathrm{u}})|^2 \left[1 - \prod_{\mathrm{j}=1}^{\mathrm{A}} \mathrm{ReS}_{\mathrm{hN}}(\vec{\mathrm{b}} - \vec{\mathrm{r}}_{\mathrm{j}\perp},\mathrm{s}) \right]
\end{aligned}$$

These equations show how the knowledge of elementary hadron–nucleon scattering and of the nuclear ground state is sufficient to compute all relevant cross sections without any further assumption and/or information.

It is customary to define a cross section for *quasi–elastic* scattering as the difference between $\sigma_{hA\ \Sigma f}$ and the elastic cross section:

$$\sigma_{hA\ qe}(s) \equiv \sigma_{hA\ \Sigma f}(s) - \sigma_{hA\ el}(s) \tag{101}$$

It is worthwhile to point out that $\sigma_{hA\ qe} \geq 0$, since for whichever function f it holds that $\left|\int \mathrm{dx\ f}\right| \leq \int \mathrm{dx\ |f|}$.

The physical interpretation of the quasi–elastic cross section is the following: besides the "true" elastic scattering (often called *coherent–elastic*) there are contributions coming from interactions where the nucleus is no longer left in the ground state, but still no elementary inelastic hadron–nucleon interaction occurred. Therefore such interactions do not give rise to direct particle production (particle emission could always occur during the following nuclear deexcitation process), leaving the target nucleus in an excited state. Naively speaking, quasi–elastic scattering stems from elastic hadron–nucleon interactions which leaves the nucleus excited; for this reason it is also called *incoherent–elastic*. From an experimental point of view, quasi–elastic scattering is difficult to discriminate from genuine elastic scattering, since high energy hadron–nucleon scattering, as we already discussed, is strongly forward peaked and the resulting momentum transfer is often too small to be discriminated from the "true" elastic one within experimental resolutions. From a practical point of view, quasi–elastically scattered hadrons behave in a very similar way to elastically scattered ones and both are not the dominant ingredients of high energy cascades which are mostly ruled by *absorption* reactions.

Absorption reactions are those reactions where at least one hadron–nucleon non–elastic interaction ($\rightarrow$ particle production) occurs. It is common practice among high energy physicists to quote the absorption cross section as the "reaction" or "non–elastic" cross section, even though the last two terms should be referred to all non-elastic channels including those contained in the quasi–elastic cross section. Let us define the absorption cross section as:

$$\begin{aligned} \sigma_{hA\ abs}(s) &\equiv \sigma_{hA\ T}(s) - \sigma_{hA\ el}(s) - \sigma_{hA\ qe}(s) = \sigma_{hA\ T}(s) - \sigma_{hA\ \Sigma f}(s) = \\ &= \sigma_{hA\ r}(s) - \sigma_{hA\ qe}(s) \equiv \int \mathrm{d}^2\vec{\mathrm{b}}\ \mu_{\mathrm{hA\ abs}}(\vec{\mathrm{b}}, \mathrm{s}) \end{aligned} \tag{102}$$

At this stage the equivalence of eq. 102 with our definition of absorption cross section is still to be proved.

Absorption Cross Section and Multiple Collisions

Using eqs. 98,100 and 102

$$\mu_{hA\ abs}(\vec{b},s) = \int \mathrm{d}^3\vec{\mathrm{u}}\ |\Psi_{\mathrm{i}}(\vec{\mathrm{u}})|^2 \left[2\mathrm{Re}\tilde{\Gamma}_{\mathrm{hA}}(\vec{\mathrm{b}},\mathrm{s}) - |\tilde{\Gamma}_{\mathrm{hA}}(\vec{\mathrm{b}},\mathrm{s})|^2\right] =$$
$$= \int \mathrm{d}^3\vec{\mathrm{u}}\ |\Psi_{\mathrm{i}}(\vec{\mathrm{u}})|^2 \left[1 - |\tilde{\mathrm{S}}_{\mathrm{hA}}(\vec{\mathrm{b}},\mathrm{s})|^2\right] \qquad (103)$$

Using eq. 79 and the definition of μ_r given in eq. 194 in Appendix B:

$$|\tilde{S}_{hA}(\vec{b},s)|^2 = \prod_{j=1}^{A} |S_{hN}(\vec{b}-\vec{r}_{j\perp},s)|^2 =$$
$$= \prod_{j=1}^{A} \left\{1 - \left[1 - |S_{hN}(\vec{b}-\vec{r}_{j\perp},s)|^2\right]\right\} =$$
$$= \prod_{j=1}^{A} \left[1 - \mu_{hN\ r}(\vec{b}-\vec{r}_{j\perp},s)\right] \qquad (104)$$

one can finally derive the fundamental formula:

$$\sigma_{hA\ abs}(s) \equiv \int \mathrm{d}^2\vec{\mathrm{b}}\ \mu_{\mathrm{hA\ abs}}(\vec{\mathrm{b}},\mathrm{s}) = \qquad (105)$$
$$= \int \mathrm{d}^2\vec{\mathrm{b}} \int \mathrm{d}^3\vec{\mathrm{u}}\ |\Psi_{\mathrm{i}}(\vec{\mathrm{u}})|^2 \left\{1 - \prod_{\mathrm{j=1}}^{\mathrm{A}} \left[1 - \mu_{\mathrm{hN\ r}}(\vec{\mathrm{b}}-\vec{\mathrm{r}}_{\mathrm{j}\perp},\mathrm{s})\right]\right\}$$

The probabilistic interpretation of eq. 105 is straightforward and consistent with our definition of $\sigma_{hA\ abs}$. Indeed $\prod_{j=1}^{A}[1-\mu_{hN\ r}]$ is the probability that the projectile impinging along impact parameter $\vec{b}$ will escape inelastic collisions will all A nucleons for the given nucleon configuration. Therefore the absorption probability is given by $1-\prod_{j=1}^{A}[1-\mu_{hN\ r}]$, and eq. 105 is nothing else that the average of such probability over all impact parameters and nucleon configurations. The fact that the phase shift additivity hypothesis alone implies this result is striking and gives a further confirmation of the validity of the Glauber approach.

Let us assume that the ground state wave–function, Ψ_i, can be expressed as a product of independent particle wave–functions, ψ_{ji}:

$$\Psi_i(\vec{r}_1,...,\vec{r}_A) = \left[\prod_{j=1}^{A} \psi_{ji}(\vec{r}_j)\right] \delta^3\left(\sum_{j=1}^{A} \vec{r}_j\right) \qquad (106)$$

$$\rho_j(\vec{r}_j) \equiv \psi^*_{ji}(\vec{r}_j)\cdot\psi_{ji}(\vec{r}_j) \tag{107}$$

$$\int \mathrm{d}^3\vec{\mathrm{r}}\ \rho_{\mathrm{j}}(\vec{\mathrm{r}}) = 1 \tag{108}$$

The delta function expresses the centre-of-mass constraint for the A nucleon positions. For all nuclei but the lightest ones, such term can be safely neglected: for the lightest nuclei there are exact ways of keeping track of it using shell model wave–functions, and approximate ones for heavier nuclei (for details see [138]). Under these approximations, and writing (using eq. 194):

$$\begin{aligned} \mu_{hN\ r}(\vec{b},s) &\equiv \sigma_{hN\ r}(s)\cdot\kappa_{hN}(\vec{b},s) \\ \kappa_{hN} &= \frac{1-|S_{hN}(\vec{b},s)|^2}{\sigma_{hN\ r}(s)} = \frac{\mu_{hN\ r}(\vec{b},s)}{\sigma_{hN\ r}(s)} \end{aligned} \tag{109}$$

where, by construction, $\kappa_{hN}(\vec{b},s)$ is real and:

$$\int \mathrm{d}^2\vec{\mathrm{b}}\ \kappa_{\mathrm{hN}}(\vec{\mathrm{b}},\mathrm{s}) = 1 \tag{110}$$

expression 105 for $\mu_{hA\ abs}$ transforms into:

$$\mu_{hA\ abs}(\vec{b},s) = 1-\prod_{j=1}^{A}\left[1-\sigma_{hN\ rj}(s)T_{rj}(\vec{b},s)\right] \tag{111}$$

$$\begin{aligned} T_{rj}(\vec{b},s) &\equiv \int \mathrm{d}^3\vec{\mathrm{r}}\ \rho_{\mathrm{j}}(\vec{\mathrm{r}})\ \kappa_{\mathrm{hN\ j}}(\vec{\mathrm{b}}-\vec{\mathrm{r}}_\perp,\mathrm{s}) = \\ &= \int_{-\infty}^{+\infty}\mathrm{dz}\int \mathrm{d}^2\vec{\mathrm{s}}\ \rho_{\mathrm{j}}(\mathrm{z},\vec{\mathrm{s}})\kappa_{\mathrm{hN\ j}}(\vec{\mathrm{b}}-\vec{\mathrm{s}},\mathrm{s}) \\ \mathrm{d}^3\vec{\mathrm{r}} &= \mathrm{dz}\ \mathrm{d}^2\vec{\mathrm{s}} = \mathrm{dz}\ \mathrm{sds}\ \mathrm{d}\phi \end{aligned} \tag{112}$$

where the *thickness function* for non-elastic reactions, T_{rj}, has been introduced. Note that the index j has been explicitly written in this case to stress both that densities can be different for different nucleons (i.e. for light nuclei when using shell model densities), and that $\sigma_{hN\ r}$ and κ_{hN} depend on the nucleon type (proton or neutron). $T_{rj}(\vec{b},s)$ obviously represent the amount of nuclear matter seen by the incident hadron travelling along the impact parameter $\vec{b}$, when properly folded with its profile function.

The thickness function has an important normalization property, that derives from the normalization of ρ_j and κ_{hN}, and from the property that the integral of a convolution of two functions is the product of the integrals. This

result is a direct consequence of two properties of the Fourier transforms, namely that the transform of a n-dimensional convolution is the product of the transforms, and that the n-dimensional integral of a funtion is equal to its transform evaluated in the origin. Therefore:

$$\begin{aligned}\int \mathrm{d}^2\vec{\mathrm{b}}\ \mathrm{T_{rj}}(\vec{\mathrm{b}},\mathrm{s}) &= \int_{-\infty}^{+\infty}\mathrm{dz}\int \mathrm{d}^2\vec{\mathrm{b}}\int \mathrm{d}^2\vec{\mathrm{s}}\ \rho_{\mathrm{j}}(\mathrm{z},\vec{\mathrm{s}})\ \kappa_{\mathrm{hN\ j}}(\vec{\mathrm{b}}-\vec{\mathrm{s}},\mathrm{s}) = \\ &= \int_{-\infty}^{+\infty}\mathrm{dz}\ \left[\int \mathrm{d}^2\vec{\mathrm{s}}\ \rho_{\mathrm{j}}(\mathrm{z},\vec{\mathrm{s}})\right]\left[\int \mathrm{d}^2\vec{\mathrm{s}}\ \kappa_{\mathrm{hN\ j}}(\vec{\mathrm{s}},\mathrm{s})\right] = \\ &= \int \mathrm{d}^3\vec{\mathrm{r}}\ \rho_{\mathrm{j}}(\vec{\mathrm{r}}) = 1 \end{aligned} \tag{113}$$

For ρ and κ depending only on the modulus of $\vec{r}$ and $\vec{b}-\vec{s}$ respectively, which is a very common situation, and omitting the dependence on the center-of-mass squared energy s to prevent confusion with $\vec{s}$:

$$\begin{aligned} T_{rj}(b) &= \int_{-\infty}^{+\infty}\mathrm{dz}\int \mathrm{d}^2\vec{\mathrm{s}}\ \rho_{\mathrm{j}}(\sqrt{\mathrm{z}^2+\mathrm{s}^2})\ \kappa_{\mathrm{hN\ j}}(\sqrt{\mathrm{b}^2+\mathrm{s}^2-2\mathrm{bs}\cos\phi}) = \\ &= \int_{-\infty}^{+\infty}\mathrm{dz}\int \mathrm{d}^2\vec{\mathrm{s}}\,'\rho_{\mathrm{j}}(\sqrt{\mathrm{z}^2+\mathrm{b}^2+\mathrm{s}'^2-2\mathrm{bs}'\cos\phi})\ \kappa_{\mathrm{hN\ j}}(\mathrm{s}') \end{aligned} \tag{114}$$

Eq. 114 is a useful starting point for practical calculations. Simple exponential amplitudes like those depicted in Appendix C are well adequate in order to parameterize hadron–nucleon scattering, and to make calculations rather comfortable. In order to further understand how multiple collisions are described by eq. 105, let us make the further assumption that ρ_j does not depend on the nucleon index, and that $\sigma_{hn\ r} = \sigma_{hp\ r} \equiv \sigma_{hN\ r}$. Then (again omitting the dependence on the centre-of-mass energy):

$$\begin{aligned} \mu_{hA\ abs}(b) &= 1-[1-\sigma_{hN\ r}T_r(b)]^A = \\ &= [1-\sigma_{hN\ r}T_r(b)+\sigma_{hN\ r}T_r(b)]^A-[1-\sigma_{hN\ r}T_r(b)]^A = \\ &= \sum_{\nu=0}^{A}\left(\begin{array}{c}A\\ \nu\end{array}\right)[\sigma_{hN\ r}T_r(b)]^\nu\,[1-\sigma_{hN\ r}T_r(b)]^{A-\nu}+ \\ &\quad -[1-\sigma_{hN\ r}T_r(b)]^A = \\ &= \sum_{\nu=1}^{A}\left(\begin{array}{c}A\\ \nu\end{array}\right)[\sigma_{hN\ r}T_r(b)]^\nu\,[1-\sigma_{hN\ r}T_r(b)]^{A-\nu} \\ &= \sum_{\nu=1}^{A}\left(\begin{array}{c}A\\ \nu\end{array}\right)P_r^\nu(b)\,[1-P_r(b)]^{A-\nu} \end{aligned} \tag{115}$$

$$
\begin{aligned}
&= \sum_{\nu=1}^{A} P_{r\ \nu}(b) \\
P_r(b) &\equiv \sigma_{hN\ r} T_r(b) \\
P_{r\ \nu}(b) &\equiv \left(\begin{array}{c} A \\ \nu \end{array} \right) P_r^{\nu}(b)\,[1 - P_r(b)]^{A-\nu} \qquad (116) \\
T_r(b) &= \int_{-\infty}^{+\infty} \mathrm{dz} \int \mathrm{d}^2\vec{\mathrm{s}}\ \rho(\sqrt{\mathrm{z}^2 + \mathrm{s}^2})\kappa_{\mathrm{hN}}(\sqrt{\mathrm{b}^2 + \mathrm{s}^2 - 2\mathrm{bs}\cos\phi}) = \\
&= \int_{-\infty}^{+\infty} \mathrm{dz} \int \mathrm{d}^2\vec{\mathrm{s}}\,'\rho(\sqrt{\mathrm{z}^2 + \mathrm{b}^2 + \mathrm{s}'^2 - 2\mathrm{bs}'\cos\phi})\kappa_{\mathrm{hN}}(\mathrm{s}') \qquad (117) \\
\left(\begin{array}{c} A \\ \nu \end{array} \right) &= \frac{A!}{\nu!(A-\nu)!}
\end{aligned}
$$

Since $P_r(b)$ is the probability of getting one specific nucleon hit (for our assumptions it is the same for all nucleons) and there are A possible trials, $P_{r\ \nu}(b)$ is exactly the binomial distribution for getting ν successes out of A trials, with probability $P_r(b)$ each. Therefore the absorption cross section is just the integral in the impact parameter plane of the probability of getting at least one non-elastic hadron-nucleon collision. The average number of non-elastic hadron-nucleon for a given impact parameter b can be easily obtained observing that we have A independent trials with probability $P_r(b)$ each:

$$
< \nu(b) >= A\ P_r(b) \qquad (118)
$$

and the overall average number of collision is given by:

$$
\begin{aligned}
< \nu > &= \frac{\int \mathrm{d}^2\vec{\mathrm{b}}\ < \nu(\mathrm{b}) >}{\int \mathrm{d}^2\vec{\mathrm{b}}\ \mu_{\mathrm{hA\ abs}}(\mathrm{b})} \\
&= \frac{A\sigma_{hN\ r}}{\sigma_{hA\ abs}} \int \mathrm{d}^2\vec{\mathrm{b}}\ \mathrm{T_r(b)} = \frac{A\sigma_{hN\ r}}{\sigma_{hA\ abs}} \qquad (119)
\end{aligned}
$$

where the integral has been estimated according to eq. 113. Therefore the result 73 has been demonstrated under very general assumptions in the framework of the Glauber model. The extension of the previous equations to the case of different densities and/or cross sections for protons and neutrons is straightforward and left to the reader. The final result for the average number of collisions reads:

$$
< \nu >= \frac{Z\sigma_{hp\ r} + N\sigma_{hn\ r}}{\sigma_{hA\ abs}} \qquad (120)
$$

In order to make a quick evaluation of $T_r(b)$, which can be required in order to compute $\sigma_{hA\ abs}$ or for example in a MonteCarlo model to select the

number of collisions occuring for a randomly sampled impact parameter, one can resort to the so called *nuclear thickness approximation* (sometimes also called *optical limit*). It consists in making the substitution $\kappa_{hN}(s') \rightarrow \delta^2(0)$ in eq. 114 and 117, which is justified whenever κ_{hN} takes significant values over a spatial extension << of the nuclear radius. According to Appendix C, the typical spatial extent for κ_{hN} is of the order of 1 fm, and therefore this approximation is reasonably justified for medium and heavy nuclei. In this case:

$$T_r(b) \approx \int_{-\infty}^{+\infty} \mathrm{dz}\ \rho(\sqrt{\mathrm{z}^2 + \mathrm{b}^2}) \tag{121}$$

with an obvious geometrical interpretation.

When computing absorption cross sections a small correction[143,144], known as *inelastic screening*, should be taken into account. This correction arises because expression 80 contains only contributions from elastic hadron-nucleon scattering. There are additional contributions in second and higher order diagrams from intermediate states in which the incoming hadron is diffractively excited on one target nucleon, and reverts to its ground state in a later interaction.

The same approach used to derive the absorption cross section can be extended at least partially to the total one, making the substitutions:

$$\begin{aligned} \kappa_{hN\ j}(\vec{b}) &\rightarrow \gamma_{hN\ j}(\vec{b}) \\ \sigma_{hN\ rj} &\rightarrow \frac{1 - \mathrm{i}\rho_0}{2}\sigma_{hN\ Tj} \\ T_{rj}(\vec{b}) &\rightarrow T_{Tj}(\vec{b}) \end{aligned}$$

where the new quantities are defined by:

$$\gamma_{hN}(\vec{b}) \equiv \frac{2\Gamma_{hN}(\vec{b})}{(1 - \mathrm{i}\rho_0)\sigma_{\mathrm{hN\ T}}} \tag{122}$$

$$\rho_0 \equiv \frac{\mathrm{Ref_{hN}}(0)}{\mathrm{Imf_{hN}}(0)} \tag{123}$$

$$\mu_{h\,A\ T}(\vec{b}) = 2\left\{1 - \mathrm{Re}\prod_{\mathrm{j=1}}^{\mathrm{A}}\left[1 - (1 - \mathrm{i}\rho_0)\frac{\sigma_{\mathrm{hN\ Tj}}}{2}\mathrm{T_{Tj}}(\vec{\mathrm{b}})\right]\right\} \tag{124}$$

$$\begin{aligned} T_{Tj}(\vec{b}) &\equiv \int \mathrm{d}^3\vec{\mathrm{r}}\ \rho_{\mathrm{j}}(\vec{\mathrm{r}})\ \gamma_{\mathrm{hN\ j}}(\vec{\mathrm{b}} - \vec{\mathrm{r}}_\perp) = \\ &= \int_{-\infty}^{+\infty} \mathrm{dz} \int \mathrm{d}^2\vec{\mathrm{s}}\ \rho_{\mathrm{j}}(\mathrm{z}, \vec{\mathrm{s}})\ \gamma_{\mathrm{hN\ j}}(\vec{\mathrm{b}} - \vec{\mathrm{s}}) \end{aligned} \tag{125}$$

The definition of γ_{hN} is such that, using the definition 193 of Appendix B, it holds:

$$\int \mathrm{d}^2\vec{\mathrm{b}}\ \gamma_{\mathrm{hN\ T}}(\vec{\mathrm{b}}) \quad = \quad 1$$
$$\mathrm{Im}\gamma_{\mathrm{hN}}(0) = 0$$

In general the imaginary part of γ_{hN} can be different from zero for $b \neq 0$. γ_{hN} is real for every $\vec{b}$ when the ratio of the imaginary-to-real part of the hadron-nucleon scattering amplitude is constant and equal to ρ_0 for whichever momentum transfer. The simplified scattering amplitudes described in Appendix C fulfill this requirement. Whenever γ_{hN} is not completely real little can be done in expanding eq. 124 in a way similar to the one adopted for the absorption cross section. However the real part of high energy hadron scattering amplitudes is usually small and therefore can be safely neglected. Under this approximation ($\rho_0 \approx 0$, $\gamma_{hN}(\vec{b})$ real) it is easy to show that:

$$\begin{aligned}
\mu_{hA\ T}(b) &= 2\sum_{\nu=1}^{A} \left(\begin{array}{c} A \\ \nu \end{array} \right) \left[\frac{\sigma_{hN\ T}}{2} T_T(b)\right]^{\nu} \left[1 - \frac{\sigma_{hN\ T}}{2} T_T(b)\right]^{A-\nu} \qquad (126) \\
&= 2\sum_{\nu=1}^{A} \left(\begin{array}{c} A \\ \nu \end{array} \right) P_T^{\nu}(b) \left[1 - P_T(b)\right]^{A-\nu} \\
&= \sum_{\nu=1}^{A} P_{T\ \nu}(b) \\
P_T(b) &\equiv \frac{\sigma_{hN\ T}}{2} T_T(b) \\
P_{T\ \nu}(b) &\equiv 2 \left(\begin{array}{c} A \\ \nu \end{array} \right) P_T^{\nu}(b) \left[1 - P_T(b)\right]^{A-\nu} \qquad (127) \\
T_T(b) &= \int_{-\infty}^{+\infty} \mathrm{dz} \int \mathrm{d}^2\vec{\mathrm{s}}\ \rho(\sqrt{\mathrm{z}^2 + \mathrm{s}^2})\gamma_{\mathrm{hN}}(\sqrt{\mathrm{b}^2 + \mathrm{s}^2 - 2\mathrm{bs}\cos\phi}) = \\
&= \int_{-\infty}^{+\infty} \mathrm{dz} \int \mathrm{d}^2\vec{\mathrm{s}}\,'\rho(\sqrt{\mathrm{z}^2 + \mathrm{b}^2 + \mathrm{s}'^2 - 2\mathrm{bs}'\cos\phi})\gamma_{\mathrm{hN}}(\mathrm{s}') \qquad (128)
\end{aligned}$$

where the meaning of the various terms is obvious. Of course the physical interpretation of eq. 126 is much less obvious than in the absorption case. A part the overall factor of 2, It describes a multiple scattering expansion, where individual scatterings are governed by $\sigma_{hN\ T}/2$. This is a direct consequence of the wave nature of the whole problem and in particular of the optical theorem, since the total cross section is linked to the forward scattering amplitude

and not to an amplitude squared. In the nuclear thickness approximation ($\gamma_{hN}(s') \to \delta^2(0)$), it holds:

$$T_T(b) \quad = \quad T_r(b) \approx \int_{-\infty}^{+\infty} \mathrm{dz}\ \rho(\sqrt{\mathrm{z}^2 + \mathrm{b}^2})$$

It is worthwhile to point out that for whichever b:

$$P_{T\nu}(b) \quad \geq \quad P_{r\nu}(b)$$

The proof of this inequality is straightforward in the nuclear thickness approximation, for a purely imaginary amplitude with zero phase shifts δ_l (in this case $\sigma_{hN\ T} \geq \sigma_{hN\ r} \geq \sigma_{hN\ T}/2$).

Diagram Interpretation of Multiple Collisions

Most of the interest of the Glauber multiple collision model lies in the possibility of formulating it as a field theory (the so called Glauber-Gribov model[139]) based on general principles such as unitarity and analyticity. The various multiple collision terms can be shown to be in a one-to-one correspondence with the various Feynman graphs describing the interaction. In this approach, for example, at high energies where the scattering amplitude can be assumed to be dominated by exchanges in the t-channel with the quantum numbers of vacuum (the so called *pomeron*, see Appendix C), the projectile partons exchange one or more pomerons according to the multiple scattering formula, with one or more target nucleons.

In the DPM language, neglecting the contributions from higher order diagrams (those called multiple soft collisions in the DPM paragraph) that is considering at most one pomeron exchange with each target nucleon, a collision where the projectile is undergoing interactions with n target nucleons is described by $2n$ chains, out of which, two result from the combination of the projectile valence quarks with the valence quarks of one target nucleon ($\to$ 2 valence-valence chains), and $2(n-1)$ chains are stretched among $2(n-1)$ couples $q - \bar{q}$ of sea quarks of the projectile and the valence quarks of the remaining $2(n-1)$ target nucleons ($\to 2(n-1)$ sea-valence collisions).

The whole procedure for describing hA absorption interactions can be summarized as follows, striclty following what can be done in a MonteCarlo implementation:

- an impact parameter b is randomly selected over the geometrical area of the target nucleus

- the distribution for the number of collision is then computed according to eq. 116, and the actual number of collisions randomly sampled from such distribution. If no collision is selected the procedure restarts from the first step
- the position and Fermi momenta of the hit nucleons are sampled
- the momentum fractions of the projectile and target partons as well as chain ends are selected according to DPM prescriptions. Sea–valence chains which result in too small invariant masses are discarded
- all chains are hadronized into stable hadrons or resonances

One of the most critical points is connected with the treatment of low energy chains. The Glauber approach has widely demonstrated its validity at projectile energies as low as few hundreds MeV in the laboratory for what concerns cross section calculations and elastic scattering distributions. However the multiple scattering regime is approached only at much higher energies. Indeed the number of primary interactions extracted from the experiments saturates at the level given by Glauber approach ($< \nu >$ is fairly independent on energy, due to the slow variation of both σ_{hN} and σ_{hA}) at several tens of GeV. At lower energies the average number of collisions start to decrease, eventually approaching one at few GeV (see for example ref[145] where exp. data for p-Ta interactions at 8 GeV/c are reported and discussed). This behaviour is not in contradiction with the Glauber approach, but rather reflects that more and more interactions with decreasing energy do not possess enough invariant mass to give rise to particle production, and do not show up as real interactions, therefore reducing the effective number of primary collisions. Models can tentatively take into account these effects by setting proper thresholds for the minimum energy carried by a chain and for the minimum momentum fraction carried by a parton. These thresholds are a sort of free parameters, which reflect our ignorance in treating the whole business with finite masses and energies, and they are usually set in such a way to achieve agreement with the experimental data in the transition region from ordinary INC (with just one primary interaction) to the full Glauber cascade.

5.12 Formation Zone

It has been known for many years that a plain treatment of INC at high energies, on the basis of elementary hadron-nucleon cross sections, overestimates measured particle yields, if the incident energy exceeds a few GeV[22,21]. In particular, experiments support the effect of some mechanism in limiting the reinteractions of energetic particles. In emulsion experiments for example, while

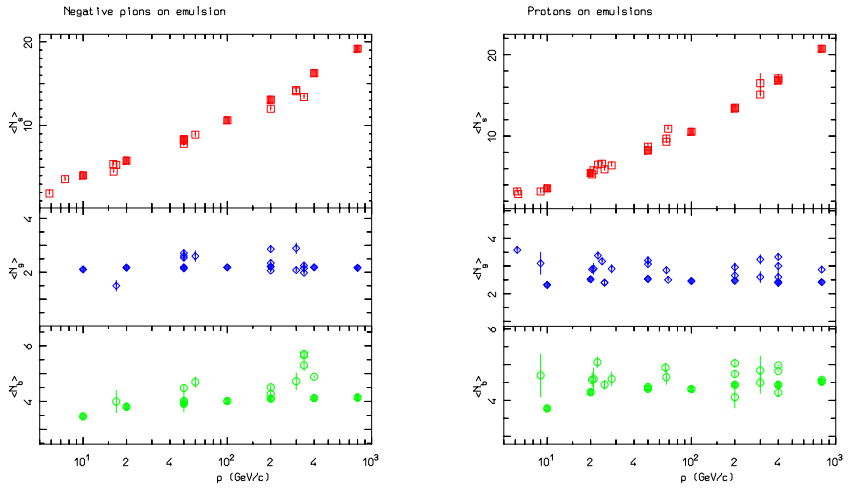

Figure 17: Shower, grey, and black tracks multiplicities for π^- (left) and protons (right) incident on emulsion, as a function of the projectile momentum. Open symbols are experimental data, full symbols are FLUKA results

shower particle multiplicities increase steadily with the energy of the primary particle, the multiplicities of grey and black tracks rapidly saturate at few tens of GeV, and stay constant (see fig. 17, the exp. data are taken from [146,147]). The physical mechanism which is believed to be at work in limiting high energy secondary reinteractions in nuclei, is the so called "formation zone" [92,148,149]. This concept has a strong analogy with the Landau-Pomeranchuk-Migdal [150] (LPM) effect which reduces electron bremsstrahlung and photon pair production at very high energies.

Naively, it can be understood considering that hadrons are composite objects and that the typical time of strong interactions is of the order of 1 fm (please note that space units are used for time in all this paragraph, $x = ct$). If one thinks about the hadrons emerging from an inelastic interaction, it requires some time to them to "materialize" and be able to undergo further interactions. The amount of time can be qualitatively estimated considering a secondary particle of mass M and of momentum components $p_{\|}$ and p_T with respect to the original projectile direction. Making a Lorentz transformation to the frame where the longitudinal momentum is null (remember that p_T is invariant under Lorentz transformations), the uncertainty principle tell us:

$$\bar{t} = \Delta t \approx \frac{\hbar}{E_T} = \frac{\hbar}{\sqrt{p_T^2 + M^2}} \tag{129}$$

This time interval can be translated into the particle proper time, τ, and the lab frame time, t, taking care of the Lorentz dilation among the various frames:

$$\tau = \frac{M}{E_T}\bar{t} = \frac{\hbar M}{p_T^2 + M^2} \tag{130}$$

$$t_{lab} = \frac{E_{lab}}{E_T}\bar{t} = \frac{E_{lab}}{M}\tau = \frac{\hbar E_{lab}}{p_T^2 + M^2} \tag{131}$$

The time interval in the lab frame can be also expressed as a function of the particle rapidity, y, by:

$$t_{lab} = \bar{t}\cosh y = \frac{\hbar}{\sqrt{p_T^2 + M^2}}\cosh y \tag{132}$$

If such an interaction takes place inside a nucleus, the condition for having (possible) reinteractions of our secondary particle is expressed by :

$$v \cdot t \leq R_A \approx r_0 A^{\frac{1}{3}} \tag{133}$$

Such an equation can be used to define a critical rapidity, above which particles have no chance to reinteract and will "materialize" already outside the nucleus. Inserting typical values for pions inside eq. 132, $E_T \approx 0.3$ GeV, $E \approx 10$ GeV, it can be easily checked that the formation time can easily exceed heavy nuclei radii. All this derivation must be taken with a lot of care: among all other uncertainties, it is not clear whether the particle entering the formulae must be the final one, or rather the "mother" resonance. Nevertheless the concept is very powerful, and using a scale factor for the formation time as a free parameter, very nice agreement for hadron-nucleus and nucleus-nucleus interactions have been obtained [149,151]. Examples of complete models including all effects described above can be found in [152,153].

6 Elastic Nuclear Interactions

The elastic scattering of nucleons on nuclei is normally described in terms of the optical model. An optical potential as described in sec. 5.3 is used to model the nucleus as a scattering centre. The potential is most frequently chosen as a sum of a central and a spin-orbit part, with a Woods-Saxon radial dependence for the real part, and a more periphery-peaked shaped imaginary part. The parameters of the optical potential are determined by fitting the existing data, after corrections for the Coulomb effect on proton scattering: they are found to vary both with A and with projectile energy.

The behaviour of the differential elastic cross section exhibits a shape similar to a diffraction pattern, and becomes more strongly forward peaked as the projectile energy increases. In first approximation, this pattern can be reproduced with the expression of the scattering from a grey disk. The formulae relevant for scattering from a grey disk can be obtained from Appendix B, for a purely real profile function ($\rightarrow$ a purely imaginary scattering amplitude), and assuming that:

$$\begin{aligned} \Gamma(b) &= 1-a, \quad b \leq R \\ \Gamma(b) &= 0, \quad b > R \end{aligned}$$

where R is the scattering sphere radius, and a gives the opacity of the sphere. Under these assumptions it is easy to show starting from the expressions reported in Appendix B, that:

$$\frac{\mathrm{d}\sigma}{\mathrm{d}\Omega} = (1-a)^2 R^2 \left[\frac{J_1(2kR\sin\theta/2)}{2\sin\theta/2} \right]^2 \tag{134}$$

and:

$$\begin{aligned} \sigma_{el} &= \pi R^2 (1-a)^2 \\ \sigma_r &= \pi R^2 (1-a^2) \\ \sigma_T &= 2\pi R^2 (1-a) \end{aligned}$$

For complete absorption $a = 0$, and the reaction cross section becomes equal to the geometrical one, and one half of the total one.

The same diffractive pattern is found in pion-nucleus scattering. At resonance, the diffraction minima and the total cross section can be very well described by the black disk formulation with $a = 0$, due to the strong pion-nucleus interaction.

At higher energies (> 1 GeV), the pion and nucleon elastic scattering on nuclei is more and more forward peaked: the first minimum of eq.134 is at $\theta \approx 0.61 \frac{h}{pR}$, that means that for a 1 GeV nucleon on Carbon it is situated at about 12°. Eventually, the usual exponential form becomes appropriate. One remark to be made is that these forward-peaked scatterings involve very small energy losses, thus the importance of elastic scattering on particle propagation becomes increasingly small at high energies.

Elastic Scattering in the Glauber Model

The formulae developed in the previous paragraphs can be used to derive a closed expression for the elastic scattering amplitude in the Glauber approach.

With a bit of algebra, and using approximation 106 with ρ and hN scattering amplitudes not depending on the nucleon type, it can be shown that:

$$f_{hA\ el}(\vec{q},s) = \frac{ik}{2\pi}\int d^2\vec{b}e^{i\vec{q}\cdot\vec{b}}\left\{1+ - \left[1-\frac{1}{2\pi ik}\int d^2\vec{q}\,'e^{-i\vec{q}\,'\cdot\vec{b}}f_{hN}(\vec{q}\,',s)F(\vec{q}\,')\right]^A\right\} \quad (135)$$

where F is the nuclear form factor, that is the Fourier transform of the nuclear density:

$$F(\vec{q}\,') = \int d^3\vec{r}e^{i\vec{q}\,'\cdot\vec{r}}\rho(\vec{r}) \quad (136)$$

In case of charged particle scattering, the previous expression should be properly modified to take into account interference with Coulomb scattering [138]. Similar expressions can be derived also for the quasielastic scattering amplitude.

Experimental examples of high energy hadron-nucleus elastic scattering and of its analysis in terms of Glauber scattering can be found in [130,131,132].

6.1 Examples of hadron-nucleus cross sections

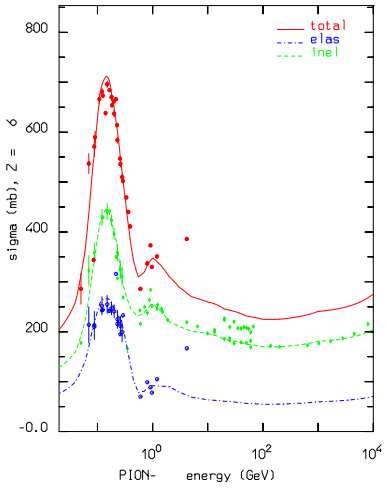

Figure 18: Total, elastic and inelastic cross section for negative pions on Carbon

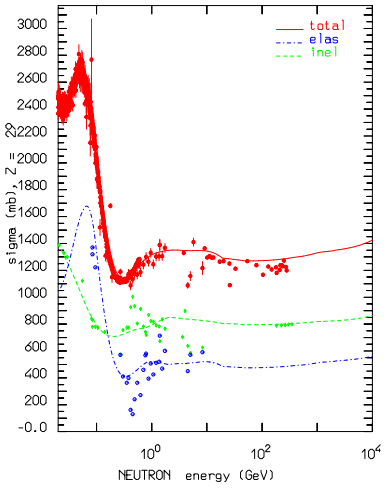

Figure 19: Total, elastic and inelastic cross section for neutrons on Copper

Actually hA cross sections at intermediate and high energies resemble the behaviour of the corresponding hN ones (see figs. 1 and 3), and this is not unexpected due to the strong relationship between σ_{hA} and σ_{hN} (see paragraph 5.11). The main differences are in the resonance region, where cross section features are smoothed by the Fermi motion, and at very high energies where the increase of hA cross sections is slower than in the corresponding hN ones. This feature can be easily explained in the Glauber model, observing that both total and absorption cross sections are determined by the probability of having at least one collision in the corresponding multiple scattering expansions. Moderate increases in the elementary hN cross section are therefore effective only for large impact parameters where this probability is small, while for more central collisions they simply result in an increase of the average number of collisions rather than in an increase of the cross section. Typical behaviours of cross sections for neutrons on Copper and for negative pions on Carbon are reported in figs. 18 and 19, together with some representative experimental data.

7 Practical Examples of (G)INC calculations

In the previous sections, a brief description of the processes occurring during hadronic inelastic interactions in the energy range of interest has been given. In the present section, a few representative comparisons between model results and experimental data on particle production in the energy range of interest are presented. All the presented results have been obtained with the last version of the FLUKA [40,41,27,42] code, and most of them rely on the model used for the intermediate energy range [27] and called PEANUT (PreEquilibrium-Approach-to-NUclear-Thermalization). As already explained, this model combines both an INC part, and a preequilibrium part. Nuclear potential effects (refraction and reflection) are modeled into the code, as well as quantum effects, like Pauli blocking, nucleon-nucleon correlations, fermion antisymmetrization, coherence length and formation zone. The results obtained with such a code are not at all representative of the majority of the INC models, usually based on some flavour of the Bertini INC code [21,29,30], or similar approaches. Among the available INC codes, possibly only CEM92 [28] and the LAHET version with the preequilibrium model included [26] can be compared with this model for nucleon induced interactions. For pion induced interactions, the approach of PEANUT is very different from all other mentioned codes, none of which includes a complex optical potential or absorption effects computed according to modern approaches [5,6,7] including three body absorption (for example, CEM92 [154] derives 2-body absorption cross sections just multiplying the deuteron one by a

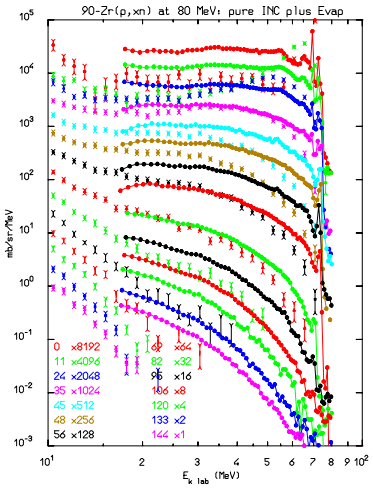

Figure 20: ^{90}Zr(p,xn) at 80.5 MeV, plain INC (see text) calculation

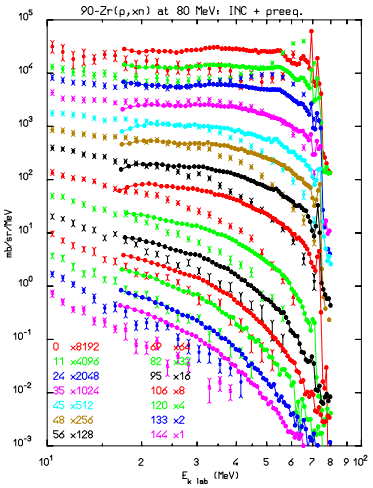

Figure 21: ^{90}Zr(p,xn) at 80.5 MeV, plain INC plus preequilibrium (see text) calculation

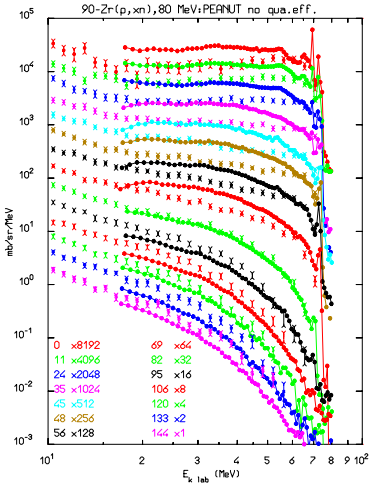

Figure 22: ^{90}Zr(p,xn) at 80.5 MeV, PEANUT (see text) calculation with no quantum effect, but Pauli blocking

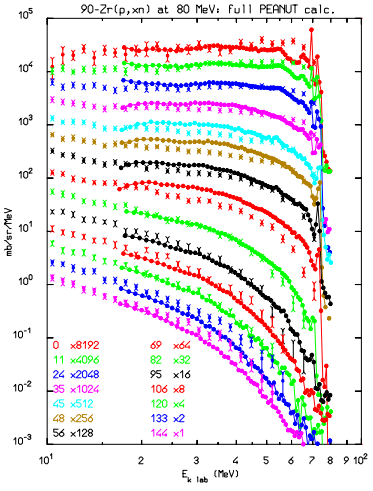

Figure 23: ^{90}Zr(p,xn) at 80.5 MeV, full PEANUT (see text) calculation

tunable factor, and uses a square well potential of fixed depth for pions).

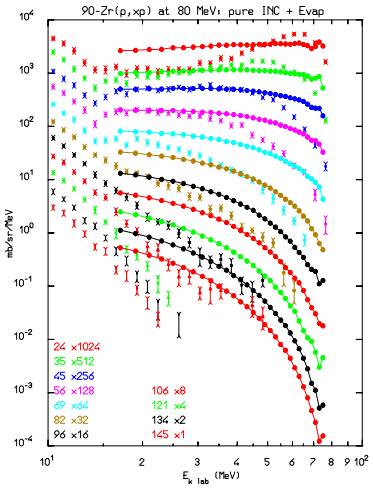

Figure 24: ^{90}Zr(p,xp) at 80.5 MeV, plain INC (see text) calculation

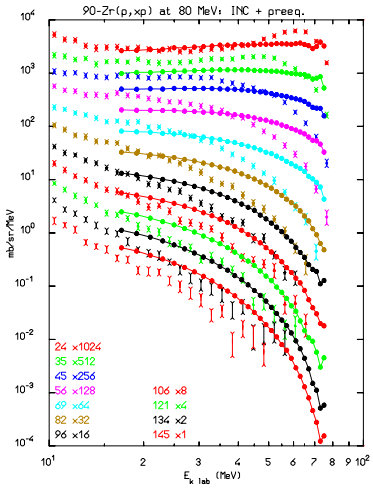

Figure 25: ^{90}Zr(p,xp) at 80.5 MeV, plain INC plus preequilibrium (see text) calculation

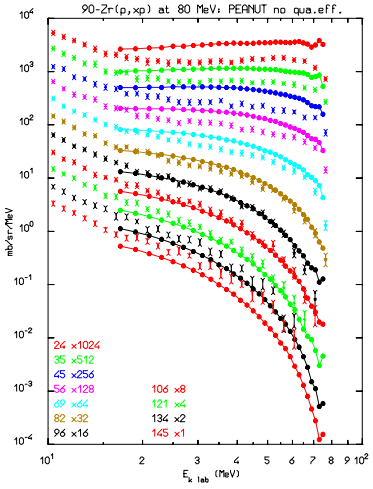

Figure 26: ^{90}Zr(p,xp) at 80.5 MeV, PEANUT (see text) calculation with no quantum effect, but Pauli blocking

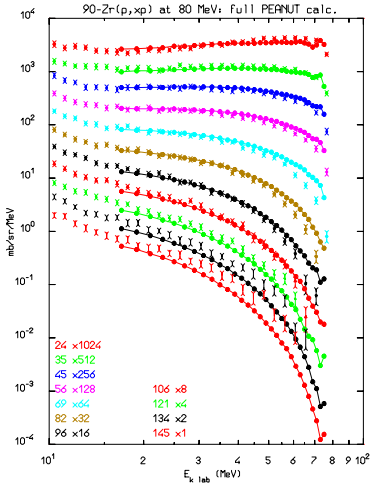

Figure 27: ^{90}Zr(p,xp) at 80.5 MeV, full PEANUT (see text) calculation

7.1 From plain INC to more Complex Models

In paragraph 3.3 a list of known weaknesses of INC codes has been presented. Here some examples are given, trying to illustrate the sources of such deficien-

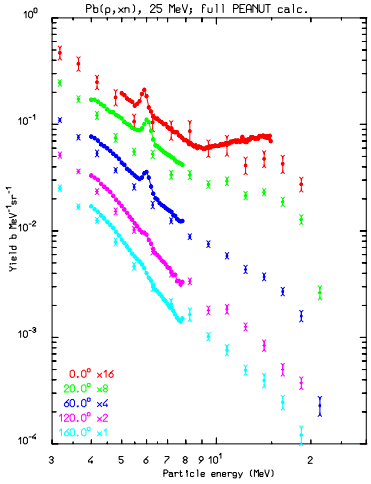

Figure 28: ^{208}Pb(p,xn) at 25 MeV, PEANUT calculation

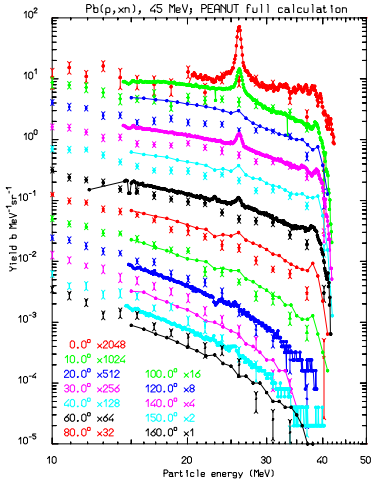

Figure 29: ^{208}Pb(p,xn) at 45 MeV, at several emission angles

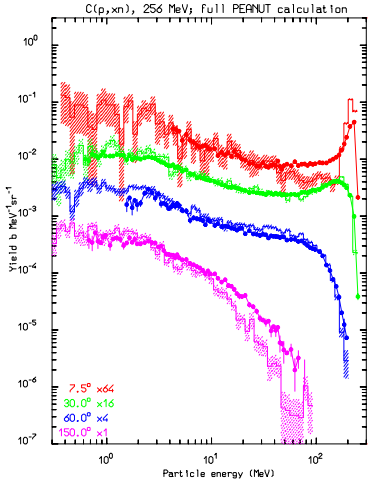

Figure 30: ^{12}C(p,xn) at 256 MeV, at several emission angles

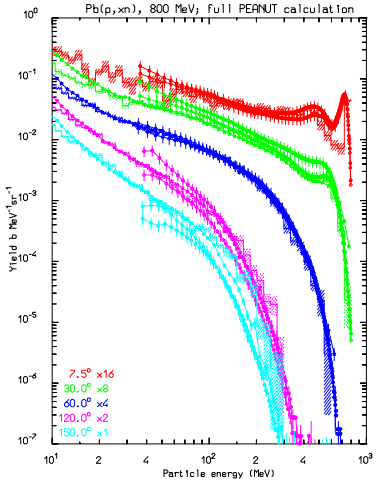

Figure 31: Pb(p,xn) at 800 MeV, at several emission angles

cies. Examples of the problems met by classical INC codes based on the plain Bertini model or similar approaches can be found in[36], PSI and Julich contributions, where the results of an intercomparison carried by the Nuclear Energy

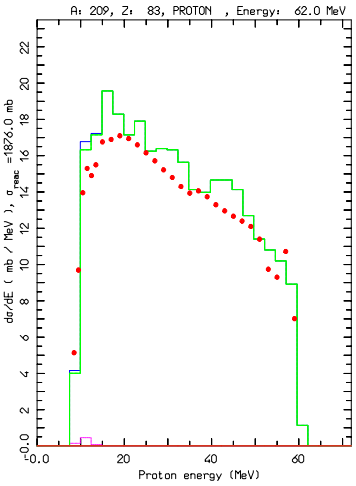

Figure 32: ^{209}Bi(p,xp) at 62 MeV, angle integrated spectrum preequilibrium only

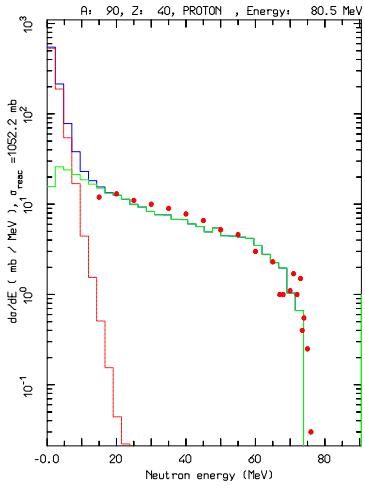

Figure 33: ^{90}Zr(p,xn) at 80.5 MeV, angle integrated spectrum preequilibrium only

Agency are reported. Results on ^{208}Pb(p,xn), and ^{90}Zr(p,xn), ^{90}Zr(p,xp) reactions where the topic of the intercomparison. The equivalent set of data computed with PEANUT , 1994 status, can be found in [155]. It is important to remind that the Bertini model does not include reflection or refraction, neither includes any preequilibrium stage. Furthermore an average binding energy is used throughout all cascading process without account for actual Q values of the different reaction channels.

In order to illustrate the effect of the various ingredients, the same projectile-target combination, 80.5 MeV protons on ^{90}Zr, has been computed under different assumptions and the results compared with experimental data [156,157]. Four different trials have been performed, always using PEANUT with all or only a few of the ingredients at work. The results of the exercise are presented in figs. 20,21,22,23, for (p,xn), and in figs. 24,25,26,27, for (p,xp). In all these figures as well as in following ones, experimental data are plotted as full symbols joined by a line, while model results are given or by symbols with error bars, or by histograms with shaded areas representing the statistical error.

The first attempt (figs. 20,24) has been performed using a plain INC approach with no preequilibrium stage, no refraction and reflection, and only Pauli blocking activated among the quantum effects. The transport threshold for secondary nucleons was set equal to the average binding energy. As can be easily seen results are very poor, with an overestimation of the forward peak

and a strong underestimation of backward angle emission. These results have been obtained with assumptions which are quite consistent with those used by the Bertini model, but the binding energy which, as usual in PEANUT , has been correctly set at each emission stage to match the actual reaction Q-value. This is the explanation, maybe paradoxically, of the slightly worse results of this trial at medium/large angles with respect for example to the PSI contribution in [36]. The use of a constant binding energy value in [36] overestimates the available ejectile energy of about 6.9 MeV, shifting the spectra of the same amount towards larger energies.

The second trial does not yet use refraction and reflection, but the preequilibrium stage is there. There is a clear improvement in the results, particularly at backward angles, but still there are large discrepancies.

The third trial has been performed switching on all the refraction and reflection business, but still limiting the quantum effects to Pauli blocking alone. There is a great improvement, with still discrepancies at the forward angles, but a reasonable description of backward ones. The reason for these last deficiencies is related to the effect of particle curvature in the nucleus which both increases the particle track length and hence the reinteraction probability, and at the same time "pushes" particles towards the nucleus centre, again increasing the interaction probability.

The fourth and last trial has been performed with all quantum effects on, that is with coherence length, nucleon correlation, and fermion antisymmetrization effects on. Clearly these are effective in increasing particle mean free paths in the nuclear medium resulting in a quite reasonable description of the whole spectrum at all angles (see also [93] for the effect of nucleon correlations).

The effect of particle curvature on interaction rates are typical of INC codes which include refraction and reflection [23]. The reason for the good results, at least for angle integrated spectra, of INC models based on straight trajectories (like the Bertini INC) probably lies in the compensating effect of the lack both of mechanisms able to lengthen particle mean free paths, and of the curvature effect which operates in the opposite direction. The price is the poor description of angular distributions, at least for energies not much larger than typical potential energies. Such a picture is consistent with what has been already reported in the literature [31,33,34,35].

Other examples of complete calculations of neutron double differential spectra are reported in figs. 28,29,30, and 31. The experimental data have been taken from ref. [33,35,158,160]. It is particularly interesting to note that in the PEANUT model at 25 MeV incident energy no INC stage is performed and all the emission is due to preequilibrium. At 45 MeV the INC stage starts to con-

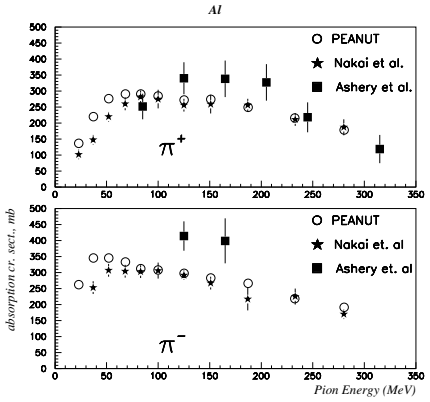

Figure 34: Pion absorption cross section on Aluminum as a function of energy

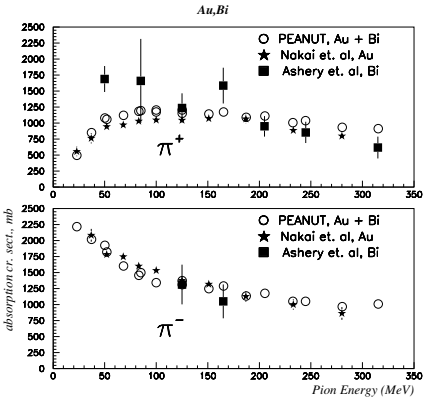

Figure 35: Pion absorption cross section on Gold or Bismuth as a function of energy

tribute (compare fig. 29 with ref.[35] to appreciate the improvement over plain INC models), while at higher energies it dominates the most energetic part of the spectra. Neutron double differential spectra following C(p,xn) at 256 MeV (exp. data from[33]), and Pb(p,xn) at 800 MeV (exp. data from[158,160]) are presented in figs. 30,31. In the latter figure three experimental curves are drawn, two come from[160] and correspond to two possible choices for the efficiencies of the scintillators used in the experiment, the third one comes from[158]. The relative disagreement among these curve can give an idea of the experimental uncertainties in this energy range. An inspection of the literature data for 113, 256, 597, and 800 MeV proton energies[31,33,158,159], shows how "classical" INC are more and more reliable with increasing energy. However, it must be taken into account that the onset of the effects discussed in paragraph 5.10, and the need for physical models other than those based on isobar production and decay (see paragraph 4.4,4.5), limit the validity range to a maximum of 1.5–3 GeV.

Two examples of angle integrated spectra computed with the preequilibrium model alone (no INC) are reported in fig. 32, and 33, for ^{209}Bi(p,xp) at 62 MeV and ^{90}Zr(p,xn) at 80.5 MeV (exp. data from refs.[34] and[156] respectively). Again a comparison with the Bertini results reported in the original reference shows the superior capabilities of preequilibrium models in this energy range. Examples about pion absorption are presented in figs. 34,35 and fig. 36. The former two figures show the experimental[162,161] and calculated absorption cross section for incident π^+ and π^- on Aluminium, and on

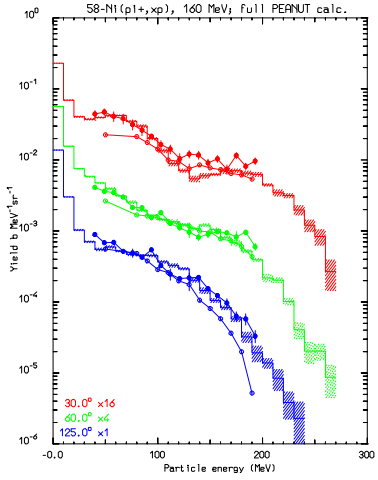

Figure 36: ^{58}Ni(π^+,xp) at 160 MeV, at several emission angles. Symbols exp. data from [163,164], dahsed histogram PEANUT calculations

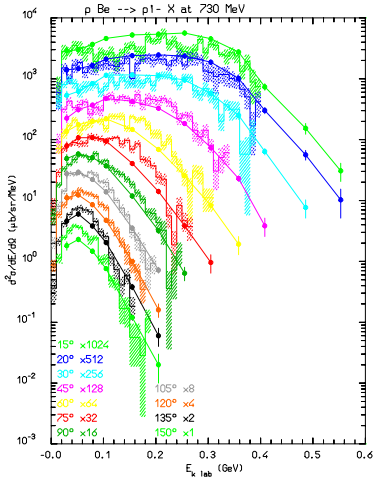

Figure 37: Double differential distribution of negative pions in the reaction p+Be at 730 MeV. Dashed histograms are PEANUT results, points are experimental data [165]

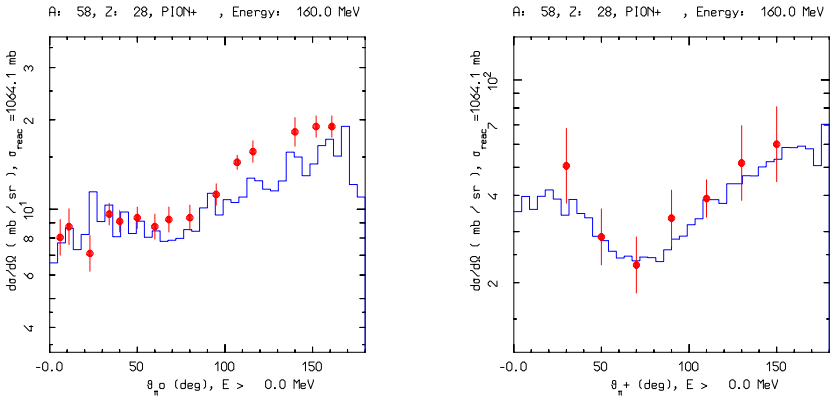

Figure 38: Angular distribution of positive (right) and neutral (left) pions following ^{58}Ni(π^+,π^+x) and ^{58}Ni(π^+,π^0x)

Bismuth and Gold. The comparison is made on an absolute scale, since the calculated results have been obtained making use of the capability of PEANUT (as of all other INC models) of computing reaction cross sections. The latter

figure presents the double differential emission spectrum of protons, following π^+ interactions on ^{58}Ni at 160 MeV (exp. data from [163,164]). The contribution of absorption in the energetic part of the spectra is evident.

An example of pion production at intermediate energy is reported in fig. 37, where calculated and experimental [165] double differential negative pion yields are compared for the reaction ^{9}Be(p,π^-x) at 730 MeV. An example of pion inelastic and charge exchange scattering in the Δ region is reported in fig. 38, where the calculated and experimental [166,167] angular distributions of positive and neutral pions for ^{58}Ni(π^+,πx) are shown.

Finally two examples for high energy interactions, besides those already discussed in the previous sections, are presented in figs. 39 and 40. The former presents the multiplicity distribution of negative shower particles emitted by 250 GeV positive kaons on Aluminium and Gold targets [134]: this distribution if of course mainly sensitive to the details of the Glauber cascade undergone by the projectile into the target nucleus. The latter is instead related to intranuclear cascading and shows the mutual correlations of black and grey tracks [168].

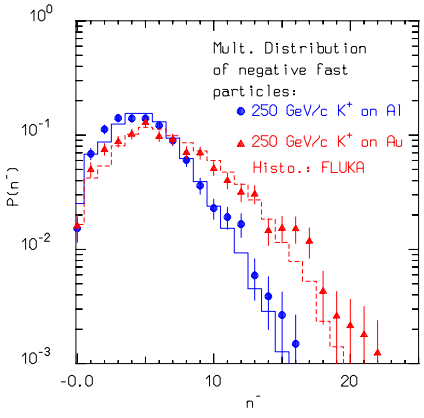

Figure 39: Multiplicity distribution of neagtive shower particles for 250 GeV/c K^+ on Aluminium and Gold targets. Symbols exp. results [134], histo FLUKA results

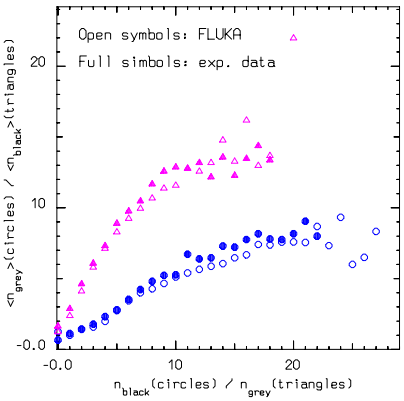

Figure 40: Mutual correlations ($< n_g >$ vs n_b and $< n_b >$ vs n_g) between black and grey charged tracks for 400 GeV/c p on emulsion. Full symbols are exp. data from [168]

7.2 Residual Nuclei

The problem of a reliable description of individual isotopes produced in spallation reactions is still an open one. While the general features of the residual nuclei distributions are usually well reproduced by INC with the possible

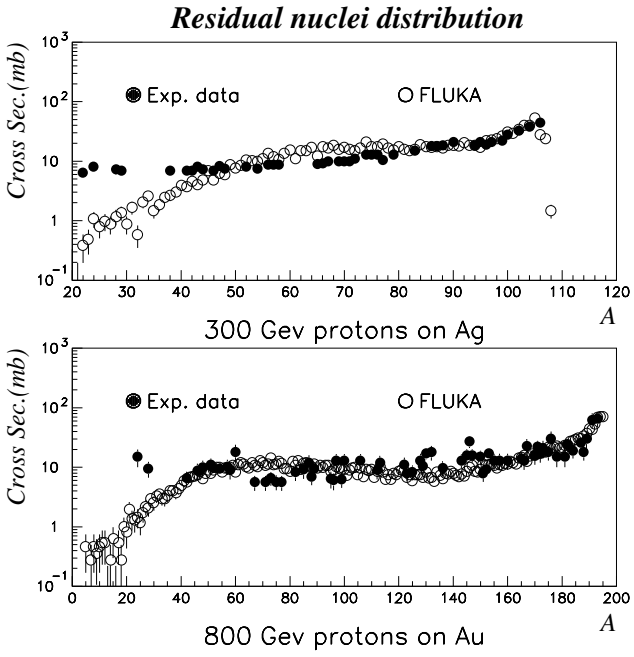

Figure 41: Residual nuclei mass distribution. Experimental data are from [169] for silver, and [170] for gold.

exception of fragmentation products, (see paragraph 5.8), predictions on individual isotopes can be out of large factors. Many reasons contribute to this uncertainty:

- Slight inaccuracies in excitation energy spectra reaching the evaporation stage can results in small shifts in particle multiplicities, but in substantial shifts among close isotope yields
- The lack of spin and parity dependent (Hauser-Feshbach) calculations in the last stage can also bias the very last steps and hence the final residual nucleus
- Charged particle emission channels of low probability can be badly reproduced because of sub-barrier effects etc
- No prediction about metastable states is possible

- Fragmentation is usually not included

Besides these physical reasons, there are also "technical" ones. What is often required when looking for residual nuclei production, is the production cross section of some specific isotopes, for example because of its toxicity or long life time etc, which however can be a very small fraction of the total reaction cross section. Therefore a good agreement over the gross part of emission spectra is not at all a proof of a similar agreement on some specific and relatively unlikely isotope production channel. Sticking however at our previous statement, that

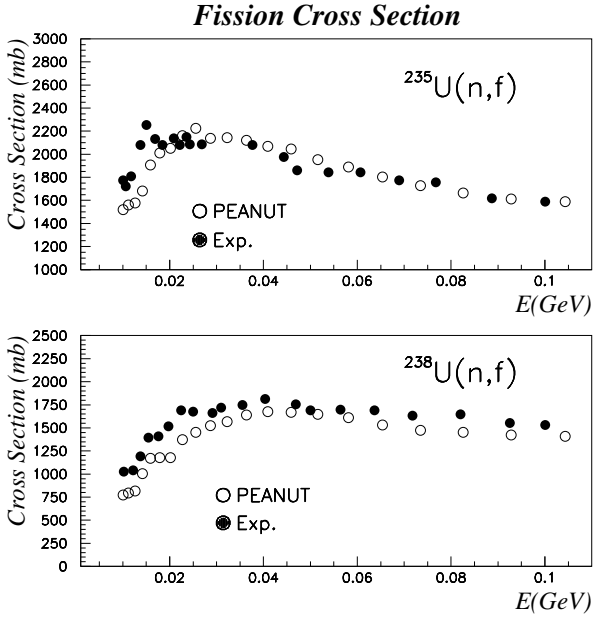

Figure 42: Neutron induced fission cross sections on Uranium. Experimental data are from [171]

is that the general features of isotope production are reasonably reproduced, in fig. 41 the computed and measured mass distributions of residuals after 300 GeV proton interactions on Silver, and 800 GeV protons on Gold are shown. The agreement is fairly good in the spallation region close to the target mass, and still reasonable down to very light masses where the lack of fragmentation in the model shows up clearly.

Fission models developed for INC codes often contain "ad hoc" parameters

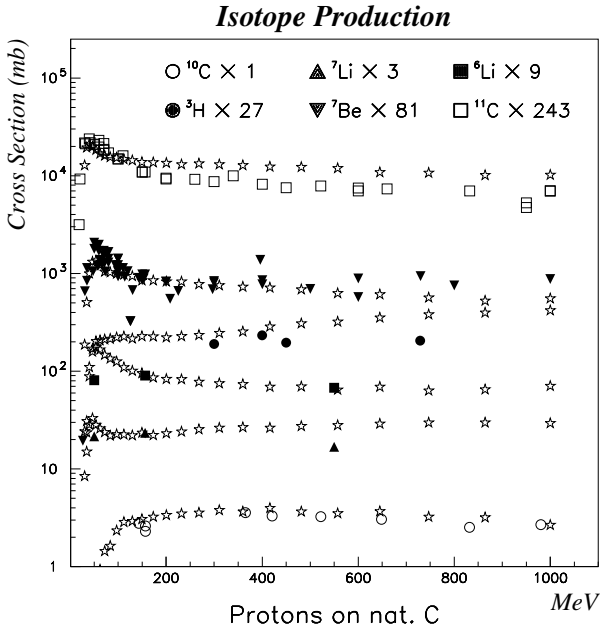

Figure 43: Residual nuclei excitation functions. Experimental data are from [114,172] with various symbols, open stars are PEANUT results

to adjust the calculations, like the unphysical reduction factor that was applied to the fission width in the original Atchison work [155] for the Bertini model. This excitation-dependent factor was introduced in HETC to cut off the fission process at high excitation energies and bring the calculations in agreement with measured data. Our explanation is that an INC without preequilibrium emission leads to an average overestimation of the nuclear excitation energy at the equilibrium stage. This is not the case for PEANUT , and the agreement with experiment is nice without any arbitrary factor, as shown in fig. 42 for Uranium (exp. data from [171]).

Regarding light nuclei, the inclusion of Fermi Break–up allows reasonable predictions about residual nuclei also for light nuclei, which are known to be "difficult" targets. In fig. 43 the excitation functions for the production of different isotopes by proton bombardment of Carbon are shown (exp. data from [114,172]. The evaporation model alone could never have explained the abundance of isotopes like ^{7}Be, while it would have grossly overestimated the

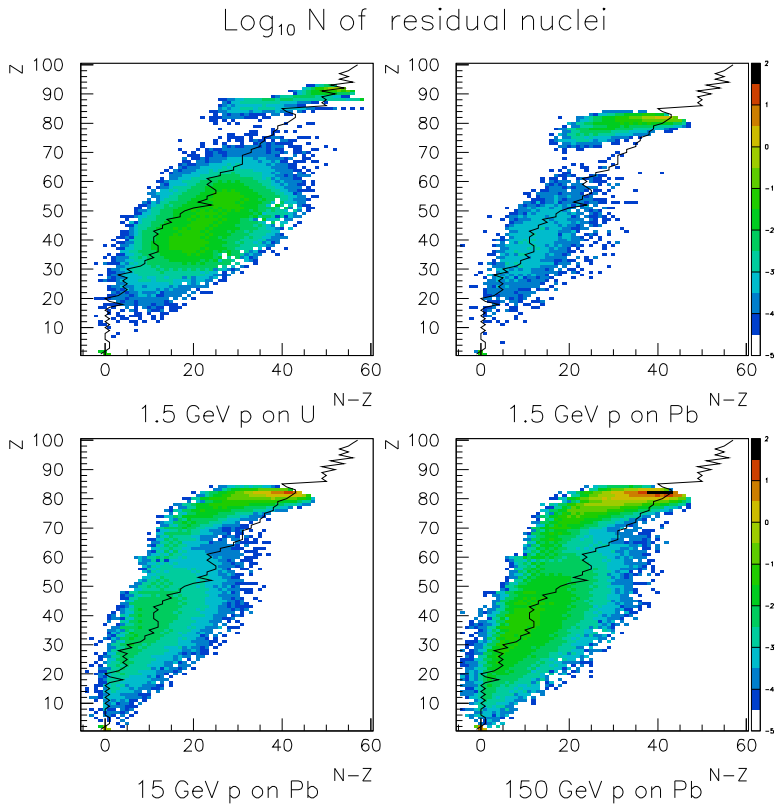

Figure 44: Residual nuclei distribution produced by proton cascades on Pb and U at different energies. Only residuals produced by all particles but neutrons below 20 MeV are presented. The abscissa is the neutron excess, N-Z, and the ordinate the atomic number Z. The stability line is also shown.

emission of neutrons α particles.

As an example of the inventory of residual nuclei produced by whole high energy cascades, in fig. 44 the residual nuclei distributions produced by protons of 1.5 GeV on a depleted Uranium target, and of 1.5, 15, and 150 GeV on a natural Lead target are presented. The isotopes shown, are only those produced by particles other than low energy neutrons (those below 20 MeV).

A few important features can be seen in these plots, taking into account that neutron-rich isotopes sit to the right of the stability line, and proton-rich

ones to the left:

- The fission zone in the U plot, and to a lesser extent also in the Pb, 1.5 GeV one
- The spallation zone, with the characteristic peak close to the original target A and Z, populated mainly by proton-rich isotopes
- The increasing extension of the spallation zone with increasing energy

The production of proton-rich isotopes is one of the distinct features of spallation induced by energetic particle. It is mainly due to the reduced emission probability of charged particles in the evaporation stage, due to the Coulomb barrier. A last word must be spent about the life times of these impressive inventories of nuclides: a good fraction of them are very short half-life ones, created relatively far from the stability line. Codes able to model the evolution with time of such inventories are therefore required for a proper evaluation of incineration rates or other effects of interest. However a bit of caution must always be taken when considering INC code results on residual nuclei, particularly for isotopes far from the original target.

Acknowledgments

The authors are greatly indebted to A. Fassò and J. Ranft for the many stimulating discussions and the continuous support, and to dr. G. Reffo for the invitation to give this lecture.

Appendix A: useful kinematical quantities

It is customary in high energy physics to make use of a few "strange" kinematical variables to describe particle kinematical properties. Let us assume to deal with a particle, c, of mass M, total energy E, and momentum $\vec{p} = (p\sin\theta\cos\phi, p\sin\theta\sin\phi, p\cos\theta)$, possibly emerging from an interaction of the kind $a + b \rightarrow c + X$. From, now variable with an asterisk (e.g. E^*, p^*) are supposed to be evaluated in the Centre of Mass System (CMS) of the collision, variables labelled with $_L$ are suppose to be computed in the lab frame (that is the frame where particle b is at rest), and variables with no particular labelling can be in whichever frame. Four-momenta are indicated by tilded characters, and are defined by:

$$\tilde{p}_a \equiv (E_a, \vec{p}_a) \tag{137}$$

$$\tilde{p}_a \cdot \tilde{p}_b = E_a E_b - \vec{p}_a \cdot \vec{p}_b \tag{138}$$

$$\tilde{p}_a^{\,2} \equiv \tilde{p}_a \cdot \tilde{p}_a = M_a^2 \tag{139}$$

The invariant mass squared of the system, s, ($\sqrt{s} \equiv$ the total energy of the system in the CMS frame) is given by:

$$s = (E_a^* + E_b^*)^2 = (E_a + E_b)^2 - (\vec{p}_a + \vec{p}_b)^2 = M_a^2 + M_b^2 + 2M_b E_{aL} \tag{140}$$

In particular, for $a+b \to c+d$, it is customary to use the Mandelstam invariants:

$$s \equiv (\tilde{p}_a + \tilde{p}_b)^2 = (\tilde{p}_c + \tilde{p}_d)^2 \tag{141}$$
$$t \equiv (\tilde{p}_a - \tilde{p}_c)^2 = (\tilde{p}_d - \tilde{p}_b)^2 \tag{142}$$
$$u \equiv (\tilde{p}_a - \tilde{p}_d)^2 = (\tilde{p}_c - \tilde{p}_b)^2 \tag{143}$$

which are related by:

$$s + t + u = M_a^2 + M_b^2 + M_c^2 + M_d^2 \tag{144}$$

The 4-momentum transfer t in case of elastic scattering is simply related to the 3-momentum transfer $\vec{q} = \vec{p}_c^{\,*} - \vec{p}_a^{\,*}$ and to the scattering angle θ^* in the centre-of-mass frame by:

$$t = -\vec{q}^{\,2} = -2p^{*\,2}(1 - \cos\theta^*) \tag{145}$$
$$q = 2p^* \sin\frac{\theta^*}{2} \tag{146}$$

The Lorentz transformation required to go from the original frame to another one moving with velocity $\vec{v}$ with respect to the first one, are given by:

$$\vec{\beta} = \frac{\vec{v}}{c} \tag{147}$$
$$\gamma = \frac{1}{\sqrt{1 - \vec{\beta}^2}} \tag{148}$$
$$\vec{\eta} = \vec{\beta}\gamma, \ (\gamma^2 - \vec{\eta}^{\,2} = 1) \tag{149}$$
$$\vec{p}\,' = \vec{p} - \vec{\eta}\left(E - \frac{\vec{\eta}\cdot\vec{p}}{\gamma + 1}\right) \tag{150}$$
$$E' = \gamma E - \vec{\eta}\cdot\vec{p} \tag{151}$$

The inverse transformation is readily obtained exchanging non-primed variables with primed ones, and $\vec{\eta} \to -\vec{\eta}$. In particular, for a system of particles

with total energy E_{tot}, and total momentum $\vec{p}_{tot}$, the transformation to the Center of Mass System can be accomplished using:

$$\gamma_{CM} = \frac{E_{tot}}{\sqrt{s}} \tag{152}$$

$$\vec{\eta}_{CM} = \frac{\vec{p}_{tot}}{\sqrt{s}}, (s = E_{tot}^2 - \vec{p}_{tot}^{\,2}) \tag{153}$$

The single particle inclusive cross section for particle c is defined as:

$$\sigma_{inv} = E_c \frac{d^3\sigma_{ab}}{d^3\vec{p}_c}\left(\sqrt{s}, p_\parallel^*, p_T\right) \equiv F_{ab}^c\left(\sqrt{s}, p_\parallel^*, p_T\right) \tag{154}$$

where the labels a, b, c are there just to remind that this is the inclusive distribution of particle c after an interaction with particle a impinging on particle b. Such a distribution is often called the *invariant cross section*, since $\frac{d^3\vec{p}}{E}$ can be shown to be Lorentz invariant, and therefore:

$$E_c^* \frac{d^3\sigma}{d^3\vec{p}_c^*} = E_c \frac{d^3\sigma}{d^3\vec{p}_c} \tag{155}$$

The transverse momentum p_T and the transverse mass E_T or M_T (which are all invariant under Lorentz transformation), are defined by:

$$p_T = p\sin\theta = \sqrt{E^2 - M^2}\sin\theta \tag{156}$$

$$M_T = E_T = \sqrt{p_T^2 + M^2} \tag{157}$$

The longitudinal momentum, $p_\parallel$ is instead frame dependent. A very useful quantity connected with longitudinal momentum is the so called x Feynman variable, defined as the ratio of the particle longitudinal momentum and the maximum possible longitudinal momentum, in a given frame, usually assumed to be the CMS (but sometimes also the lab frame is used):

$$x_F^* = \frac{p_\parallel^*}{p_\parallel^*(Max)} \approx \frac{2p_\parallel^*}{\sqrt{s}} \tag{158}$$

Please note that $-1 \leq x_F^* \leq 1$. The regions $x_F^* > 0$ and $x_F^* < 0$ are usually called the *projectile fragmentation region*, and the *target fragmentation region*, the region $x_F^* \sim 0$ is called the *central region*. The *hypothesis of limiting fragmentation*[53] supposes that in the projectile and target fragmentation regions the following scaling holds (see eq. 154):

$$F_{ab}^c\left(\sqrt{s}, p_\parallel^*, p_T\right) \overset{\sqrt{s}\to\infty}{\to} \bar{F}_{ab}^c\left(x_F^*, p_T\right) \tag{159}$$

A stronger version of the scaling hypothesis, due to Feynman, assumes that such a scaling holds also in the central region. As a consequence $\bar{F}^c_{ab}(0, p_T))$ is energy independent, and the produced particle multiplicity can be shown to scale like $< n_{ab} > \propto n_0 + n_1 \ln s$. Both predictions are violated, but they can be used as order of magnitude guesses without too much danger. Other variables very frequently used are the *rapidity*, y (dy is again Lorentz invariant, that is ys differ in different frames only of a constant factor), and the *pseudorapidity*, η, whose major (and unique) advantages are that it can be easily measured and it coincides with rapidity for $p_T \gg M$

$$y = \mathrm{acosh}(\frac{\mathrm{E}}{\mathrm{M_T}}) = \mathrm{atanh}(\frac{\mathrm{p_\parallel}}{\mathrm{E}}) = \frac{1}{2}\ln\left(\frac{\mathrm{E}+\mathrm{p_\parallel}}{\mathrm{E}-\mathrm{p_\parallel}}\right) \tag{160}$$

$$\eta = -\ln\left(\tan\frac{\theta}{2}\right) = \frac{1}{2}\ln\left(\frac{p+p_\parallel}{p-p_\parallel}\right) \tag{161}$$

Appendix B: partial waves and cross sections

Let us start from the standard partial wave expansion of the scattering amplitude f for a spinless scattering:

$$f_{cm}(t,s) = \frac{1}{k_{cm}}\sum_{l=0}^{\infty}(2l+1)\,P_l(\cos\theta)\,\frac{\eta_l \mathrm{e}^{2\mathrm{i}\delta_l}-1}{2\mathrm{i}} \tag{162}$$

where cm indicates the centre of mass system, k_{cm} is given by

$$k_{cm} = k = \frac{p_{cm}}{\hbar} = \frac{1}{\lambda\!\!\!^{-}} \tag{163}$$

and η_l, δ_l are real with $0 \leq \eta_l \leq 1$. The last condition follows from flux conservation and it is often called the *unitarity* condition. The physical interpretation of η_l's (often called *inelasticities*) is the following: they are linked to the fraction of the incident wave which survives the scattering (therefore they must be ≤ 1) or conversely $1-\eta_l^2$ is the fraction of the incident flux which is removed by inelastic processes. Indeed $\eta_l \to 0$ maximizes the reaction cross section for the lth partial wave, while $\eta_l \to 1$ implies purely elastic (or charge exchange when possible) scattering. Introducing:

$$a_l = \frac{\eta_l \mathrm{e}^{2\mathrm{i}\delta_l}-1}{2\mathrm{i}} = \frac{S_l - 1}{2\mathrm{i}} \tag{164}$$

$$\mathrm{Re_l} = -\eta_l\frac{\sin 2\delta_l}{2} = \frac{\mathrm{Im(S_l)}}{2} \tag{165}$$

$$\mathrm{Ima_l} = \frac{1-\eta_l\cos 2\delta_l}{2} = \frac{1-\mathrm{ReS_l}}{2} \tag{166}$$

$$\tag{167}$$

the expansions for the scattering amplitude and the total, elastic and reaction cross sections, σ_T, σ_{el} and $\sigma_r = \sigma_T - \sigma_{el}$, can be written as:

$$\begin{aligned} f_{cm}(\theta) &= \lambda\!\!\!^{-}\sum_{l=0}^{\infty}(2l+1)a_l P_l(\cos\theta) \qquad (168)\\ &= \lambda\!\!\!^{-}\sum_{l=0}^{\infty}(2l+1)\frac{S_l-1}{2\mathrm{i}}P_l(\cos\theta)\\ &= \lambda\!\!\!^{-}\sum_{l=0}^{\infty}(2l+1)\frac{\eta_l\,\mathrm{e}^{2\mathrm{i}\delta_l}-1}{2\mathrm{i}}P_l(\cos\theta) \end{aligned}$$

$$\begin{aligned} \sigma_T = \frac{4\pi}{k_{cm}}\mathrm{Imf_{cm}}(0) &= 4\pi\lambda\!\!\!^{-2}\sum_{l=0}^{\infty}(2l+1)\mathrm{Ima_l} \qquad (169)\\ &= 2\pi\lambda\!\!\!^{-2}\sum_{l=0}^{\infty}(2l+1)(1-\mathrm{ReS_l})\\ &= 2\pi\lambda\!\!\!^{-2}\sum_{l=0}^{\infty}(2l+1)(1-\eta_l\cos 2\delta_l) \end{aligned}$$

$$\begin{aligned} \sigma_{el} = \int_{4\pi}\mathrm{d}\Omega|\mathrm{f_{cm}}(\theta)|^2 &= 4\pi\lambda\!\!\!^{-2}\sum_{l=0}^{\infty}(2l+1)|a_l|^2 \qquad (170)\\ &= \pi\lambda\!\!\!^{-2}\sum_{l=0}^{\infty}(2l+1)|1-S_l|^2\\ &= \pi\lambda\!\!\!^{-2}\sum_{l=0}^{\infty}(2l+1)(1+\eta_l^2-2\eta_l\cos 2\delta_l) \end{aligned}$$

$$\begin{aligned} \sigma_r = \sigma_T - \sigma_{el} &= 4\pi\lambda\!\!\!^{-2}\sum_{l=0}^{\infty}(2l+1)(\mathrm{Ima_l}-|\mathrm{a_l}|^2) \qquad (171)\\ &= \pi\lambda\!\!\!^{-2}\sum_{l=0}^{\infty}(2l+1)(1-|S_l|^2)\\ &= \pi\lambda\!\!\!^{-2}\sum_{l=0}^{\infty}(2l+1)(1-\eta_l^2) \end{aligned}$$

When a large number of partial waves are involved, it is convenient to re-

sort to the so called *impact parameter representation*, which is readily obtained from the previous formulae with the following substitutions:

$$\lim_{l>>1, or \theta<<1} P_l(\cos\theta) = \mathrm{J}_0\left[(2\mathrm{l}+1)\sin\frac{\theta}{2}\right] \tag{172}$$

$$b = \frac{l+\frac{1}{2}}{k} = (l+\frac{1}{2})\lambda\!\!\!^{-} \tag{173}$$

$$f(\theta) \to f(q,s) \tag{174}$$

$$a_l \to a(b,s) \tag{175}$$

$$\eta_l \to \eta(b) = \mathrm{e}^{-\mathrm{Im}\chi(\mathrm{s,b})} \tag{176}$$

$$\delta_l \to \delta(b) = \frac{\mathrm{Re}\chi(\mathrm{s,b})}{2} \tag{177}$$

hence

$$\begin{aligned} kb &= l+\frac{1}{2} \\ (2l+1)\sin\frac{\theta}{2} &= qb \\ (2l+1)P_l(\cos\theta) &\approx 2kb\ \mathrm{J}_0(\mathrm{qb}) \\ \sum_{l=0}^{\infty} &\to \int_0^{\infty} \mathrm{dl} = \int_0^{\infty} \mathrm{k\ db} \\ f(q,s) &= k\int_0^{\infty} \mathrm{d^2b\ J}_0(\mathrm{qb})\ \mathrm{a(b,s)} \\ &= \mathrm{ik}\int_0^{\infty} \mathrm{bdb\ J}_0(\mathrm{qb})\left[1-\mathrm{e}^{\mathrm{i}\chi(\mathrm{b,s})}\right] \end{aligned} \tag{178}$$

where we used the momentum transfer q (for a definition of q and of the four-momentum transfer t see Appendix A), and the complex phase shift $\chi(b,s)$, according to:

$$a(b,s) = \frac{\mathrm{e}^{\mathrm{i}\chi(\mathrm{b,s})}-1}{2\mathrm{i}} \tag{179}$$

and we made explicit the dependence on the centre–of–mass squared energy s. Furthermore, making use of one of the many explicit definitions of the Bessel function J_0

$$\mathrm{J}_0(\mathrm{z}) = \frac{1}{2\pi}\int_0^{2\pi} \mathrm{e}^{\mathrm{iz}\cos\phi}\mathrm{d}\phi \tag{180}$$

one can write:

$$f(\vec{q},s) = \frac{\mathrm{ik}}{2\pi} \int \mathrm{d}^2\vec{\mathrm{b}}\ \mathrm{e}^{\mathrm{i}\vec{\mathrm{q}}\cdot\vec{\mathrm{b}}} \left[1 - \mathrm{e}^{\mathrm{i}\chi(\vec{\mathrm{b}},\mathrm{s})}\right], \quad \mathrm{d}^2\vec{\mathrm{b}} = \mathrm{bdbd}\phi \tag{181}$$

where $\vec{b}$ is a vector perpendicular to the incident momentum $\vec{k}$ which is the analogue of the classical impact parameter between the incident particle and the scattering centre, and the assumption $\vec{q}\cdot\vec{b} = qb\cos\phi$ has been made. Eq. 181 is usually called the *impact parameter representation* of the scattering amplitude. The relations between q, Ω and t are the following (being ϕ and θ the azimuthal and polar angle of the scattered particle):

$$\mathrm{d}\Omega = \mathrm{d}\cos\theta\mathrm{d}\phi = 2\mathrm{d}\sin^2\frac{\theta}{2}\mathrm{d}\phi = \frac{\mathrm{qdqd}\phi}{\mathrm{k}^2} \tag{182}$$

$$\frac{\mathrm{d}\Omega}{\mathrm{dt}} = \frac{\pi}{k^2} \tag{183}$$

$$\sigma_{el}(s) = \int \mathrm{d}\Omega|\mathrm{f}|^2 = \frac{1}{k^2}\int \mathrm{d}^2\mathrm{q}\ |\mathrm{f}(\vec{\mathrm{q}},\mathrm{s})|^2 \tag{184}$$

in which $\mathrm{d}^2\vec{\mathrm{q}} = \mathrm{qdqd}\phi$ is a two-dimensional element of integration in the plane perpendicular to $\vec{k}$. It is also customary to introduce the *profile function* $\Gamma(\vec{b},s)$, defined by:

$$\Gamma(\vec{b},s) = 1 - \mathrm{e}^{\mathrm{i}\chi(\vec{\mathrm{b}},\mathrm{s})} \tag{185}$$

Comparing eqs. 181 and 185, it is obvious that the profile function is the scattering amplitude in impact parameter space, that is the Fourier transform of the scattering amplitude $f(\vec{q},s)$:

$$\Gamma(\vec{b},s) = \frac{1}{2\pi\mathrm{ik}}\int \mathrm{d}^2\vec{\mathrm{q}}\ \mathrm{e}^{-\mathrm{i}\vec{\mathrm{q}}\cdot\vec{\mathrm{b}}}\mathrm{f}(\vec{\mathrm{q}},\mathrm{s}) \tag{186}$$

$$f(\vec{q},s) = \frac{\mathrm{ik}}{2\pi}\int \mathrm{d}^2\vec{\mathrm{b}}\ \mathrm{e}^{\mathrm{i}\vec{\mathrm{q}}\cdot\vec{\mathrm{b}}}\Gamma(\vec{\mathrm{b}},\mathrm{s}) \tag{187}$$

Introducing the analogue of S_l:

$$S(\vec{b},s) = \mathrm{e}^{\mathrm{i}\chi(\vec{\mathrm{b}},\mathrm{s})} = \eta(\vec{\mathrm{b}},\mathrm{s})\mathrm{e}^{2\mathrm{i}\delta(\vec{\mathrm{b}},\mathrm{s})} \tag{188}$$

the following relations defining the *S-matrix* approach, hold;

$$S(s) = \int \mathrm{d}^2\vec{\mathrm{b}}\ \mathrm{e}^{\mathrm{i}\chi(\vec{\mathrm{b}},\mathrm{s})} \tag{189}$$

$$S(\vec{b},s) = 1 - \Gamma(\vec{b},s) \tag{190}$$

$$f(\vec{q},s) = \frac{\mathrm{ik}}{2\pi}\int \mathrm{d}^2\vec{\mathrm{b}}\ \mathrm{e}^{\mathrm{i}\vec{\mathrm{q}}\cdot\vec{\mathrm{b}}}\left[1 - \mathrm{S}(\vec{\mathrm{b}},\mathrm{s})\right] \tag{191}$$

and the unitarity condition translates into:

$$|S(\vec{b},s)| \leq 1 \tag{192}$$

where the equality holds when all inelasticities go to zero, that is $\mathrm{Im}\chi(\vec{\mathrm{b}},\mathrm{s}) = 0$, while in general eq. 192 simply states that part of the incident flux is removed by the inelastic channels.

The expressions for the total, elastic and reaction cross section can be readily obtained from 187 or 191:

$$\sigma_T(s) = 2\int \mathrm{d}^2\vec{\mathrm{b}}\ \mathrm{Re}\Gamma(\vec{\mathrm{b}},\mathrm{s}) \equiv \int \mathrm{d}^2\vec{\mathrm{b}}\ \mu_{\mathrm{T}}(\vec{\mathrm{b}},\mathrm{s}) \tag{193}$$

$$\sigma_r(s) = \int \mathrm{d}^2\vec{\mathrm{b}}\ \left[1 - |\mathrm{S}(\vec{\mathrm{b}},\mathrm{s})|^2\right] \equiv \int \mathrm{d}^2\vec{\mathrm{b}}\ \mu_{\mathrm{r}}(\vec{\mathrm{b}},\mathrm{s}) \tag{194}$$

$$\sigma_{el}(s) = \int \mathrm{d}^2\vec{\mathrm{b}}\ |\Gamma(\vec{\mathrm{b}},\mathrm{s})|^2 \equiv \int \mathrm{d}^2\vec{\mathrm{b}}\ \mu_{\mathrm{el}}(\vec{\mathrm{b}},\mathrm{s}) \tag{195}$$

The physical interpretation of μ_T, μ_r, and μ_{el} is rather obvious: they represent the probability of undergoing an interaction, or an inelastic one or an elastic one, for a particle impinging along the impact parameter $\vec{b}$.

Assuming that Γ/S depend on b and not on its azimuthal orientation (as it is for most practical situation, or anyway when averaging over the initial spins and summing over the final ones), the scattering amplitude can be written as:

$$f(q,s) = \mathrm{ik}\int_0^\infty \mathrm{bdb}\ \mathrm{J}_0(\mathrm{qb})\Gamma(\mathrm{b},\mathrm{s}) \tag{196}$$

$$f(q,s) = \mathrm{ik}\int_0^\infty \mathrm{bdb}\ \mathrm{J}_0(\mathrm{qb})\left[1 - \mathrm{S}(\mathrm{b},\mathrm{s})\right] \tag{197}$$

Appendix C: Toy Model of High Energy Hadron-Nucleon Scattering

Whenever the elastic scattering distribution is a simple exponential function of the 4-momentum transfer t, $\frac{\mathrm{d}\sigma_{\mathrm{el}}}{\mathrm{dt}} \propto \exp(B_s t)$, the scattering amplitude for high energy hadron-nucleon scattering can be written as (in this paragraph the natural unit system $\hbar = c = 1$ will be used unless explicitly indicated):

$$\begin{aligned} f(t,s) &= [\rho(s) + \mathrm{i}]\frac{\mathrm{k}\sigma_{\mathrm{T}}(\mathrm{s})}{4\pi}\mathrm{e}^{\frac{\mathrm{B_{sl}(s)t}}{2}} \\ \tilde{f}(t,s) &= [\rho(s) + \mathrm{i}]\frac{\sigma_{\mathrm{T}}(\mathrm{s})}{4\pi}\mathrm{e}^{\frac{\mathrm{B_{sl}(s)t}}{2}} \\ \bar{f}(t,s) &= \frac{s[\rho(s) + \mathrm{i}]\sigma_{\mathrm{T}}(\mathrm{s})}{4\pi}\mathrm{e}^{\frac{\mathrm{B_{sl}(s)t}}{2}} \end{aligned} \tag{198}$$

which fulfills by construction the various possible definitions of the optical theorem:

$$\begin{aligned}\sigma_T(s) &= \frac{4\pi}{k}\mathrm{Im f}(0,\mathrm{s}) = \\ &= 4\pi\ \mathrm{Im}\tilde{\mathrm{f}}(0,\mathrm{s}) = \\ &= \frac{4\pi}{s}\mathrm{Im}\bar{\mathrm{f}}(0,\mathrm{s})\end{aligned}$$

and where the *slope parameter*, B_{sl}, and the ρ parameter are defined in the usual way:

$$\begin{aligned}B_{sl}(s) &\equiv \frac{\mathrm{d}\left[\ln\left(\mathrm{d}\sigma_{\mathrm{el}}/\mathrm{dt}\right)\right]}{\mathrm{dt}}(t=0) \\ \rho(s) &\equiv \frac{\mathrm{Re f}(0,\mathrm{s})}{\mathrm{Im f}(0,\mathrm{s})}\end{aligned}$$

The differential and integrated elastic scattering cross sections are given by:

$$\begin{aligned}\frac{\mathrm{d}\sigma_{\mathrm{el}}(\mathrm{t},\mathrm{s})}{\mathrm{dt}} &= [1+\rho^2(s)]\frac{\sigma_T^2(s)}{16\pi}\mathrm{e}^{\mathrm{B_{sl}(s)t}} = \\ &= \frac{\pi}{k^2}|f(t,s)|^2 \\ &= \pi|\tilde{f}(t,s)|^2 \\ &= \frac{\pi}{k^2}|f(t,s)|^2 \\ \sigma_{el}(s) &= \int_{-\infty}^{0}\mathrm{dt}\ \frac{\mathrm{d}\sigma_{\mathrm{el}}(\mathrm{t},\mathrm{s})}{\mathrm{dt}} = [1+\rho^2(s)]\frac{\sigma_T^2(s)}{16\pi B_{sl}(s)}\end{aligned} \tag{199}$$

Therefore, summarizing, the following relations among the elastic cross section, the total cross section, the ratio, ρ, of the real–to–imaginary part of the forward scattering amplitude, and the slope parameter, B_{sl}, hold:

$$\sigma_T(s) = \sqrt{\frac{16\pi B_{sl}(s)\sigma_{el}(s)}{1+\rho^2(s)}} \tag{200}$$

$$\sigma_{el}(s) = [1+\rho^2(s)]\frac{\sigma_T^2(s)}{16\pi B_{sl}(s)} \tag{201}$$

$$B_{sl}(s) = [1+\rho^2(s)]\frac{\sigma_T^2(s)}{16\pi\sigma_{el}(s)} \tag{202}$$

$$\rho(s) = \sqrt{\frac{\sigma_T^2(s)-16\pi B_{sl}(s)\sigma_{el}(s)}{\sigma_T^2(s)}} \tag{203}$$

Applying eq. 186 of Appendix B, the profile function for the scattering amplitude of eq. 198 can be readily obtained as ($t = -q^2 = -2k^2(1-\cos\theta)$ for elastic scattering):

$$\Gamma(b,s) = [1 - \mathrm{i}\rho(\mathrm{s})]\frac{\sigma_{\mathrm{T}}(\mathrm{s})}{4\pi \mathrm{B}_{\mathrm{sl}}(\mathrm{s})}\mathrm{e}^{-\frac{\mathrm{b}^2}{2\mathrm{B}_{\mathrm{sl}}(\mathrm{s})}} \tag{204}$$

Therefore the gaussian scattering amplitude in the 3-momentum transfer q described by eq. 198 translates into a gaussian profile function in the impact parameter b, with their respective variances given by (with now all c and $\hbar$ factors):

$$\sigma_q = \frac{1}{\sqrt{B_{sl}(s)}} \tag{205}$$

$$\sigma_b = (\hbar c)\sqrt{B_{sl}(s)} \tag{206}$$

For example, a typical slope parameter of the order of $\approx$10 $[\mathrm{GeV/c}]^{-2}$ corresponds to an effective interaction radius of $\approx$0.7 fm, which gives us the order of magnitude of the "range" of the interaction between two hadrons. The $S(b,s)$ function for our simplified scattering amplitude would read (eq. 190):

$$S(b,s) = 1 - [1 - \mathrm{i}\rho(\mathrm{s})]\frac{\sigma_{\mathrm{T}}(\mathrm{s})}{4\pi \mathrm{B}_{\mathrm{sl}}(\mathrm{s})}\mathrm{e}^{-\frac{\mathrm{b}^2}{2\mathrm{B}_{\mathrm{sl}}(\mathrm{s})}} \tag{207}$$

Finally the total, elastic and inelastic scattering probabilities for a given impact parameter b, according to eqs. 193,195,194 can be written as:

$$\mu_T(b,s) = \sigma_T(s)\left[\frac{\mathrm{e}^{-\frac{\mathrm{b}^2}{2\mathrm{B}_{\mathrm{sl}}(\mathrm{s})}}}{2\pi B_{sl}(s)}\right] \tag{208}$$

$$\mu_{el}(b,s) = \sigma_{el}(s)\left[\frac{\mathrm{e}^{-\frac{\mathrm{b}^2}{\mathrm{B}_{\mathrm{sl}}(\mathrm{s})}}}{\pi B_{sl}(s)}\right] \tag{209}$$

$$\mu_r(b,s) = \sigma_T(s)\left[\frac{\mathrm{e}^{-\frac{\mathrm{b}^2}{2\mathrm{B}_{\mathrm{sl}}(\mathrm{s})}}}{2\pi B_{sl}(s)}\right] - \sigma_{el}(s)\left[\frac{\mathrm{e}^{-\frac{\mathrm{b}^2}{\mathrm{B}_{\mathrm{sl}}(\mathrm{s})}}}{\pi B_{sl}(s)}\right] \tag{210}$$

where all terms within square brackets are normalized to unity when integrated over $\mathrm{d}^2\vec{\mathrm{b}}$.

Suppose now that the total cross section for high energy hadron–nucleon scattering can be expressed as a function of the squared centre-of-mass energy

s as:

$$\sigma_T(s) = \sum_i \tilde{\sigma}_i \left(\frac{s}{s_0}\right)^{\eta_i} \equiv \sum_i \sigma_{Ti}(s) \tag{211}$$

where s_0 is a scale factor, with a corresponding scattering amplitude f given by, as a function of s and of the 4-momentum transfer $t = -q^2$:

$$\begin{aligned} f(t,s) &= \sum_i f_i(t,s) = \sum_i \frac{k\ \sigma_{Ti}(s)}{4\pi}(\rho_i + \mathrm{i})\theta_{\mathrm{i}}(\mathrm{t},\mathrm{s}) \\ &= \sum_i \frac{k\ \tilde{\sigma}_i \left(\frac{s}{s_0}\right)^{\eta_i}}{4\pi}(\rho_i + \mathrm{i})\bar{\beta}_{\mathrm{i}}(\mathrm{t}) \left(\frac{\mathrm{s}}{\mathrm{s}_0}\right)^{\gamma(\mathrm{t})} \end{aligned} \tag{212}$$

where the functions $\bar{\beta}(t)$ and $\gamma(t)$ satisfy:

$$\begin{aligned} \mathrm{Re}\bar{\beta}_{\mathrm{i}}(0) &= 1 \\ \mathrm{Im}\bar{\beta}_{\mathrm{i}}(0) &= 0 \\ \mathrm{Im}\gamma_{\mathrm{i}}(\mathrm{t}) &= 0 \\ \gamma_i(0) &= 0 \end{aligned} \tag{213}$$

Under these assumptions, eqs. 211 and 212 automatically fulfill the optical theorem, and the real-to-imaginary ratio of the forward scattering amplitude, $\rho(s)$, is given by:

$$\rho(s) \equiv \frac{\mathrm{Ref}(0,\mathrm{s})}{\mathrm{Imf}(0,\mathrm{s})} = \frac{\sum_i \rho_i \mathrm{Imf}_{\mathrm{i}}(0,\mathrm{s})}{\sum_i \mathrm{Imf}_{\mathrm{i}}(0,\mathrm{s})} = \frac{\sum_i \rho_i \sigma_{Ti}(s)}{\sum_i \sigma_{Ti}(s)} \tag{214}$$

where

$$\rho_i \equiv \frac{\mathrm{Ref}_{\mathrm{i}}(0,\mathrm{s})}{\mathrm{Imf}_{\mathrm{i}}(0,\mathrm{s})} \tag{215}$$

are assumed to be independent of s.

Using dispersion relations it is possible to derive an approximate explicit expression for the ratio of the real-to-imaginary forward scattering amplitude [173]:

$$\begin{aligned} \rho &\approx \frac{1}{\sigma_T(s)} \left[\tan\left(\frac{\pi}{2}\frac{\mathrm{d}}{\mathrm{dlns}}\right)\right] \sigma_t(s) = \\ &= \frac{1}{\sigma_T(s)} \left[\sum_{k=0}^{\infty} \left(\frac{\pi}{2}\right)^{2k+1} \frac{\mathrm{d}^{2\mathrm{k}+1}\sigma_{\mathrm{T}}(\mathrm{s})}{\mathrm{dln}^{2\mathrm{k}+1}\mathrm{s}}\right] \end{aligned} \tag{216}$$

which gives the following result when applied to σ_{Ti}:

$$\rho_i = \tan\left(\eta_i \frac{\pi}{2}\right) \tag{217}$$

Eqs. 211,212, and 217 have been introduced in such a way, that they match the corresponding results of Regge theory [57] for the scattering of two hadrons mediated by n Reggeons IR or pomerons IP, with trajectories, $\alpha_i(t)$, (see [57] for the definition of trajectory) given by:

$$\alpha_i(t) \quad \equiv \quad \alpha_{0i} + \alpha_i' t = 1 + \eta_i + \gamma_i(t)$$

Therefore, identifying the trajectory intercept, α_{0i}, with $1+\eta_i$, and $\gamma_i(t)$ with $\alpha_i' t$, these equations describe Regge amplitudes and cross sections.

Regge theory applications to high energy scattering are based on crossed symmetry between reactions occurring with exchange of mediators in the t-channel, $a + b \to c + d$, and the crossed reaction, $a + \bar{c} \to \bar{b} + d$, occuring via s-channel intermediate states. The same scattering amplitude is supposed to describe both processes when suitable prolonged under analyticity requirements into the unphysical region of one process, which corresponds to the physical region of the crossed one. Crossed symmetry is at the basis of the duality concept.

High energy elastic scattering is supposed to be mediated by the exchange of a variety of neutral mesons with the proper quantum numbers. However, the trajectory associated with these mesons (Reggeons) has a typical intercept $\alpha_{0IR} \approx 0.5$ and therefore gives rise to cross sections which decrease with energy approximately like $1/\sqrt{s}$. The asymptotic behaviour of all hadronic cross sections is indeed dominated by a trajectory, the pomeron, with the vacuum quantum numbers and intercept slightly larger than one, $\alpha_{0IP} = 1 + \epsilon_{IP}$, $\epsilon_{IP} << 1$, which is not associated to any physical particle. The exact nature of the Pomeron is still a matter of debate. The name comes from the observation that this trajectory is dominating the high energy behaviour of cross sections, and since it has the vacuum quantum numbers it couples in the same way to a particle and its antiparticle, therefore assuring the fulfillment of the Pomeranchuk theorem which states that asymptotically particle and antiparticle cross sections must be equal. These simple formulae give astonishing results when used to fit all known hadron-hadron cross sections with very few parameters (see [174] for details).

References

1. R. Brun et al., CERN DD/EE/84-1(1987).

2. O.G. Ryazhskaya, report LNGS 94/110 1994.
3. R. Bonetti, A.J. Koning, J.M. Akkermans, and P.E. Hodgson, *Phys. Rep.* 247, 1 (1994).
4. E. Gadioli, and P.E. Hodgson, *Pre-equilibrium Nuclear Reactions*, (Clarendon Press, Oxford, 1992).
5. M.J. Vicente Vacas, and E. Oset, *Nucl. Phys.* A568, 855 (1994).
6. E. Oset, and L.L. Salcedo, *Nucl. Phys.* A468, 631 (1987).
7. L.L. Salcedo et al., *Nucl. Phys.* A484, 557 (1988).
8. J. Aichelin, *Phys. Rep.* 202, 233 (1991) and references therein.
9. K. Niita et al., *Phys. Rev.* C52, 2620 (1995).
10. A. Ferrari, and P.R. Sala, *Improvements to the Electromagnetic part of the FLUKA code*, to be published; P. A. Aarnio, A. Fassò, A. Ferrari, J. -H. Moehring, J. Ranft, P.R. Sala, G.R. Stevenson, and J.M. Zazula, Proc. of the *MC93 Int. Conf. on Monte Carlo Simulation in High-Energy and Nuclear Physics*, Feb. 22-26, 1993, (Ed. P. Dragovitsch, S.L. Linn, M. Burbank, World Scientific, Singapore, 1994) 100.
11. M. Herman, and G. Reffo, *Recent Progress in Nuclear Reaction Theory and Models*, lecture given at the *Workshop on Nuclear Reaction Data and Nuclear Reactors - Physics, Design and Safety*, International Centre for Theoretical Physics, May 15–17 1996, Trieste, these proceedings.
12. P. Young, E.D. Arthur, and M.B. Chadwick, *Comprehensive Nuclear Model Calculations: Theory and Use fo the GNASH Code*, lecture given at the *Workshop on Nuclear Reaction Data and Nuclear Reactors - Physics, Design and Safety*, International Centre for Theoretical Physics, May 15–17 1996, Trieste, these proceedings.
13. P. Young, *Comprehensive Nuclear Model Calculations: Theory and Use fo the GNASH Code - Part II*, lecture given at the *Workshop on Nuclear Reaction Data and Nuclear Reactors - Physics, Design and Safety*, International Centre for Theoretical Physics, May 15–17 1996, Trieste, these proceedings
14. M. Blann, *Recent Progress and Current Status of Preequilibrium Reaction Theories and Computer Code ALICE*, Proc. of the *Workshop in Computation and Analysis of Nuclear Reaction Data Relevant to Nuclear Energy and Safety*, Trüste, 1992, (M.K. Mehta and J.J. Schmidt eds., World Scientific, Singapore 1993) 517.
15. A.J. Koning, and J.M. Akkermans, *Phys. Rev.* C47, 724 (1993).
16. M. Blann, in *Intermediate Energy Nuclear Data: Models and codes*, Proc. of a specialits' meeting, Issy-les-Moulineaux, May 30th - June 1st 1994, (published by OECD/NEA 1994), p. 23.
17. M.B. Chadwick, P.G. Young, and F.S. Dietrich, in *Intermediate Energy*

Nuclear Data: Models and codes, Proc. of a specialits' meeting, Issy-les-Moulineaux, May 30th - June 1st 1994, (published by OECD/NEA 1994), p. 67.
18. A. Koning, O. Bersillon, and J.P. Delaroche in *Intermediate Energy Nuclear Data: Models and codes*, Proc. of a specialits' meeting, Issy-les-Moulineaux, May 30th - June 1st 1994, (published by OECD/NEA 1994), p. 87.
19. A. Ferrari and P.R. Sala, *Physics of Showers induced by Accelerator Beams*, in Proceedings of the *1995 Frederic Joliot Summer School in Reactor Physics*, August 22–30 1995, Cadarache, France, (CEA ed., Vol. 4 1996), Lecture 5b.
20. N. Metropolis et al., *Phys. Rev.* 100, 185 (1958); N. Metropolis et al., *Phys. Rev.* 100), 204 (1958).
21. H.W. Bertini, *Phys. Rev.* 131, 1801 (1963).
22. V.S. Barashenkov et al., *Sov. Phys. Usp.* 16, 31 (1973); V.S. Barashenkov et al., *Nucl. Phys.* A222, 204 (1974).
23. K. Chen et al., *Phys. Rev.* 166, 949 (1968); K. Chen et al., *Phys. Rev.* 176, 1208 (1968).
24. R. Serber, *Phys. Rev.* 72, 1114 (1947).
25. M.L. Goldberger, *Phys. Rev.* 74, 1269 (1948).
26. R.E. Prael and M. Bozoian, Los Alamos report LA-UR-88-3238 (1988).
27. A. Ferrari, and P. R. Sala, Proc. of the *MC93 Int. Conf. on Monte-Carlo Simulation in High-Energy and Nuclear Physics*, Tallahassee, Florida, 22-26 february (1993), (World Scientific ed. 1994), p. 277; A. Fassò, A. Ferrari, J. Ranft, and P. R. Sala, Proc. of the *Specialists' Meeting on Shielding Aspects of Accelerators, Targets & Irradiation Facilities*, Arlington, April 28-29 1994, (published by OECD/NEA 1995), p. 287; A. Fassò, A. Ferrari, J. Ranft, and P. R. Sala, in *Intermediate Energy Nuclear Data: Models and codes*, Proc. of a specialist' meeting, Issy-les-Moulineaux, May 30th - June 1st 1994, (published by OECD/NEA 1994), p. 271.
28. S.G Mashnik and S.A. Smolyansky, JINR preprint E2-94-353 , Dubna (1994)
29. H.W. Bertini, *Phys. Rev.* C1), 1801 (1970).
30. H.W. Bertini, *Phys. Rev.* 6(2), 631 (1972).
31. M.M. Meier, D.A. Clark, C.A. Goulding, J.B. McClelland, G.L. Morgan, and C.E. Moss, *Nucl. Sci. and Eng.* 102, 310 (1989).
32. M.M. Meier et al, *Nucl. Sci. and Eng.* 104, 339 (1990).
33. M.M. Meier, W.B. Amian, C.A. Goulding, G.L. Morgan and C.E. Moss, *Nucl. Sci. and Eng.* 110, 289 (1992).

34. F.E. Bertrand, and R.W. Peelle, *Phys. Rev.* C8, 1045 (1973).
35. A. Galonsky et al., *Phys. Rev.* C14, 748 (1976).
36. *International Code Comparison for Intermediate Energy Nuclear Data*, (M. Blann, H. Gruppelaar, P. Nagel and J. Rodens eds., OECD/NEA 1994).
37. G.Q. Li, R. Machleidt, and Y.Z. Zhuo, *Phys. Rev.* C48, 1062 (1993).
38. G.Q. Li, and R. Machleidt, *Phys. Rev.* C48, 1702 (1993).
39. G.Q. Li, and R. Machleidt, *Phys. Rev.* C49, 566 (1993).
40. A. Fassò, A. Ferrari, J. Ranft, P. R. Sala, G. R. Stevenson, and J. M. Zazula, Proc. of the workshop on *Simulating Accelerator Radiation Environment, SARE*, Santa Fè, 11-15 january (1993), (A. Palounek ed., Los Alamos LA-12835-C 1994), p. 134.
41. A. Fassò, A. Ferrari, J. Ranft and P. R. Sala, Proc. of the *IV International Conference on Calorimetry in High Energy Physics*, La Biodola (Elba), September 19-25 1993, (A. Menzione and A. Scribano eds., World Scientific 1994), p. 493.
42. A. Fassò, A. Ferrari, J. Ranft and P. R. Sala, Proc. of the 2nd workshop on *Simulating Accelerator Radiation Environment, SARE2*, CERN-Geneva, October 9–11 1995, Yellow report CERN in press.
43. P. Cloth et al., *HERMES, a Monte Carlo program system for beam-materials interaction studies*, Report KFA/Jül–2203 (1988).
44. K.C. Chandler, and T.W. Amstrong, *Operating instructions for the high-energy nucleon-meson transport code HETC*, ORNL–4744 (1972); K.C. Chandler, and T.W. Amstrong, *Nucl. Sci. and Eng.* 49, 110 (1972).
45. R.G. Alsmiller, F.S. Alsmiller and O.W. Hermann, *Nucl. Instr. Meth.* A295, 337 (1990).
46. R. E. Prael and H. Lichtenstein, LA-UR-89-3014 Los Alamos (1989).
47. W. O. Lock and D. F. Measday, *Intermediate Energy Nuclear Physics* (Methuen & co, London 1970).
48. Phase shift solutions KH78, KH80, in *Landolt-Börnstein , new series* , Vol. 9, part II, (Springer-Verlag 1983).
49. C.J. Joachain, *Quantum Collision Theory* (North-Holland, Amsterdam 1975).
50. K. Hänssgen, and J. Ranft, *Nucl. Sci. Eng.* 88, 537 (1984).
51. J.Bystricky et al., *Energy dependence of nucleon-nucleon inelastic total cross sections*, DPhPE 87-03 (1987).
52. B.J. VerWest, and R.A. Arndt, *Phys. Rev.* C25, 1979 (1982).
53. J. Benecke, T.T. Chou, C.N. Yang, and E. Yen, *Phys. Rev.* 188, 2159 (1969).

54. M.E Law et al., *A Compilation of Data on Inclusive Reactions*, Internal Report LBL-80 (1972).
55. A. Capella, U. Sukhatme, and J. Tran Thanh Van, *Z. Phys.* C3, 329 (1980); A. Capella, and J. Tran Thanh Van, *Phys. Lett.* B93, 146 (1980).
56. A. Capella et al., *Phys. Rep.* 236, 225 (1994).
57. P.D.B. Collins, *An Introduction to Regge Theory & High Energy Physics*, (Cambridge University Press, Cambridge 1977).
58. T. Sjostrand, CERN Report CERN-TH 6488/92 (1992).
59. S. Ritter, *Comput. Phys. Commun.* 31, 393 (1984); J. Ranft, and S. Ritter, *Acta Phys. Pol.* B11 259 (1980).
60. A.B. Kaidalov, and O.I. Piskunova, *Z. Phys.* C30, 141 (1986).
61. A. Capella, A. Kaidalov, A. Kouider Akil, C. Merino, and J. Tran Thanh Van, *Z. Phys.* C70, 507 (1996).
62. K. Goulianos, *Phys. Rep.* 101, 169 (1983).
63. S. Roesler, R. Engel, and J. Ranft, *Z. Phys.* C59, 481 (1993).
64. J. Ranft, and S. Roesler, *Z. Phys.* C62, 329 (1994).
65. K. Hahn, and J. Ranft, *Phys. Rev.* D41, 1463 (1990).
66. F.W. Bopp, R. Engel, D. Pertermann, and J. Ranft, *Phys. Rev.* D49, 3236 (1994).
67. P. Aurenche et al., *Phys. Rev.* D45, 92 (1992).
68. A. Kaidalov, *Phys. Lett.* B117, 459 (1982); A. Kaidalov, and K.A. Ter-Martirosyan, *Phys. Lett.* B117, 247 (1982).
69. J. Ranft and S. Ritter, *Z. Phys.* C27, 413 (1985).
70. M. Adamus, *Z. Phys.* C39, 311 (1988).
71. A. Ferrari, P.R. Sala, J. Ranft, and S. Roesler, *Z. Phys.* C70, 413 (1996).
72. A. Ferrari, P.R. Sala, J. Ranft, and S. Roesler, *Z. Phys.* C71, 75 (1996).
73. A. Fassò, A. Ferrari, and P. R. Sala, Proceedings of the *8th International Conference on Radiation Shielding*, Arlington, April 24-28 1994, (American Nuclear Society ed., 1994), Vol. 2, 643.
74. J. J. Griffin, *Phys. Rev. Lett.* 17, 438 (1966).
75. K. Kikuchi and M. Kawai, *Nuclear Matter and Nuclear Interactions*, (North-Holland, Amsterdam, 1968).
76. M.E. Grypeos, G.A. Lalazissis, S.E. Massen and C.P. Panos, *J. Phys.* G17, 1093 (1991).
77. L.R.B. Elton, *Nuclear Sizes*, (Oxford University Press, Oxford 1961).
78. W.D. Myers, *Nucl. Phys.* A204, 465 (1973).
79. W.D. Myers, *Droplet Model of Atomic Nuclei*, (IFI/Plenum Data Company, New York 1977).
80. A. deShalit and H. Feshbach *Theoretical Nuclear Physics, Vol. 1: Nu-*

clear Structure, (Wiley 1974).
81. A.G. Sitenko and V.K. Tartakovskij,*lektsii po teorii iadra*, (Atomizdat, Moskow 1972).
82. A. Bohr, B.R. Mottelson, *Nuclear Structure* Vol. 1, (W.A. Benjamin, Inc. 1969).
83. T. Ericson and W. Weise, *Pions and Nuclei*, (Clarendon Press, Oxford, 1988).
84. M. Krell and T.E.O. Ericson, *Nucl. Phys.* B11, 521 (1969).
85. H. J. Weyer, *Phys. Rep.* 195, 295 (1990).
86. J.N. Ginocchio and M.B. Johnson, *Phys. Rev.* C21, 1056 (1980).
87. M.B. Johnson and H.A. Bethe, *Nucl. Phys.* A305, 418 (1978).
88. M.B. Johnson and B.D. Keister, *Nucl. Phys.* A305, 461 (1978).
89. K. Stricker, H. McManus, and J.A. Carr, *Phys. Rev.* C19, 929 (1979).
90. J.N. Ginocchio, *Phys. Rev.* C17, 195 (1978).
91. K. Chen et al., *Phys. Rev.* 166, 4, 949 (1968).
92. L. Stodolski, Proc. of the *Vth Intern. Coll. on Multiparticle Reactions*, Oxford, 577 (1975).
93. K. Chen et al., *Phys. Rev.* C4, 2234 (1971).
94. H. Feshbach, A. M. Kerman, S. Koonin, *Ann. Phys.* 125, 429 (1975).
95. M. Blann, *Ann. Rev. Nucl. Sci.* 25, 123 (1975).
96. M. Blann, *Phys. Rev. Lett.* 27, 337 (1971).
97. M. Blann, *Phys. Rev. Lett.* 28, 757 (1972).
98. M. Blann and H.K. Vonach, *Phys. Rev.* C28, 1475 (1983).
99. M. Blann, *Phys. Rev.* C28, 1648 (1983).
100. S. Shlomo, *Nucl. Phys.* A539, 17 (1992).
101. G. Mantzouranis, D. Agassi, and H. A. Weidenmüller, *Phys. Lett.* 57B, 220 (1975).
102. J. M. Akkermans, H. Gruppelaar and G. Reffo, *Phys. Rev.* C22, 73 (1980).
103. V.F. Weisskopf, *Phys. Rev.* 52, 295 (1937).
104. A.S. Iljinov and M.V. Mebel, *Nucl. Phys.* A543, 517 (1992).
105. S.G. Mashnik, *Acta Phys. Slov.* 43, 86 (1993).
106. I. Dostrowsky, Z. Fraenkel and G. Friedlander, *Phys. Rev.* 116, 683 (1959).
107. A.V. Ignatyuk, G.N. Smirenkin and A.S. Tishin, *Sov. J. Nucl. Phys.* 21, 255 (1975).
108. A.V. Ignatyuk et al., *Sov. J. Nucl. Phys.* 21, 612 (1975).
109. A. Gilbert and A.G.W. Cameron, *Can. J. Phys.* 43, 1446 (1965).
110. R. Vandenbosh and J. R. Huizenga, *Nuclear Fission*, (Academic Press, New York 1973).

111. N Bohr and J.A. Wheeler, *Phys. Rev.* 56, 426 (1939).
112. F. Atchison, *Meeting on Targets for neutron beam spallation sources*, (ed. G. Bauer, KFA Jülich Germany, Jül-conf-34 1980).
113. E. Fermi, *Prog. Theor. Phys.* 5, 1570 (1950).
114. M. Epherre and E. Gradsztajn, *J. Physique* 18, 48 (1967.
115. A.S. Botvina et al., *Nucl. Phys.* A475, 663 (1987).
116. S. Leray et al., *Nucl. Phys.* A511, 414 (1990).
117. W. G. Lynch, *Ann. Rev. Nucl. Part. Sci.* 37, 493 (1987).
118. J. Richert, report CRN 93-11.
119. X. Campi et al., *Phys. Lett* 142, 8 (1984).
120. L. G. Moretto and G. J. Wozniak, *Ann. Rev. Nucl. Part. Sci.* 43, 379 (1993).
121. P.A. AArnio and M. Huhtinen, Proc. of the *MC93 Int. Conf. on Monte Carlo Simulation in High-Energy and Nuclear Physics*, Feb. 22-26, 1993, (Ed. P. Dragovitsch, S.L. Linn, M. Burbank, World Scientific, Singapore, 1994), p. 1.
122. G.A. Bartholomew et al., *Advances in Nuclear Physics* 7, 229 (1975).
123. I. Bergqvist and N. Starfelt, *Progress in Nuclear Physics* 11, 1 (1970).
124. D.H. Wilkinson, in *Nuclear Spectroscopy B*, (ed. F. Ajzenberg-Selove , Academic Press, New York 1960).
125. P.M. Endt, *Atomic Data and Nuclear data Tables* 26, 46 (1981).
126. W.Dilg, W.Schantl and H.Vonach, *Nucl. Phys.* A217, 269 (1973).
127. H. Morinaga and T. Yamazaki, *In-Beam Gamma-Ray Spectroscopy*, (North Holland 1976).
128. G.L. Morgan, report ORNL-5563 (1979).
129. J.K. Dickens , T.A. Love and G. L. Morgan, report ORNL-4847 (1973).
130. G.D. Alkhazov et al., *Nucl. Phys.*bf A381, 430 (1982).
131. A. Schiz et al., *Phys. Rev.* D21(11), 3010 (1980).
132. G. Bellettini et al. *Nucl. Phys.* 79, 609 (1966).
133. C. De Marzo et al., *Phys. Rev.* D26, 1019 (1982).
134. I.V. Ajinenko et al., *Z. Phys.* C42, 377 (1989).
135. R.J. Glauber, *Phys. Rev.* 100, 242 (1955).
136. R.J. Glauber, in *Lectures in Theoretical Physics*, Vol. 1 (1959).
137. R.J. Glauber, in *High Energy Physics and Nuclear Structure*, (North Holland 1967), 311.
138. R.J. Glauber and G. Matthiae, *Nucl. Phys.* B21, 135 (1970).
139. V.N. Gribov, *Sov. Phys. JETP* 29, 483 (1969); V.N. Gribov, *Sov. Phys. JETP* 30, 709 (1970); L. Bertocchi, *Nuovo Cimento* 11A, 45 (1972).
140. K. Zalewski, *Ann. Rev. Nucl. Part. Sci.* 35, 55 (1985).
141. A. Capella, and A. Krzywicki, *Phys. Rev.* D18, 3357 (1978).

142. A. Capella, *Nucl. Phys.* A25, 133c (1991).
143. V.A. Karmanov and L.A. Kondratuk, *JETP Lett.* 18, 266 (1973).
144. D. Diamond and B. Margolis, *Phys. Rev.* D16, 1365 (1977).
145. N. Fujiwara et al., *Nucl. Phys.* A404, 509 (1983).
146. A. Tufail et al., *Phys. Rev.* D42, 2187 (1990).
147. S. Fredriksson et al., *Phys. Rep.* 144, 187 (1987).
148. Z. Pengfei, and C. Weiqin, *Nucl. Phys.* A552, 620 (1993).
149. J. Ranft, *Z. Phys.* C43, 439 (1988).
150. L. Landau, I. Pomeranchuk, *Dokl. Akad. Nauk SSSR* 92, 535 (1953); A.B. Migdal, *Phys. Rev.* 103, 1811 (1956).
151. H.-J. Möring, J. Ranft, *Z. Phys.* C52, 643 (1991).
152. J. Ranft, *Phys. Rev.* D51, 64 (1995).
153. G. Battistoni, C. Forti, and J. Ranft, *Astroparticle Physics* 3, 157 (1995).
154. S.G Mashnik, JINR preprint E2-93-470 (1993).
155. *Intermediate Energy Nuclear Data: Models and codes*, Proc. of a specialits' meeting, Issy-les-Moulineaux, May 30th - June 1st 1994, (published by OECD/NEA 1994).
156. M. Trabandt et al., *Phys. Rev.* C39, 452 (1989).
157. A.A. Cowley et al., *Phys. Rev.* C43, 678 (1991).
158. W.B. Amian et al., *Nucl. Sci. Eng.* 112, 78 (1992).
159. W.B. Amian et al., *Nucl. Sci. Eng.* 115, 1 (1993).
160. S. Stamer et al., *Phys. Rev.* C47, 1647 (1993).
161. K.Nakai et. al., *Phys. Rev. Lett.* 44, 1446 (1979).
162. D. Ashery et al., *Phys. Rev.* C23, 2173 (1981).
163. W.J. Burger et al., *Phys. Rev.* C41, 2215 (1990).
164. R.D. McKeown et al., *Phys. Rev.* C24, 211 (1981).
165. D.R.F. Cochran et al., *Phys. Rev.* D6, 3085 (1972).
166. S.M. Levenson et al., *Phys. Rev.* C28, 326 (1983).
167. D. Ashery et al., *Phys. Rev.* C30, 946 (1984).
168. E. Stenlund, and I. Otterlund, *Nucl. Phys.* B198, 407 (1982).
169. N.Y.T. Porile, G.T. Cole and C.Rudy, *Phys. Rev.* C19, 2288 (1979).
170. L.Sihver et al., *Nucl. Phys.* A543, 703 (1992).
171. P.W. Lisowski et al., in *Proc. Int. Conf. on Nuclear Data for Science and Technology*, Jülich, Germany, (Springer Berlin 1992), p. 732.
172. A.S. Iljinov et al., (Landolt-Börnstein, Springer–Verlag, New Series, Vol. 13a 1991).
173. U. Amaldi, M. Jacon, and G. Matthiae, *Ann. Rev. Nucl. Sci.* 26, 385 (1976).
174. A. Donnachie, and P.V. Landshoff, *Phys. Lett.* B296, 227 (1992).